Water resources assessment in cold regions: the Upper Tuul River basin, Mongolia

Ph.D. Thesis

Dept. of Geotechnical Eng. And Geosciences

Technical University of Catalonia, UPC-BarcelonaTech.

Institute of Environmental Assessment and Water Research, IDAEA-CSIC,

Barcelona, Spain

Enkhbayar Dandar

Advisor:

Jesús Carrera Ramírez

Co-Advisors:

Maarten W. Saaltink

( ), 2017

This thesis was supported in financial from a project of IWRM in Water Authority of Mongolia (old name) and the Institute of Environmental Assessment and Water Research (IDAEA-CSIC) of Spain.

A mi familia

I. Abstract

Groundwater withdrawals are growing in most developing countries, including Mongolia, where freshwater resources are limited and unevenly distributed, and most surface waters are frozen during winter. Groundwater represents some 80% of the water supply in the country. Computation of recharge is important, but is complicated in cold regions, because of phase change and permafrost, which is found on 63 percent of the country, and causes conventional physically-based land surface models to be inaccurate.

We have developed a two-compartment water and energy balance model that accounts for freezing and melting and includes vapor diffusion as a water and energy transfer mechanism. It also accounts for the effect of slope orientation on radiation, which may be important for mountain areas. We applied this model to the Upper Tuul River Basin to evaluate recharge under different soil and vegetation types. The basin is divided into 12 zones (models) based on elevation ranges, orientation and slope. Due to the limited number of observation data in this area, precipitation, air temperature and relative humidity were corrected as a function of elevation by means of lapse rates. Results show that recharge is relatively high and delayed with respect to snowmelt during spring, because it is mainly associated to thawing at depth, which may occur much later. Most importantly, we find that vapor diffusion plays an important quantitative role in the energy balance and a relevant qualitative role in the water balance. Except for a few large precipitation events, most of the continuous recharge is driven by vapor diffusion fluxes. Large vapor fluxes occur during spring and early summer, when surface temperatures are moderate, but the subsoil remains cold, creating large downwards vapor pressure gradients. Temperature gradients reverse in fall and early winter, but the vapor diffusion fluxes do not, because of the exponential shape of the saturated vapor pressure as a function of temperature giving smaller vapor pressure differences at lower temperature. The computed sensible heat flux is higher than the latent heat flux, which reflects the dry climate of the region. The downward latent heat flux associated to vapor diffusion is largely compensated by an upward heat conduction, which is much larger than in temperate regions.

The alluvial aquifer around Ulaanbaatar supplies water to the city and is under pressure because of the growing water demand. To address this concern, we built a numerical model, which is challenging, not only because of the lack of data, but also because the river freezes during winter. River flow under the ice is sustained by groundwater, which provides the energy to prevent full freezing of the whole river thickness, but which may not occur where groundwater levels are depleted by pumping. At present, the river still flows under the ice during winter at both ends of the Ulaanbaatar alluvial aquifer. The downstream end, to the West, receives aquifer discharge, whereas the river is fed by discharge from adjacent alluvial aquifers upstream of the east end. But, in the central portion, the river is fully frozen. In fact, the river bed in this portion becomes dry in April most years, probably because of sublimation and because melted water immediately infiltrates into the aquifer. If groundwater pumping increases, either at the Ulaanbaatar alluvial aquifer or at the alluvial aquifer near Gachuurt village, it is likely that the currently winter flowing portion of the river will also dry or, rather, become fully frozen during winter. This will not be a major problem from a quantitative point of view because aquifer storage is sufficient to support winter pumping, even if pumping is increased. However, it may have other environmental and cultural implications. Therefore, further study is needed to monitor at both the upper and downstream stream parts of the aquifer.

II. Resumen

La extracción de agua subterránea crece en la mayoría de los países en desarrollo y representa un problema en Mongolia, donde los recursos de agua son limitados, están distribuidos de manera irregular, y la mayoría de las aguas superficiales se congelan en invierno. El agua subterránea representa la principal (del orden del 80%) fuente de suministro, lo que hace importante el cálculo de la recarga. El cálculo se complica en zonas frías por los cambios de fase y el permafrost, que cubre el 63% del país, y hace que los modelos convencionales de balance de agua en el suelo sean imprecisos.

Hemos desarrollado un modelo de balance de agua y energía de dos compartimentos que incluye sublimación, congelación y fusión, así como la difusión de vapor como mecanismo de transferencia de agua y energía. También reconoce el efecto de la orientación de la pendiente sobre la radiación, que puede ser importante en zonas de montaña. Hemos aplicado este modelo a la Cuenca Alta del Río Tuul. Para incluir el efecto de los distintos tipos de suelo y vegetación, dividimos la cuenca en 12 zonas en función de la elevación, la orientación y la pendiente. Por otro lado, hemos tenido que corregir, en función de la altitud, los datos de precipitación y temperatura y humedad relativa del aire, solo disponibles en estaciones situadas en valles. Los resultados muestran que la recarga es relativamente alta y retrasada respecto al deshielo, ya que una parte se asocia a la fusión del hielo profundo, que ocurre mucho más tarde. Lo más importante es que la difusión de vapor desempeña un importante papel tanto en el balance energético como en el hídrico. Exceptuando algunos eventos de alta precipitación, la mayor parte de la recarga está asociada al flujo difusivo de vapor, que aporta no solo agua sino también energía para fundir el hielo profundo. La difusión de vapor es máxima al final de la primavera y principios del verano, cuando el suelo se calienta, favoreciendo la evaporación, pero el subsuelo permanece frío, lo que produce condensación. El gradiente térmico se invierte en otoño e invierno, pero no tanto el flujos de vapor porque las diferencias de presión de vapor disminuyen al bajar la temperatura. El flujo de calor latente descendente asociado a la difusión de vapor se compensa en gran medida por una conducción de calor hacia arriba, que es mucho mayor que en regiones templadas.

El acuífero aluvial de Ulán Bator suministra agua a la ciudad y sufre la creciente demanda de agua. Para abordar esta inquietud, hemos construido un modelo numérico, que es un desafío, no sólo por la falta de datos, sino también porque el río se congela en invierno. Los ríos fluyen bajo el hielo gracias al agua subterránea, que aporta energía para impedir la congelación total del río, que desaparece cuando los niveles del agua subterránea se deprimen por bombeo. En la actualidad, el río sigue fluyendo bajo el hielo en ambos extremos del acuífero aluvial. El de aguas abajo, hacia el oeste, recibe la descarga del acuífero, mientras que en el extremo este recibe la descarga de acuíferos aguas arriba. Pero, en la parte central, el río está completamente congelado. De hecho, el lecho del río llega a secarse en Abril, probablemente debido a la sublimación y a que el agua derretida se infiltra. Si el bombeo del agua subterránea aumenta, ya sea en el acuífero aluvial de Ulán Bator o en los de aguas arriba, es probable que la parte del río que actualmente fluye también se seque o se congele completamente en invierno. Esto no será un problema importante desde un punto de vista cuantitativo, porque el almacenamiento del acuífero es suficiente para soportar el bombeo invernal, incluso si se aumenta, pero podría tener otras implicaciones ambientales y culturales. Por ello, sería deseable hacer estudios de detalle en ambos extremos del acuífero.

III. Хураангуй

Цэвэр усны нөөц хязгаарлагдмал, жигд бус тархалттай, гадаргын ус нь өвлийн улиралд хөлддөг онцлогтой Монгол зэрэг хөгжиж буй орнуудад газрын доорх усны хэрэглээ өсөж байна. Усны нийт хэрэглээний 80 орчим хувийг газрын доорх усаар хангадаг. Газрын доорх усны тэжээмжийг тооцох нь чухал боловч нийт газар нутгийн 60 хувьд нь олон жилийн цэвдэг чулуулгийн тархалттай, фазын өөрчлөлттэй, физикд суурилсан газрын гадаргын загварууд нь тодорхой бус байдаг шалтгаанаас хүйтэн уур амьсгалтай бүс нутгуудын хувьд хүндрэлтэй байдаг.

Иймд хөлдөлт, гэсэлтийг тооцоолох болон ус ба энергийн шилжилийн механизм болох усны уурын диффузыг (vapor diffusion) багтаасан хоёр хэсэг ус ба энергийн балансын загварыг хийсэн. Уг загварт уулархаг районы чухал хүчин зүйл болох газрын гадаргын налуугийн байрлал, нийлбэр цацрагийн нөлөөллийг тооцож үзсэн. Загварыг янз бүрийн хөрс, ургамалтай нөхцөлд тэжээмжийг үнэлэх зорилгоор Туул голын сав газрын дээд хэсэгт хэрэглэсэн. Тус талбайг газрын гадаргын налуу, байрлал болон өндөржилтөөр нь 12 бүсэд (загварт) хувааж үзэв. Талбайн цаг уурын ажиглалтын мэдээ хязгаарлагдмал тул хур тунадас, агаарын температур болон харьцангуй чийгшил өндөржилтөөс хамаарсан хамаарлыг (lapse rate) ашиглан засварыг гүйцэтгэлээ. Загварын үр дүнгээс харахад, тэжээмж харьцангуй их, ихэвчлэн хөрсний гэсэлтийн гүнээс хамаарч хожуу тохиолдох хаврын цасны хайлалтаас ирдэг байна. Хамгийн чухал нь усны уурын диффузи энергийн балансад тоон чухал үүрэг гүйцэтгэж усны балансад чанарын үүрэг гүйцэтгэдгийг тогтоосон. Нэг удаагийн их хэмжээний хур тунадаснаас бусад тохиодолд газрын доорх усны тэжээмж нь усны уурын диффузын урсацаар бий болно. Газрын гадаргын өнгөн хэсгийн температур өсөх үед (>0°C), хавар болон зуны улиралын эхэн үед их хэмжээний усны уурын диффузи явагддаг ч газрын өнгөн хэсгээс доошхи гүнд хөрс хөлдүү байж доош чиглэсэн их хэмжээний усны уурын даралтын зөрүү бий болдог. Газрын өнгөн хэсгийн болон гүн дэх температурын зөрүү намар, өвлийн улирлын эхэнд эсэргээрээ тохиолдоход бага температурт усны уурын даралтын ялгааг бага өгөх ханасан усны уурын даралтын экспоненциал хэлбэр температураас хамаарсан функц байдаг тул дээш чиглэсэн усны уурын диффузийн хөдөлгөөн маш бага байна. Тооцсон турбулент босоо дулааны урсгал (sensible heat) нь ууршилтанд зарцуулагдах дулааны урсгалаас (latent heat) их байгаа нь хуурай уур амьсгалтайг илтгэнэ. Доош чиглэсэн дулааны урсгал усны уурын диффузтэй холбоотой. сэрүүн бүс нутагт их байдаг дээш чиглэсэн хөрсний дулааны урсгалаар нөхөгдөж байдаг.

Улаанбаатар хотын усан хангамжийг аллювийн уст давхаргаас хангадаг ба өсөн нэмэгдэж буй усны хэрэглээнээс болж асуудал үүсээд байгаа билээ. Энэ асуудлыг шийдвэрлэхийн тулд мэдээлэл хомсдолоос гадна өвлийн улиралд голын ус хөлддөг хүндрэлтэй нөхцөлд тоон загварыг хийж гүйцэтгэсэн. Голын мөсний дор гол бүрэн хөлдөх үйл явцыг удаашруулдаг дулааны хөдөлгөөн газрын доорх усны урсгалаар бий болдог ч газрын доорх усны түвшин шавхалтын улмаас багассан тохиолдолд дээрх үйл явц явагдах боломжгүй. Одоогийн байдлаар Улаанбаатар орчмын аллювийн уст давхаргын дээд болон доод хэсгүүдэд өвлийн улиралд голын ус урсгалтай байна. Талбайн дээд буюу зүүн хэсэгт (Гачуурт орчимд) голын ус нь зэргэлдээх аллювийн уст давхаргаас тэжээгддэг онцлогтой. Харин төв хэсэгт голын ус ёроолоо хүртэл хөлддөг. Энэ хэсэгт өвлийн улиралд явагддаг ууршилт (sublimation) болон хайлсан ус тэр дороо уст давхарга руу нэвчдэгийн улмаас ихэнхдээ 4-р сард хуурай, усгүй болдог байна. Хэрэв Улаанбаатар орчмын аллювийн уст давхарга, Гачуурт тосгон орчмын уст

давхаргад усны шавхалт нэмэгдвэл өвлийн улиралд голын ус ёроолоо хүртэл хөлдөх нөхцөлийг бүрдүүлэх ба мөсний доор усны урсгал явагдах боломжгүй болох магадлалтай. Өвлийн улирлын шавхалтанд газрын доорх усны нөөц хангалттай байдаг тул тоо хэмжээний хувьд тийм ч чухал асуудал биш ч хүрээлэн буй орчин, соёлын ач холбогдолтой байж болох юм. Иймд уст давхаргын дээд болон доод хэсгүүдэд хяналт хийх нэмэлт судалгаа шаардлагатай байна.

IV. Acknowledgments

A large number of people have supported me in my doctoral research. First and foremost, I would like to thank sincerely my supervisor Dr. Jesus Carrera, for allowing me to do doctoral thesis in Barcelona and to join the Hydrolgeology Group. His breadth of knowledge and profession have contributed greatly to the completion of this work. I want to thank Dr. Maarten W. Saaltink, my co-supervisor, for his excellent assistance and helpful comments on this thesis. I thank also my co-supervisor Dr. Buyankhishig Nemer, for her full support and help. She gave me an opportunity to study abroad. I have benefited greatly from my advisors.

Many colleagues, friends have inspired me as well as given me moral support all these years. I am grateful to my colleagues of the Hydrogeology group from the UPC and IDAEA-CSIC. I want to thank them for all their help and support. I could not learn Spanish without them. Special thanks go to Silvia for her brilliant counsel and constant encouragement. And more, I wish to acknowledge Gonzalo, Estanis, Anna, Bruno, Mar, Alex Serrano, Quim, Victor, Berta, Sheila, Alessandro, Laura, Alba, Carme, Rotman, Enric Bonet, Jordi Belles, Miguel Angel, Violeta, Yoar, Cristina, Maria Pool, Lazaro and Linda for their unconditional friendship and their valuable help during these years.

I would also like to thank the professors of Hydrogeology Group, they always give a salute with politely: Enric Vazquez, Jordi Cama, Carlos Ayora, Marco Dentz, Xavier Sanchez-Vila and Josep Soler, and special thanks to Teresa Garcia, Ana Martínez and Monica Prats for their help and guidance.

I am further gratitude to my colleagues from Mongolia, Naranchimeg, Batdemberel, Erdenetsetseg and other members of department of Hydrogeology and Engineering geology at MUST for their support and for their help in obtaining data from the monitoring wells.

Thanks to my friends who supported me throughout my thesis: Tumenjargal, Batxi, Sainsanaa, Tuvshinjargal and Naranbaatar.

Finally I would like to thank my dear wife (Munkhbayar), my daughter (Khaliunaa) and my son (Enkhsuld), my parents and all family for their great support, patience, understanding and love with all my heart.

Table of Contents

I. Abstract i
II. Resumen ii
III. Хураангуй iii
IV. Acknowledgments v
V. List of figures viii
VI. List of tables x
1. Chapter 1: Introduction 1
1.1. Motivation and objectives 1
1.2. Thesis Outline 4
1.3. The Mongolian context 5
2. Chapter 2: A surface model for water and energy balance in cold regions accounting for vapor diffusion 8
2.1. Introduction 8
2.2. Methodology 10
2.2.1. Model description 10
2.2.2. Water balance 11
2.2.3. Energy balance 14
2.2.4. Numerical solution and implementation 19
2.2.5. Data of meteorological stations and parameters 20
2.3. Results 22
2.4. Discussion and Conclusions 29
3. Chapter 3: Water and energy balance in the Upper Tuul basin, Mongolia 31
3.1. Introduction 31
3.2. Methodology 33
3.2.1. Study area 33
3.2.2. Available data 34
3.2.3. Model description 36
3.3. Results 41
3.4. Conclusions 49
4. Chapter 4: Surface and groundwater interaction in cold region and leakage 51

4.1. Introduction 51
4. 2. Methodology and materials 55
4.2.1. Study area 55
4.2.2. Available data 56
4.2.3. Conceptual model 59
4.2.4. Numerical model. Calibration strategy 63
4.3. Results 63
4.3.1. Preliminary calibration 63
4.3.2. Head fluctuations 64
4.3.3. Calibration 66
4.4. Discussion and Conclusion 68
5. Chapter 5: General Conclusions 70
6. References 73
Annexes 87

V. List of figures

Figure 1.1. Map of Mongolia (source: SRTM with 90m)

Figure 1.2. Map of permafrost in Mongolia (source: Sharkhuu, 2003). 1) Permafrost monitoring site, 2) Continuous and discontinuous permafrost, 3) Islands permafrost and 4) Sporadic permafrost

Figure 2.1. Schematic diagram of the water balance (a) and energy balance (b) models

Figure 2.2. Temperature versus total energy

Figure 2.3. Daily evolution of (a) precipitation and recharge, (b) other water fluxes, (c) water content at surface (solid line) and subsoil (dashed line), (d, e) heat fluxes, and (f) temperatures of the base model

Figure 2.4. Zoom of recharge (red dashed line) and vapor diffusion (blue line) during 2003 (Temperatures are also shown). Note that, except for the two heavy rainfall events of May and August, recharge during the warming period (after the subsoil has started to thaw) is identical to the vapor diffusion flux.

Figure 2.5. Zoom of ET (actually, water phase change processes) (black line) along with liquid (blue) and ice (red) water contents during 2003.

Figure 2.6. Daily evolution of surface and subsoil temperature in 2004.

Figure 3.1. Location of the study area. Elevation map (a), Soil map (b).

Figure 3.2. Upper Tuul River Basin, showing the location of gauge and whether stations, and the subdivision (color code) according to slope orientation and elevation, which correlate with soil type and vegetation.

Figure 3.3. Comparison between calculated and observed cumulative discharge (mm) for the Selbe basin from 1994 to 2013. Q* is the cumulative discharge calculated using only one type of soil (cryosols).

Figure 3.4. Comparison between calculated and observed cumulative discharge (mm) for the Uliastai basin from 1994 to 2013. Q* is the cumulative discharge calculated using only one type of soil (cryosols).

Figure 3.5. Comparison between calculated and observed cumulative discharge (mm) for the whole Upper Tuul basin from 1994 to 2013.

Figure 3.6. Comparison between the daily observed and computed snow depth at elevations below 1450 m with a horizontal slope.

Figure 3.7. Comparison between the daily observed and computed snow depth at elevations ranging from 1451 to 1750 m with a horizontal slope.
Figure 3.8. The average annual water fluxes evolution in the Upper Tuul basin
Figure 3.9. Schematic image (a) for landscape, the average annual surface (b) and subsoil layer (c) temperature (1993-2013) in different surfaces. The average annual air temperature was 0.6°C, -3.2°C, -6.2°C and 9.2°C, elevation < 1450 m, 1451-1750 m, 1751-2250 m and > 2251 m respectively.
Figure 4.1. River flows under the ice largely because inflows from groundwater, which sustain the flow rate and provide energy to keep water liquid. The resulting flow regime is similar to that without ice (a). Pumping near the river captures river flow, leading to narrow depression cones (b), but it also reduces the inflow of water and energy to the river, which may fully freeze during winter.
Figure 4.2. Study area, including the whole Upper Tuul River Basin and the Ulaanbataar alluvial aquifer.
Figure 4.3. Geological map (scale 1: 200 000)
Figure 4.4. Location of exploration boreholes for the May, 1960 campaign, including TDS (color code) and geological cross sections, such as A-A′ shown below (modified from PNIIIS, 1979).
Figure 4.5. Water temperature at observation wells versus depth.
Figure 4.6. Different leakage condition along the Tuul River near Ulaanbaatar. Date of Google Earth images are in April, 2016 and the picture was taken by Tuul River Basin Authority in March, 2016.
Figure 4.7. a) Conceptual model and boundary conditions and b) model grid.
Figure 4.8. TDS concentrations calculated under steady-state flow conditions.
Figure 4.9. Measured (red circles) and computed heads at the three observation wells for the initial base model (using the steady-state calibrated parameters), and acknowledging seasonal fluctuations of only one of the time dependent parameters (recharge, river water stage (H_{river}), lateral flow or leakage coefficient). It is clear that most of the head fluctuation is driven by fluctuations in the leakage factor.
Figure 4.10. Groundwater head fit obtained from calibration at observation wells.
Figure 4.11. Contributions to mass balance (10^6 m^3 $year^{-1}$). Positive values represent inputs.
Figure 4.12. Measured and calculated heads OW3, near the river at the upstream edge of the aquifer for several values of the leakage factor. Note that heads rise slightly at the beginning of winter, probably in response to the river head rise during freezing.

VI. List of tables

Table 2.1. Parameter and values for Base model

Table 2.2. Average in 5 years of water fluxes: evapotranspiration (ET), infiltration (I), surface runoff (SR), vapor diffusion (J_D) and Recharge (R). Precipitation is 334 kg m^{-2} $year^{-1}$)

Table 2.3. Average in 5 years of energy fluxes: net radiation (Rn), Latent heat (e_gET), sensible heat (H), heat conduction (G) and vapor convection (e_gJ_D).

Table 3.1. Description of the 12 model zones

Table 3.2. Parameters and values

Table 3.3. Water fluxes, averaged over 21 years (1993-2013): precipitation (P), evapotranspiration from the surface (ET_{sf}) and the subsoil (ET_{ss}) layer, infiltration (I), surface runoff (SR), vapor diffusion (J_D) and recharge (R). All fluxes are in kg m^{-2} $year^{-1}$. Note that $R=I+ J_D- ET_{ss}$.

Table 3.4. Heat fluxes, averaged over 21 years (1993-2013): net radiation (Rn), latent heat (e_g ET), sensible heat (H), heat conduction (G) and vapor convection (e_g J_D). Units of all fluxes are in MJ m^{-2} $year^{-1}$.

Chapter 1

Introduction

1.1. Motivation and objectives

Water demand and water shortage are gradually increasing in many countries, as a result of increasing population, expanding areas of irrigated agriculture, industrial development and massive urbanization (Lalzad, 2007). If groundwater abstraction exceeds its recharge for long time, overexploitation (Custodio, 2002) or groundwater depletion (Wada et al., 2010; Aeschbach-Hertigand Gleeson, 2012) will occur. Actually, withdrawals are growing in most developing countries, which increases the pressure on water resources.

Moreover, available groundwater resources may change as a consequence of climate change. Climate change affects indirectly groundwater resources by changing groundwater

heads and recharge over time (Green et al., 2011; Taylor et al., 2013) and it can influences groundwater systems through changes in precipitation, evapotranspiration and soil moisture as a result of increasing temperature (Kumar, 2012).In cold regions, climate change will have an impact on permafrost or frozen soil. Higher temperatures during winter will reduce ground frost (Jyrkama and Sykes, 2007), resulting in permafrost warming or degradation, which in return will alter groundwater discharge (Hinzman et al., 2013). Controlling the above issues requires sustainable water resources management which entails assessing groundwater resources. This is especially relevant in developing countries with scarce water resources. Another problem is the lack of data or data from different sources that makes it difficult to obtain a reliable estimation of water resources (Döll et al., 2012).

This thesis is motivated by the assessment of water resources in the Upper Tuul River Basin, located in the northern Mongolia. This basin is characterized by semi-arid, subarctic conditions, which has important effects on recharge and makes traditional empirical methods to be of little value because they are largely based on regions with temperate climate. Permafrost is found at high altitudes, which hampers infiltration of water towards underlying aquifers. An “active layer” that freezes and thaws seasonally is found above the permafrost (Woo, 2012). Due to long term increase of temperature the depth of the active layer increases, which leads to higher permeability of the soil and affects hydrological processes (e.g., Ge et al., 2011). The consideration of freezing and thawing makes it clear that a proper assessment of hydrological processes requires not only the water balance but also the energy balance.

Water and energy balances are the basic building blocks for any hydrological model and specifically of land surface schemes linking meteorological data with runoff, and thus water availability. Classical hydrological model codes, such as WatBal (Yates, 1996),SWAT or BALAN (e.g., Arnold et al., 1998; Hülsmann et al., 2015; Samper et al., 2007) calculate the basic terms of a river basin water balance, such as stored soil water, evapotranspiration and surface runoff. The latest version of SWAT use energy balances of the snow cover instead of the temperature-index method (e.g., Fuka et al., 2012).It has been extended by considering energy balances in the soil as well (Qi et al., 2016). Unfortunately, this code only considers conduction as a mechanism for heat transport in the soil. In this thesis, we conjecture that the large temperature differences within the soil

may drive water vapor to the cold part of the soil as proposed by Shvetzov (1978) and Gusev and Nanosova (2002).Therefore, we also need to take into account vapor diffusion flux in both the water and the energy balance of the soil.

Ulaanbaatar, capital of Mongolia, is located in the UpperTuul River Basin. The water supply of the city totally depends on groundwater abstraction from the alluvial aquifer of the Tuul River Basin because surface waters freeze during winter. The water demand of Ulaanbaatar has increased to a great extent as a result of the rapid industrial development and population growth, partly due to the migration from rural areas (Buyankhishig et al., 2009).The population of the was estimated at 1.4 million people in 2013 (NSO, 2013), which is the highest of Mongolia. Few studies have focused on the interaction between the alluvial aquifer and river water in this area. Tsujimura et al., (2013) found by using the End Member Mixing Analysis method that the alluvial aquifer is mainly fed by water from the River Tuul. Therefore, a groundwater model is needed to assess groundwater resources of the alluvial aquifer of the River Tuul.

Flow of water between the alluvial aquifer and the Tuul River is mainly controlled by the river water levels. Generally the river water levels increase in summer and drop in winter. However, in early winter, river levels increase when water starts to freeze-up (Weber et al., 2013; Hamilton, 2004). In fact, the hydrological monitoring and research in northern regions are traditionally focused on the spring and summer high flow period (Moore et al., 2002). This area is no exception. Another factor that drives the exchange between groundwater and surface water is the hydraulic conductivity of streambed and banks. Water temperature directly affects the hydraulic conductivity (e.g., Constantz, 1998; Barahona-Palomo, 2014) through the viscosity which decreases with increasing temperature. Considering this process, this thesis includes a groundwater numerical model to define the interaction between surface water and alluvial aquifer along the Tuul River near Ulaanbaatar under different leakage condition during winter months.

The objectives of this thesis are to increase understanding of hydrology of Tuul River basin as follows:

1. To develop a new method for water and energy balance accounting for vapor diffusion, including the effect of slope on radiation.

2. To apply the above method to the Upper Tuul River Basin, to evaluate the groundwater recharge under freezing and thawing soil condition and to understand the complex hydrological processes in cold regions for different landscapes (vegetation, soil, orientation and slope).
3. To model the alluvial aquifer of the Tuul River Basin near Ulaanbaatar and its interaction with the river including the leakage from Tuul River under different assumptions for leakage during winter period.

These three objectives lead to three papers (Dandar et al., 2017a,b,c) submitted (or in preparation) for publication and presented in chapter 2,3 and 4, respectively.

1.2. Thesis Outline

This thesis is organized in three main chapters (chapters 2, 3, 4), an introduction (chapter 1) and conclusions (chapter 5).

Chapter 2 introduces a new approach to calculate the water and energy balances, including vapor diffusion and the effect of slope on radiation which should be relevant for high latitudes. This model contains two layers and attempts to represent all terms relevant for simulating land surface hydrological processes, including all possible phase changes and, singularly, vapor diffusion. The model has been applied to meteorological data from the Terelj station. A semi-implicit finite difference scheme with a time step of one day was used to solve the water and energy balances equations. The algorithm was implemented in a spreadsheet that is available for the cases discussed at http://h2ogeo.upc.edu/en/investigation-hydrogeology/software.

Chapter 3 presents the application of the water and energy balance model to the Upper Tuul River Basin in order to evaluate the groundwater recharge. This basin was divided into 12 zones or models according to its slope and elevation. For the elevations higher than 1751 m, where no data are available, the precipitation, air temperature and relative humidity were obtained from lower altitude stations by means of lapse rates. The water and heat fluxes were evaluated for three sub basins under different vegetation and soil types.

In *chapter 4*, the interaction between surface water and its adjacent alluvial aquifer was investigated. In order to define their interaction, a groundwater numerical model of an alluvial aquifer was carried out for the Tuul River Basin near Ulaanbaatar. A sensitivity analysis was performed under different leakage condition along the Tuul River.

Chapter 5 presents general conclusion of thesis.

1.3. The Mongolian context

A summary of the Mongolian context is presented here for readers not familiar with Mongolia, which is a landlocked country in north central Asia, bounded in the north by Russia, and in the west, south and east by China. The topography of Mongolia consists of a high plateau surrounded by mountain ridges in the north and west, and dry steppes and semi-deserts in the east and south with elevation ranging from 524 (Huh Nuur) to 4316m.a.s.l (Khuiten Peak). It has a total area of 1,565,000 km^2 and is thus the 19^{th} largest country in the world (Dagvadorj et al., 2009). It is one of the largest countries with no access to the sea. With a population of 2.93million (NSO, 2013) it is the most sparsely populated country. The country has an extreme continental climate consisting of four seasons characterized by long and cold winters, hot summers with a distinct spring and autumn (Batimaa et al., 2007). Mongolia's territory is divided into two major geographic regions: the Khangai (including the Altai and Khangai-Khentii mountain ranges) in the central and western regions; and the Gobi (including the Steppe and Gobi-desert areas) in the southern and eastern regions.

In general, recorded precipitation in Mongolia is low. Annual mean precipitation ranges between 50-100 mm in the southern Gobi desert-steppe, 300-400 mm in the northern mountainous regions (Khangai, Khentain and Khuvsgul), and 250-300 mm in the western forest steppe regions (Natsagdorj et al., 2001). It is characterized by relatively intense rainfall events with most of the precipitation falling between April to September, of which about 50-60% falls in July and August during the summer monsoon (Dagvadorj et al., 2009).

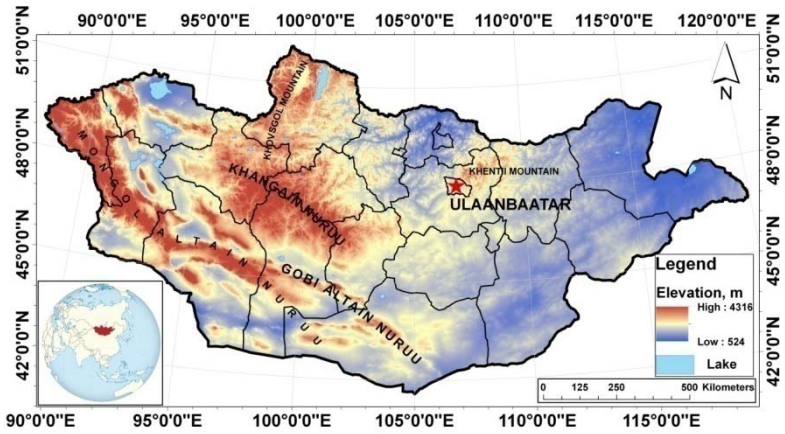

Figure 1.1. Map of Mongolia (source: SRTM with 90m)

Temperatures across Mongolia range from -15°C to -30°C in the winter and from 10°C to 27°C in the summer. The annual mean temperature in Mongolia is 0.7°C, ranging from 8.5°C in the warmest regions of southern Gobi to -7.8°C in the coldest regions of the North. July is the hottest month of the year, with an average of 15-25°C. The extreme maximum temperature recorded was 43.1°C. The coldest (-52.9°C) occurred in January (Ma et al., 2003). The average temperature in Mongolia has increased approximately 1.56°C over the last 60 years.

Permafrost zones occupy almost two thirds of Mongolia, predominantly in the Khentii, Hovsgol, Khangai and Altai Mountains and surrounding areas. A geocryological (permafrost) map for Mongolia was developed by scientists led by Gravis (1972), based on results from a Mongolian and Russian joint research expedition from 1967 to 1971. According to this map (Figure 1.2), permafrost areas distributed in the Mongolian territory are divided into four types: 1) continuous and discontinuous permafrost (50-100%), 2) isolated permafrost (1-50%), 3) sporadic permafrost (0-1%) and 4) no permafrost or seasonally frozen ground (Sharkhuu, 2000). Most of the permafrost is at temperatures close to 0 degree, and thus, thermally unstable (Sharkhuu, 2003). Batimaa et al., 2011estimated Mongolian permafrost areas using two global climate models (GCMs) to decrease 50% by 2020 compared to the current situation, 53-70% by 2050 and 77-94% by 2080.

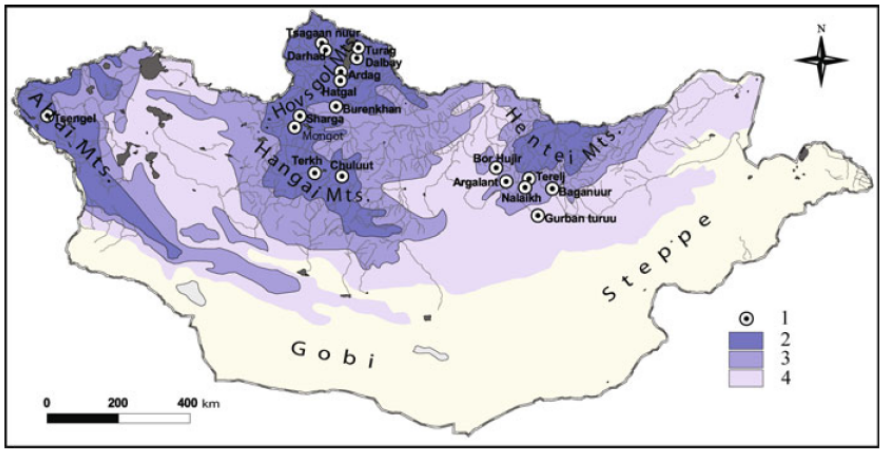

Figure 1.2. Map of permafrost in Mongolia (source: Sharkhuu, 2003). 1) Permafrost monitoring site, 2) Continuous and discontinuous permafrost, 3) Islands permafrost and 4) Sporadic permafrost

Chapter 2

A surface model for water and energy balance in cold regions accounting for vapor diffusion

2.1. Introduction

This work is motivated by the assessment of water resources in the Upper Tuul River basin, around Ulaanbaatar (Mongolia) and, in general, by subarctic continental climate regions, characterized by very low temperatures, low rainfall and, yet, sizable runoff. This causes such regions to fall very low in the Budyko curve (see, e.g., Figure 3b of Hanasaki et al., 2007). That is, total runoff is much larger than what would be expected in terms of potential evapotranspiration and rainfall.

We conjecture that increased runoff may be caused by condensation (deposition) of air moisture. Condensation and freezing may be especially significant during the spring when air temperature and moisture increase, which drives water vapor to the cold soil. This mechanism was proposed by Shvetzov (1978) and it is also mentioned by Gusev and Nanosova (2002), but has not been analyzed in detail. Since moisture condensation data are not available in such regions, and phase changes are driven by energy availability, water and energy balances are required.

Water and energy balances are the basic building blocks for any hydrological model and specifically of land surface schemes (also called large area hydrological models) linking meteorological data with runoff, and thus water availability. Hydrological modeling in cold regions has been largely motivated by climate change (Nicolsky et al., 2007) because of the fear that permafrost melting may release large amounts of methane to the atmosphere, thus accelerating global warming (Anisimov, 2007). Efforts have also been devoted to the construction of land surface schemes to be coupled to atmospheric circulation models (Ek et al., 2003), which cover the whole Earth. However, these tend to be simple to facilitate coupling to atmospheric processes, so that they may not account for all processes taking place at the soil surface. Detailed models are possible, but complex (e.g., Sapriza-Azuri et al., 2015; Bao et al., 2016). Yet, proper understanding of the hydrological cycle and water and energy fluxes in boreal regions is important not only for climate change but also for water management (Dandar et al., 2016).

Classical hydrological model codes, such as WatBal (Yates, 1996) and SWAT (e.g., Arnold et al., 1998; Hülsmann et al., 2015) calculate the basic terms of a river basin water balance, such as stored soil water, evapotranspiration and surface runoff. In its original form, SWAT calculates snowmelt by means of a water balance of the snow cover and a so called temperature-index method that estimates the snow cover temperature from previous ones and air temperature. Some later versions of SWAT use energy balances of the snow cover instead of the temperature-index method (e.g., Fuka et al., 2012). Both methods have been compared thoroughly (Debele et al., 2010; Verdhen et al., 2014). Only recently SWAT has been extended by considering energy balances in the soil as well (Qi et al., 2016). Unfortunately, this only considers conduction as a mechanism for heat transport in the soil. For our purposes we need to take into account vapor diffusion flux in both the water and the energy balance of the soil.

The aim of this work is, first, to understand the hydrological processes and to evaluate water resources in cold and semi-arid regions and, second, to assess the importance of vapor diffusion. We do this by developing a hydrological scheme that accounts for the processes that are relevant for subarctic climates, including the effect of slope on radiation, which should be relevant for high latitudes, water phase changes and soil vapor diffusion.

2.2. Methodology

2.2.1. Model description

Water and energy balances in land surface hydrological models are typically expressed on one layer that extends to root depth, where plants can extract water. However, since we are interested in water and energy dynamics including seasonal fluctuations, we formulate the balances over two layers (see Figure 2.1). The surface layer extends some 16 cm, so as to accommodate the roots of typical grass in the Tuul basin and to dampen daily temperature fluctuations. The subsoil (with length L_{ss}) layer accommodates the "active" layer that freezes and thaws seasonally. The input and output terms for the water balance of the surface layer include precipitation (as rain or snow), evapotranspiration (including both ice deposition and sublimation), infiltration into the subsoil and vapor diffusion to or into the subsoil. Those for the subsoil are infiltration, vapor diffusion from the surface and recharge to the aquifer. The energy balance considers solar radiation, latent and sensible heat fluxes, heat conduction between the two layers and energy released due to phase changes. The model also takes into account the slope of the surface. The above fluxes can be written as a function of meteorological data and two state variables: mass of water (kg m^{-2}) and energy (J m^{-2}). Details of each mass balance term are given below.

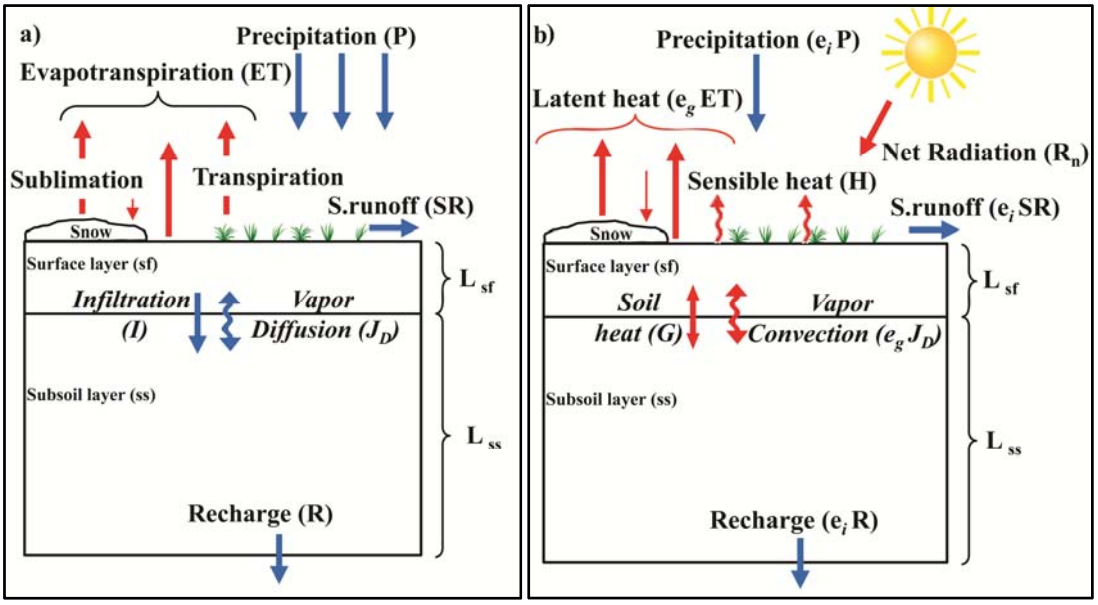

Figure 2.1. Schematic diagram of the water balance (a) and energy balance (b) models

2.2.2. Water balance

The water balance for the surface and the subsoil layers can be formulated as:

$$\frac{\partial m_{sf}}{\partial t} = P - ET_{sf} - I - SR - J_D \tag{2.1}$$

$$\frac{\partial m_{ss}}{\partial t} = I - ET_{ss} - R + J_D \tag{2.2}$$

where subscripts "sf" and "ss" refer to surface and subsoil layers, respectively, m is the mass of water (liquid or ice) (kgm^{-2}), and fluxes (all in kg m^{-2} s^{-1}) include precipitation (P), evapotranspiration (ET), infiltration (I, positive downwards), surface runoff (SR), vapor diffusion (J_D, positive downwards), and recharge (R).

Evapotranspiration is commonly used to describe both evaporation and transpiration (Brutsaert, 1982), including sublimation, the conversion of solid water directly to vapor (Zhang et al., 2004). ET is usually the most important term for returning energy to the atmosphere. Traditional methods for estimating evapotranspiration can be divided be into those that use temperature (Hargreaves and Samani, 1985), radiation (Priestley and Taylor, 1972) and an aerodynamic approach (McMahon et al., 2013 and Katul et al., 1992). We

chose the latter, because in dry climates ET is controlled by water availability rather than incoming radiation. The aerodynamic method is based on Dalton law, which establishes that ET is proportional to the difference of vapor pressures between air and soil. It is the basis of the method of Penman (1948) and has been used to estimate evaporation from water surfaces (Rosenberg et al., 1983; Xu and Singh, 2002), or bare soil (Ripple et al., 1970) and evapotranspiration from vegetated surfaces (Blad and Rosenberg, 1976). We assume that one part of the water evaporates from the soil surface controlled by an aerodynamic resistance and another part evaporates through plant transpiration controlled by both aerodynamic and stomata resistance. Moreover, we distinguish between plant transpiration from the soil surface and the subsoil. We express ET from soil surface and subsoil as:

$$ET_{sf} = \frac{M}{RT_{air}}\left[\frac{1}{r_a + r_s}\alpha\beta + \frac{1}{r_a}(1-\beta)\right] f_{sf}\left[p_{v.sf} - p_{v.air}\right] \quad (2.3)$$

$$ET_{ss} = \frac{M}{RT_{air}}\ [\frac{1}{r_a + r_s}(1-\alpha)\beta] f_{ss}[p_{v.ss} - p_{v.air}] \quad (2.4)$$

where M is the molar mass of water (0.018 kg mol^{-1}), R is the gas constant (8.314 J mol^{-1} K^{-1}), T_{air} is the air temperature (K), r_a and r_s are the aerodynamic and stomata resistances, respectively (s m^{-1}), α is the fraction of total transpiration from the surface layer and β is the fraction of vegetation cover. When the soil is frozen, no transpirations is assumed and α and β are given a zero value. Factor, f, represents the reduction of evaporation due to the lack of water in the surface and subsoil layers (see below), $p_{v.sf}$ and $p_{v.ss}$ are the saturated vapor pressures (Pa) at the surface and subsoil layers and $p_{v.air}$ is the actual vapor pressure in the atmosphere (Pa). The actual vapor pressure can be calculated from the relative humidity and saturated vapor pressure ($p_{v.sat}$), which we computed with Murray's (1967) equation as a function of temperature.

The aerodynamic resistance, r_a, describes the resistance from the vegetation upward and involves friction from air flowing over vegetative surfaces whereas the stomata surface resistance, r_s, describes the resistance of vapor flow through stomata, total leaf area and evaporating soil surface (Shuttleworth, 1979). A general form for the aerodynamic resistance to evapotranspiration (or sublimation) and sensible heat is (Evett et al., 2011):

$$r_a = \frac{1}{k^2 u_z}\left[\ln\left(\frac{z}{z_0}\right)\right]^2 \tag{2.5}$$

where z is height at which wind speed, temperature and relative humidity are measured (m), z_0 is the roughness length (m), k is von Karman's constant (k = 0.4) and u_z is the wind speed (m s^{-1}). The roughness length can vary over five orders of magnitude (from 10^{-5} m for very smooth water surfaces to several meters for forests and urban areas) and increases gradually with increasing height of roughness elements (Arya, 2001). The stomata surface resistance can be calculated by (Allen et al., 1998):

$$r_s = \frac{r_l}{0.5\ LAI} \tag{2.6}$$

where r_l is the bulk stomata resistance of a well-illuminated leaf (s m^{-1}). Monteith and Unsworth (1990) suggest that r_l=100 s m^{-1} for grassland. LAI is the leaf area index (leaf area per unit soil surface area).

Factor, f, in equations (2.3) and (2.4) expresses the decreases of ET with water content in the surface and subsoil layers, according to:

$$f_{sf/ss} = \begin{cases} 1 & \text{if } m_{sf/ss} > m_{sf/ss}^{fc} \\ \dfrac{m_{sf/ss} - m_{sf/ss}^{wp}}{m_{sf/ss}^{fc} - m_{sf/ss}^{wp}} & \text{if } m_{sf/ss} < m_{sf/ss}^{fc} \\ 0 & \text{otherwise} \end{cases} \tag{2.7}$$

where superscripts fc and wp refer to field capacity and wilting point, respectively.

For the calculation of infiltration (I) we assume that it is limited by a maximum infiltration capacity, which only liquid water exceeding the field capacity can infiltrate. Then, for a time step Δt the infiltration can be formulated as:

$$I^{k+1} = \max\left(0, \left[\min\left(\left(\frac{m_{sf}^{k+1} - m_{sf}^{wp}}{\Delta t} + P - ET_{sf} - J_D\right), I_{max},\ m_{sf,l}\right)\right]\right) \tag{2.8}$$

where m_{sf}^{k+1} is the mass of water in the surface layer at a present time step and $m_{sf,l}$ is the liquid mass of water in the surface layer (kg m^{-2}). The maximum infiltration (I_{max}) equals the saturated hydraulic conductivity (K_{sat}).

In a similar way we calculate surface runoff (SR) by assuming that only water exceeding the maximum water content in the surface layer (m_{sf}^{ϕ}) can runoff, where m_{sf}^{ϕ} (kg m^{-2}) equals the porosity (ϕ) multiplied by water density and length of the soil surface (L_{sf}). For the calculation of recharge (R) we assume that only liquid water exceeding the field capacity in the subsoil layer can percolate to the aquifer.

Vapor diffusion using Fick's Law, is written as:

$$J_D = \frac{M}{RT_{sf}} \frac{D}{L_{sf}} \frac{m_{sf}^{\phi} - m_{sf}}{m_{sf}^{\phi}} [p_{v.sf} - p_{v.ss}] \quad (2.9)$$

where D is the diffusion coefficient (m^2 s^{-1}), T_{sf} is the temperature of the surface layer (K), L_{sf} is the surface layer's length (m). Note that we use L_{sf} as length between the two layers rather than$(L_{sf} + L_{ss})/2$ because temperature gradients, which control vapor pressure, are expected to be largest near the soil surface. The value to be adopted for the diffusion coefficient deserves some discussion. The diffusion coefficient of water vapor in air is $0.3 \cdot 10^{-4}$ m^2 s^{-1} (Cussler, 1997). This value should be reduced due to reduced open area and tortuosity in a porous medium. However, for reasons that are subject to debate (Ho and Webb, 2006), vapor diffusion is enhanced (Cass et al., 1984). Gran et al., (2011) required using values above $2 \cdot 10^{-4}$ m^2 s^{-1}. Given these uncertainties we have adopted 10^{-4} m^2 s^{-1} as base value, and then analyzed the sensitivity of the model to this parameter.

2.2.3. Energy balance

Energy balance for the two layers is written as:

$$\frac{\partial U_{sf}}{\partial t} = e_{i/l} P - e_g ET_{sf} - (e_g - e_l) ET_{ss} - e_l I - e_l SR + R_n - H - G - e_g J_D \quad (2.10)$$

$$\frac{\partial U_{ss}}{\partial t} = e_l I - e_l ET_{ss} - e_l R + G + e_g J_D \quad (2.11)$$

where U is the total energy of each layer (J m^{-2}), R_n is the net radiation (J m^{-2} s^{-1}), H is the sensible heat flux (J m^{-2} s^{-1}) and G is the heat conduction (J m^{-2} s^{-1}) between surface and subsoil. Advective heat fluxes include the fluxes of water, ice (snow) or vapor (P, ET, SR, I, J, R) multiplied by the corresponding internal energies of liquid water, ice or vapor (e_l,

e_i, e_g (J kg^{-1})), which are linear functions of temperature (minus the fusion latent heat for ice or the vaporization latent heat for vapor). Although a distinction is made between evapotranspiration from the surface and the subsoil (ET_{sf} and ET_{ss}), equations (2.10) and (11) assume that the heat loss occurs only at the surface because the actual phase change takes place in the plant, which is part of the surface layer.

The total energy (U) is a sum of energy for liquid water, ice and solid (Figure 2.2):

$$U = me = m_l e_l + m_i e_i + m_s e_s \qquad (2.12)$$

where subscript s presents the solid part of the soil layers. During melting or freezing, the temperature is fixed at the melting temperature of 0°C while at higher temperature all water is liquid ($m = m_l$) and at lower temperature all water is ice ($m = m_i$). Therefore, we can calculate the temperature and mass of ice and water as a function of U and m as:

$$T = \frac{U + m\Lambda_{melt}}{mc_i + m_s c_s} \quad \text{and} \quad m = m_i \quad \text{if} \quad -m\Lambda_{melt} > U \qquad (2.13)$$

$$T = 0 \quad \text{and} \quad m_i = -\frac{U}{\Lambda_{melt}};\ m_l = m - m_i \quad \text{if} \quad -m\Lambda_{melt} < U < 0 \qquad (2.14)$$

$$T = \frac{U}{mc_l + m_s c_s} \quad \text{and} \quad m = m_l \quad \text{if} \quad U > 0 \qquad (2.15)$$

where Λ_{melt} is the melting heat ($3.34 \cdot 10^5$ J kg^{-1}), c_l is specific heat of water (4184 J kg^{-1} °C^{-1}), c_i is specific heat of ice (2092 J kg^{-1} °C^{-1}) and c_s is specific heat of soil (843 J kg^{-1} °C^{-1}). Equations (2.13) to (2.14) are also illustrated by Figure 2.2.

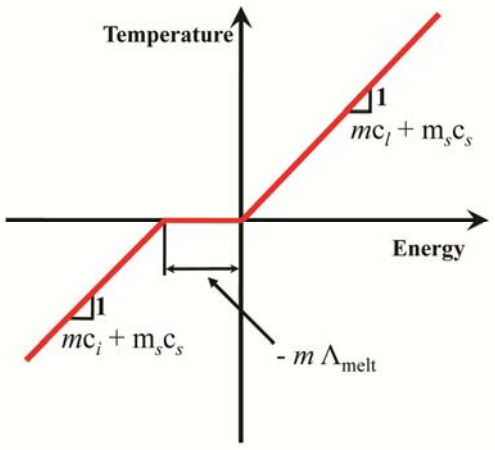

Figure 2.2. Temperature versus total energy

Radiation

Radiation is the main energy input for land surface models. Hence, it is not surprising that it has received a lot of attention. We follow a somewhat modified version of the approaches of Tian el al., (2001) and Allen et al., (2006) and divide radiation between shortwave, received from the sun, and longwave radiation, emitted by the Earth and the atmosphere. Net radiation (R_n) is the sum of the net shortwave radiation (R_{ns}) and the net longwave radiation (R_{nl}):

$$R_n = R_{ns} + R_{nl} = (1 - A)R_S + R_{L.up} + R_{L.down} \qquad (2.16)$$

where A is the albedo, fraction of solar radiation (R_S) that is reflected by the surface. The albedo depends on surface types (small for vegetated surface and high values for snow).The net longwave radiation is equal to the received (downward, $R_{L.down}$) minus the emitted ($R_{L.up}$) radiation.

Solar radiation on a horizontal and on an inclined surface

The solar radiation on a horizontal surface ($R_{S,hor}$) is measured or can be calculated from the atmospheric transmissivity (τ_a), which is the fraction of extraterrestrial solar radiation (easy to compute, see Appendix) that makes it to the land surface. Atmospheric transmissivities highly sensitive to cloudiness and moisture content. It can be estimated from the relative sunshine hours (Allen et al., 1998) or through the method of Hargreaves and Allen (2003):

$$\tau_a = K_H \sqrt{T_{air}^{max} - T_{air}^{min}} \qquad (2.17)$$

where T_{air}^{max} and T_{air}^{min} are the daily maximum and minimum air temperature and K_H is an empirical constant. Allen et al., (1998) recommends K_H = 0.16 for interior and K_H = 0.19 for coastal regions.

Shortwave radiation may reach the land surface directly from the sun, reflected by the surrounding or scattered by the atmosphere (diffuse solar radiation). The distinction is

relevant for inclined surfaces in the shade, which only receive reflected and diffuse solar radiation. Numerous relations can be found in the literature (Noorian et al., 2008) to estimate the fraction of diffuse radiation over the total solar radiation (f_{dif}). We adopted the one of Boland et al., (2008), which is simple and statistically sound:

$$f_{dif} = \frac{1}{1 + \exp\left(8.6\tau_a - 5\right)} \tag{2.18}$$

Solar radiation on an inclined surface can be calculated from the solar radiation on a horizontal surface by means of the following expression (e.g., Tian et al., 2001):

$$R_S = R_{S,hor}\left[\left(1 - f_{dif}\right)\frac{\max(\mathbf{p}^T\mathbf{s}, 0)}{s_{up}} + f_{dif}f_{sv} + A(1 - f_{sv})\right] \tag{2.19}$$

where f_{sv} is the sky view factor (see equation A14 in the Appendix). The first term represents the direct solar radiation, the second term the diffuse radiation and the third term the solar radiation reflected from the surroundings. Definitions of $\mathbf{p}^T\mathbf{s}$ and s_{up} are shown in the Appendix (equations A1 and A2). To perform daily energy balances, we calculate the daily averaged solar radiation on an inclined surface, assuming the atmospheric transmissivity (τ_a) to be constant during the day, as follows:

$$R_S = \left[\left(1 - f_{dif}\right)\frac{\int_{-\omega_{ss}}^{\omega_{ss}} \max(\mathbf{p}^T\mathbf{s}, 0)\,dt}{\int_{-\omega_{ss}}^{\omega_{ss}} s_{up}\,dt} + f_{dif}f_{sv} + A(1 - f_{sv})\right] R_{S,hor} \tag{2.20}$$

where ω_{ss} is the sunset angle, the integrals of s_{up} and $\max(\mathbf{p}^T\mathbf{s}, 0)$ are given by equations A6 and A13 of the Appendix.

Longwave radiation

Longwave radiation appears simple, but actual parameterization is hard (Herrero and Polo, 2014; Zabel et al., 2012). Upward longwave radiation is calculated from Stefan-Boltzmann law:

$$R_{L.up} = -\varepsilon_s \sigma T_{sf}^4 \tag{2.21}$$

where ε_s is the surface emissivity, σ is the Stefan-Boltzmann constant ($5.7 \cdot 10^{-8}$ J s^{-1} m^{-2} K^{-4}) and T_{sf} is the surface temperature (K). The soil surface emissivity is usually close to 1 (Saito and Šimůnek, 2009). However, small changes in ε_s may cause an imbalance between upwards and downwards longwave radiation balance, thus having a large effect on net radiation. We adopted a constant value of 0.94, but also tested 0.99 for sensitivity analysis purposes.

The Earth's surface also receives longwave radiation emitted by the atmosphere and surrounding surfaces. It can be calculated from the same law:

$$R_{L.down} = f_{sv}\varepsilon_a \sigma T_{air}^4 - (1 - f_{sv})R_{L.up} \quad (2.22)$$

where ε_a is the emissivity of the atmosphere and T_{air} the absolute temperature of the atmosphere. Note that a fraction equal to the sky view factor (f_{sv}) originates from the atmosphere and another part ($1-f_{sv}$) from the surroundings.

Clear sky emissivity is obtained from the empirical expression of Brutsaert (1975):

$$\varepsilon_{air.cs} = 1.24\left(\frac{p_{v.air}}{T_{air}}\right)^{1/7} \quad (2.23)$$

The cloudy sky emissivity (ε_a) is obtained from $\varepsilon_{air.cs}$ using the expression that Sicart et al., (2006) derived empirically for a subarctic continental climate in Yukon (Canada):

$$\varepsilon_a = \varepsilon_{air.cs}(1 + 0.44h_r - 0.18\tau_a) \quad (2.24)$$

where h_r is relative humidity.

Sensible heat

The sensible heat flux is calculated using the aerodynamic resistance (r_a) and soil surface resistance (r_{sf}):

$$H = \frac{\rho_a c_a}{r_a + r_{sf}}(T_{sf} - T_{air}) \quad (2.25)$$

where ρ_a is the air density (1.22 kg m^{-3}) and c_a is the specific heat of air (1013 J kg^{-1} K^{-1}). The soil surface resistance, r_{sf}, is calculated from the thermal conductivity of the soil:

$$r_{sf} = \frac{0.5 L_{sf} \rho_a c_a}{\lambda_s} \tag{2.26}$$

where λ_s is the thermal conductivity of soil.

Heat conduction

Heat conduction of soil can be calculated from Fourier's Law as:

$$G = \frac{\lambda}{(0.5\ L_{sf} + 0.5\ L_{ss})}(T_{sf} - T_{ss}) \tag{2.27}$$

where λ is a representative soil thermal conductivity ($\lambda = \lambda_l^{\phi}\lambda_s^{1-\phi}$), where ϕ is the porosity and λ_l, is the thermal conductivity of ice, λ_i, when water is frozen or that of liquid water, λ_l, otherwise (Côté and Konrad, 2005).

2.2.4. Numerical solution and implementation

We solve the water and energy balance equations (Eqs. (2.1), (2.2), (2.10) and (2.11), respectively) using a semi-implicit finite differences scheme with a time step of one day. The term semi-implicit means that all variables are treated explicitly (i.e., using the values from the previous day), with two exceptions to ensure stability. First, vapor pressures in equations (2.3), (2.4) and (2.9) are linearized and treated implicitly (that is, $p_{v.sf}^{k+1} - p_{v.air} = (T_{sf}^{k+1} - T_{air})\Delta + (1 - h_r)p_{v.sat}$, where Δ is the slope of the saturation vapor pressure curve (Pa $°C^{-1}$)). This type of linearization is frequent (e.g., Penman, 1948) because vapor pressure is highly sensitive to temperature and treating it explicitly may cause instability. Second, we perform a preliminary water balance to approximate the water available for evaporation, this is followed by the energy balance which yields not only energy and temperature, but also actual evaporation, that is used for the final water balance.

The algorithm was implemented in a spreadsheet that is available for the cases discussed below at http://h2ogeo.upc.edu/es/investigacion-hidrologia-subterrania/software.

2.2.5. Data of meteorological stations and parameters

The model was tested using meteorological data from 2000 through 2004 of the Terelj station (elevation 1540 m, 47.98N, 107.45E), located in northern Mongolia some 40 km east of Ulaanbaatar. This station records daily meteorological data (maximum and minimum T, precipitation, snow depth, wind and relative humidity) provided by the Institute of Meteorology and Hydrology of Mongolia. The area is mountainous with grassland and forest of Larix and Pinus. Forests dominate the north face of mountains while grassland dominates the south face of mountains and flat areas (Dulamsuren et al., 2008; Ishikawa et al., 2005). The region contains discontinuous and sparsely insular permafrost (Gravis et al., 1972; Sharkhuu, 2003; Jambaljav et al., 2008).

The average daily maximum and minimum air temperature is 5.06°C and -11.5°C, respectively. Mean air temperature averaged -3.2°C for the studied period. Annual precipitation averaged 334 mm/year, with 80% falling between June and September. Snow usually falls between mid-October and mid-April, with a maximum thickness of 31 cm. The average wind speed is 1.5 m/s and average relative humidity 70.12%.

We used parameters from the literature (Table 2.1) to define a base model that assumes that the surface is horizontal and covered by grass. Jambaljav et al., (2008) noted that the north and south facing slopes of mountains in the Terelj area are about 10-40°.Therefore, for the sensitivity analysis, we take into account both the north and south face with a slope of 20 degrees. Tuvshinjargal et al., (2004) used an albedo of 0.21 for grass meadow to calculate the surface energy balance. There are no other data for albedo from this area, especially snow albedo. The albedo (A) was taken from Oke (1987) as 0.6 during periods with snow cover and 0.23 for grass and soil surface. Most surfaces have emissivities larger than 0.9 (Arya, 2001). So, we used ε_s=0.94 for the base model. We assumed that all the roots of grass are in the surface layer (L_{sf}) which means the evapotranspiration only occurs from the surface layer. Thus, we used α equal to 1.

The surface roughness length (z_0) is defined by surface types such as soil, vegetation and snow. We used z_0=0.04 for grass and z_0=0.002 for snow surface (see figure 10.5 of Arya, 2001). The leaf area index (LAI) is defined by vegetation types. Asner et al., (2003) give LAI of 2.1 $m^2 m^{-2}$ for grass. According to the National Soil Atlas of Mongolia (1981), the soil of the study area belongs to the Gleysols-umbrisol and Cryosols-leptic type. The soil texture is mainly a silt-clay-loam. The wilting point (θ^{wp}), field capacity (θ^{fc}), porosity (ϕ) and saturated hydraulic conductivity (K_{sat}) are 0.11, 0.342, 0.365 and $4.2 \cdot 10^{-7}$ m s^{-1}, respectively, and were obtained from Schroeder et al., (1994). Length of the surface layer (L_{sf}) and subsoil layer are of 0.16 m and 1.5 m, respectively. Thermal conductivities were obtained from Bristow (2002).

For the sensitivity runs we changed eight parameters: dip of the surface (θ), roughness length (z_0), soil emissivity (ε_s), saturated conductivity (K_{sat}), wilting point (θ^{wp}), vapor diffusion coefficient (D), surface length (L_{sf}) and subsoil length (L_{ss}).

Table 2.1. Parameter and values for Base model

Parameters	**Value**	**Units**	**Reference**
Slope (θ)	0	degree	
Latitude (φ)	48	degree	
Albedo (A)	0.23 for grass and soil 0.6 for snow	-	Oke, 1987
Soil emissivity (ε_s)	0.94	-	Arya, 2001
Fraction of transpiration (α)	1	-	
Vegetation cover (β)	0.6	-	
Leaf area index (LAI)	2.1 for grass	$m^2 m^{-2}$	Asner et al., 2003
Surface roughness length (z_0)	0.04 for grass 0.002 for snow	m	Arya, 2001
Diffusion coefficient (D)	10^{-4}	$m^2 s^{-1}$	
Field capacity (θ^{fc})	0.342	$m^3 m^{-3}$	Schroeder et al., 1994
Wilting point (θ^{wp})	0.11	$m^3 m^{-3}$	Schroeder et al., 1994
Porosity (ϕ)	0.365	-	Schroeder et al., 1994

Saturated hydraulic conductivity (K_{sat})	$4.2 \cdot 10^{-7}$	m s^{-1}	Schroeder et al., 1994
Surface depth (L_{sf})	0.16	m	
Subsoil depth (L_{ss})	1.5	m	
Thermal conductivity (λ)	2.9 for soil 0.57 for water 2.2 for ice	J $s^{-1}m^{-1}K^{-1}$	Bristow (2002)

2.3. Results

Results are summarized in Figure 2.3, which displays the evolution of the water fluxes (precipitation, evapotranspiration, recharge, surface runoff and vapor diffusion), water contents, heat fluxes (net radiation, latent heat, sensible heat, vapor convection and heat conduction) and temperature (air, surface and subsoil) of the base model during the last two years. Table 2.2 and 2.3 summarize the balances averaged over the 5 years for the base model and for the sensitivity.

Direct surface runoff is very small. Figure 2.3.b only shows some surface runoff at the beginning of April 2003 during snowmelt. No surface runoff occurred during the snowmelt of 2004 probably because the accumulated snow on the surface was small that year. The sensitivity analysis suggests that the limiting factor is the infiltration capacity. When saturated hydraulic conductivity is reduced by a factor of 10, direct surface runoff increases dramatically and infiltration reduces. The reduced infiltration also implies increased ET, so that the overall runoff (SR plus recharge) is also reduced. The small surface runoff is consistent with the lack of very intense rainfall events and with the absence of indications of surface erosion.

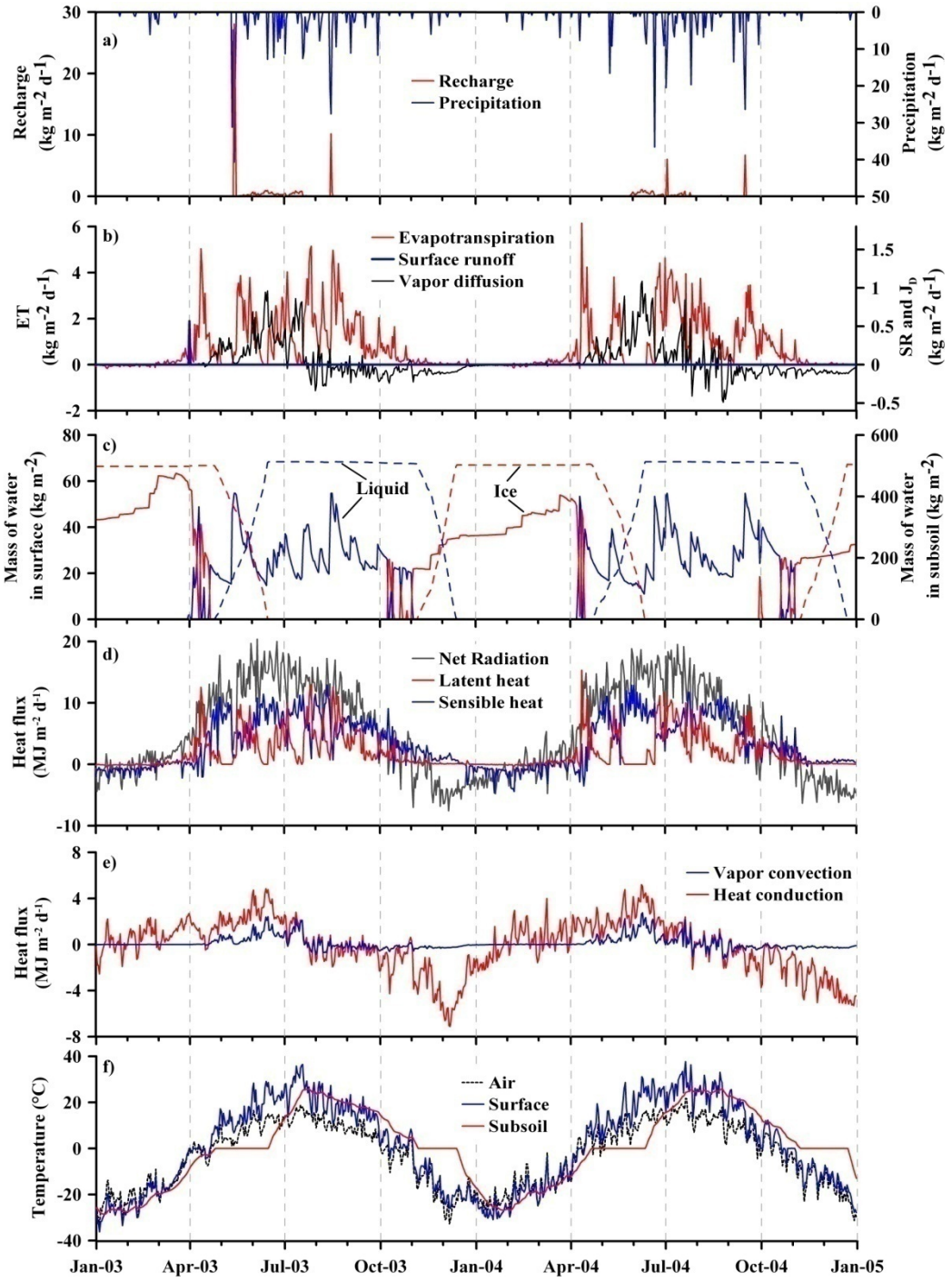

Figure 2.3. Daily evolution of (a) precipitation and recharge, (b) other water fluxes, (c) water content at surface (solid line) and subsoil (dashed line), (d, e) heat fluxes, and (f) temperatures of the base model

Infiltration and recharge are also relatively low. Infiltration occurs mainly after heavy rainfall events and it is not shown in figure 2.3 because similar pattern as recharge. Most

infiltration transforms into recharge because, in the absence of deep rooted plants, the subsoil is always close to field capacity. Recharge from rainfall infiltration can vary a lot from year to year, due to the irregular occurrence of heavy rainfall events. However, a significant amount of recharge occurs throughout the spring and summer driven by vapor diffusion into the subsoil. While the rate is small (it can hardly be seen in Figure 2.3.a, so we zoom it in Figure 2.4), it occurs throughout the late spring and summer, after the subsoil has started to thaw. Overall, it is about half of recharge from direct rainfall infiltration, but much more regular (it occurs every year) and quite robust, in that it displays little sensitivity to model results (See Table 2.2).

Vapor diffusion between the surface and subsoil layers is positive (downwards) during spring and early summer, because then the temperature and, therefore, vapor pressure is higher in the surface than in the subsoil. The flux fluctuates during late winter, when the subsoil has started to warm, so that vapor diffuses upwards during cold days and downwards during warm days. Diffusion is consistently upwards during autumn and winter, but the rate is very low because the saturated vapor pressure is low and changes little with temperature (that is, $dp_{v,sat}/dT$ is small) at low temperatures. Therefore, there is a net downward vapor flux. Its amount is not very large, but as mentioned above, it is what drives recharge during spring and early summer.

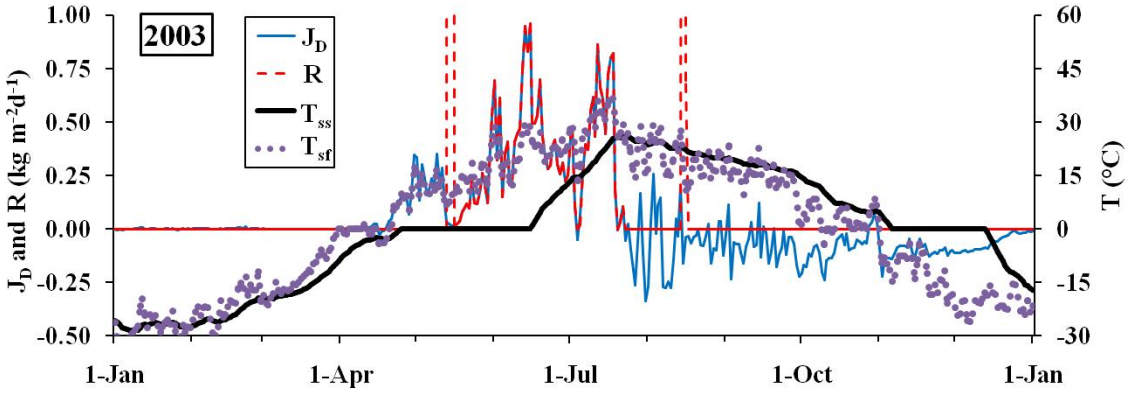

Figure 2.4. Zoom of recharge (red dashed line) and vapor diffusion (blue line) during 2003 (Temperatures are also shown). Note that, except for the two heavy rainfall events of May and August, recharge during the warming period (after the subsoil has started to thaw) is identical to the vapor diffusion flux.

Vapor diffusion is basically controlled by the diffusion coefficient (D), which is the only parameter that affects the vapor diffusion flux significantly (Table 2.2). Reducing D leads obviously to a reduction of vapor diffusion. A similar effect results from increasing the soil surface thickness, which results in an apparent reduction of the gradient. As less water is transported downwards, evapotranspiration increases and recharge decreases.

As expected, evapotranspiration is the main sink of water. In fact, it is limited by water availability during the warm season, being high only after rainfall events and during melting (Figure 2.3.b). The evapotranspiration is about 85% of rainfall (Table 2.2), which is similar to the results obtained by Ma et al., (2003) for the Selenge River basin, northern Mongolia. Note that the evapotranspiration is very small during winter because low temperatures hinder vaporization. In fact, it is negative (i.e., ice deposition) during January and February (Figure 2.5), when the soil is colder than the air. Sublimation only becomes relevant in March. Cumulative sublimation (some 29 kg m^{-2} $year^{-1}$ in 2003) is low compared to typical values of cold regions (see, e.g., Zhou et al., 2014), but large compared to winter rainfall.

The whole cycle is driven by radiation, which follows the usual seasonal patterns, high during late spring and early summer and low in winter, when net radiation may become negative, partly due to the high albedo of snow (Figure 2.3.d). The radiation balance is highly sensitive to orientation of the slope (Table 2.3). Obviously, the south face receives more radiation than the north face. But this is largely compensated by an increase in sensible heat flux. The sensible heat increases when latent heat decreases. That is, heat is returned to the atmosphere either as latent heat when water is available for evaporation, or as sensible heat when the soil is dry. According to the energy balance (Table 2.3), the sensible heat is higher than the latent heat flux, which reflects the dry climate of region. As a result the effect of slope and orientation is smaller than we had anticipated (Tables 2.2 and 2.3). The large increase in radiation of south facing slopes only results in a small increase in evaporation and latent heat because there is little water and a parallel reduction of infiltration and recharge decreases (Table 2.2).

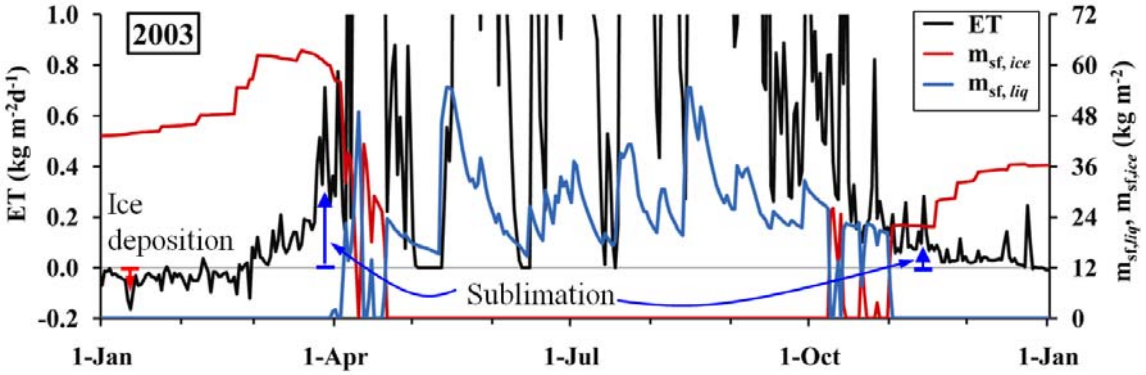

Figure 2.5. Zoom of ET (actually, water phase change processes) (black line) along with liquid (blue) and ice (red) water contents during 2003.

The dependence of the two balances on slope is non-monotonic, which points to the complexity of the system, even in the relatively simple model we are presenting here. Radiation is dramatically reduced in north facing slopes, which causes a reduction in ET, but the reduction is very small as discussed above, and not sufficient to cause an increase in infiltration. The reduction in ET is compensated by an increase in surface runoff and latent heat diffusion (vapor convection) downwards.

The non-monotonic dependence of vapor convectionon slope also illustrates the robustness of vapor diffusion. It is slightly larger in south facing slopes than in horizontal land because surface temperatures are also larger. But it is also slightly larger in north facing slopes than in horizontal land because subsoil temperatures are lower.

The limited availability of water causes most rainfall to evaporate. It also implies a low sensitivity of ET parameters to water and energy fluxes. For example, increasing roughness length (z_0) decreases the aerodynamic resistance (r_a), which leads to small increases in both latent and sensible heat fluxes and a parallel small decrease in infiltration and recharge. Similarly, increasing land surface emissivity from 0.94 to 0.99 reduces considerably net radiation as more longwave radiation is emitted, but is compensated by a decrease of sensible and, to a lesser extent, latent heat fluxes.

Table 2.2. Average in 5 years of water fluxes: evapotranspiration (ET), infiltration (I), surface runoff (SR), vapor diffusion (J_D) and Recharge (R). Precipitation is 334 kg m^{-2} $year^{-1}$)

Water Bal. [kg m^{-2} $year^{-1}$]	**ET**	**I**	**SR**	**J_D**	**R**
Base model	284.9	30.9	0.1	18.1	48.8
South face	290.8	23.8	0.0	19.5	43.3
North face	283.8	30.2	1.0	19.0	49.1
z_0 (x 2)	289.8	26.8	0.0	17.5	44.1
ε_s (0.94 → 0.99)	280.6	35.5	1.0	16.9	52.2
K_{sat} (x 0.1)	288.2	12.8	14.9	18.1	30.6
θ^{wp} (x 2)	252.9	66.0	2.1	13.1	79.1
D (x 0.25)	296.1	32.6	0.0	5.3	37.8
L_{sf} (x 2)	318.5	4.2	0.0	11.4	15.6
L_{ss} (1.5 → 2.15)	267.9	30.2	0.0	36.0	66.2

Table 2.3. Average in 5 years of energy fluxes: net radiation (Rn), latent heat (e_gET), sensible heat (H), heat conduction (G) and vapor convection ($e_g J_D$).

Water Bal. [kg m^{-2} $year^{-1}$]	**Rn**	**e_gET**	**H**	**G**	**$e_g J_D$**
Base model	2064.4	717.1	1345.6	-45.8	45.9
South face	2610.7	732.3	1876.8	-49.1	49.4
North face	1708.4	714.6	992.3	-48.0	48.1
z_0 (x 2)	2181.4	729.5	1450.5	-44.2	44.3
ε_s (0.94 → 0.99)	1739.1	706.4	1030.9	-42.9	42.9
K_{sat} (x 0.1)	2067.2	725.4	1340.1	-45.4	45.9
θ^{wp} (x 2)	2041.5	636.6	1402.1	-34.4	33.1
D (x 0.25)	2072.4	745.5	1325.8	-14.3	13.6
L_{sf} (x 2)	1980.5	801.8	1177.9	-28.6	29.0
L_{ss} (1.5 → 2.15)	2032.0	675.2	1355.5	-91.4	91.1

The most surprising energy balance terms are heat conduction (soil heat flux) and vapor convection (Figure 2.3.e). Conductive heat flux is usually considered seasonal, with yearly averages close to zero. Downward heat fluxes in summer are usually balanced by upward fluxes in winter (e.g. Alkhaier et al., 2012). In our case, even though the subsoil remains frozen for long (more than 7 months, compared to less than six the surface layer), there is a net flux upwards, to compensate the latent heat convection associated to vapor diffusion, which is downwards, as was discussed before. Therefore, it is not surprising that all factors that reduce the soil heat flux cause an increase in vapor convection, and vice versa.

The temperature oscillates more at the surface than at the subsoil layer (Figure 2.3.f). The differences of temperature of the layers are higher in summer. One can observe clearly the periods of melting and freezing of the subsoil layer with temperatures of 0°C. The annual average surface layer temperature was 0.8°C for 2003 and 2.0°C for 2004 while the air temperature was -3.6°C for 2003 and -2.4°C for 2004. For subsoil layer, -0.5°C and 0.7°C, in 2003 and in 2004 respectively.

An increase of the subsoil length (L_{ss}) leads to temperatures in the subsoil that oscillate less due to the increased heat storage capacity. This leads to larger temperature differences between surface and subsoil, which according to our model (equation 2.9, Figure 2.6) leads to larger vapor diffusion. As more water is transported downwards, evapotranspiration decreases and recharge increases.

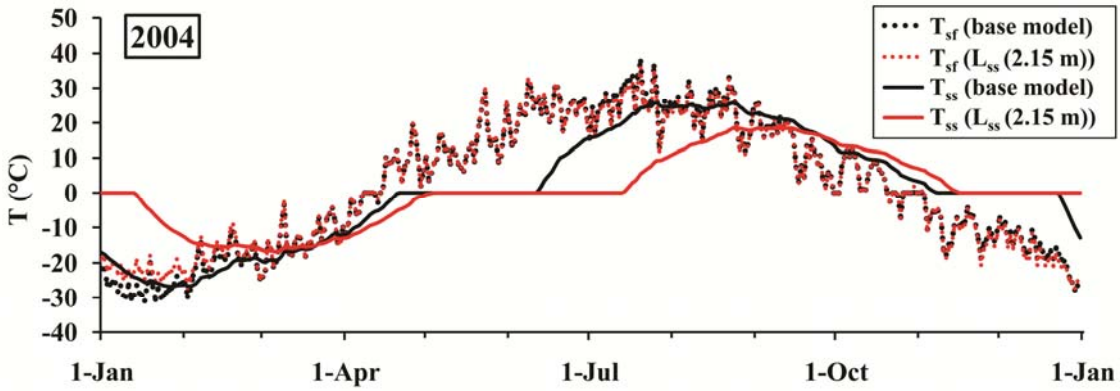

Figure 2.6. Daily evolution of surface and subsoil temperature in 2004.

2.4. Discussion and Conclusions

We have developed a water and energy balance model that contains two layers and attempts to represent all terms relevant for simulating land surface hydrological processes, including all possible phase changes and, singularly, vapor diffusion. The model has been applied using meteorological data from the Terelj station, northern Mongolia and typical soil properties of the region. Results are consistent with local observations by others:

- Direct surface runoff is negligible and restricted to snowmelt periods.
- Liquid infiltration and subsequent recharge are restricted to a few heavy rainfall events. However, a sizable recharge (about half of that from rainfall events) occurs continuously during late spring and early summer.
- Evapotranspiration is limited by water availability, as it accounts for 85% of rainfall. Sublimation is restricted to late fall and spring, but it is also large, compared to winter snowfall. Ice deposition occurs most days during January and February.
- Sensible heat is higher than latent heat flux, which reflects the dry climate of the region and low precipitation.
- The active layer remains frozen during the winter with periods of freezing or thawing of some three months, a length of time that increases when the thickness of the active layer increases.

In summary, results are qualitatively consistent with observations. Notably, total runoff would be too small, compared to observations, if vapor diffusion is reduced. The most singular result of the simulations is the relative importance of vapor diffusion, which is downwards during spring and early summer, when temperature and, therefore, vapor pressure are higher in the surface than in the subsoil. The upwards vapor diffusion flux is much smaller than the downward one, because vapor pressure is a non-linear function of temperature. This downward flux transforms into recharge, which is continuous, although fluctuating during that period.

In summary, the net downward vapor flux is relevant both in terms of water balance, accounting for a sizable portion of recharge, and energy balance, causing a net upwards

flux of heat. We conclude that land surface schemes should account for vapor diffusion. We notice that, being a diffusive process, it may be included in such schemes at a moderate effort. Still, further research is needed to ascertain the right values of diffusion coefficient to be used and the way of discretizing Fick's Law, that is, the choice of length over which diffusion takes place in equation (2.9).

Chapter 3

Water and energy balance in the Upper Tuul basin, Mongolia

3.1. Introduction

Water resources in the Upper Tuul basin (Figure 3.1) are stressed by an increasing water demand, mainly from the city of Ulaanbaatar within the basin. Groundwater is the primary source for water supply in this watershed (Hillel and Jadambaa, 2006; Emerton et al., 2009; Dolgorsuren et al., 2012). Therefore, the quantification of groundwater recharge becomes essential for water resources assessment.

The Upper Tuul basin is located in a mountainous area, characterized by semi-arid, subarctic conditions, which has important effects on recharge and makes traditional

empirical ratios to be of little value because they are largely based on regions with temperate climate. Permafrost is found at high altitudes, which hampers infiltration of water towards underlying aquifers. An “active layer” that freezes and thaws seasonally is found above the permafrost (Woo, 2012). Due to long term increase of temperature the depth of the active layer increases, which leads to higher permeability of the soil and affects hydrological processes (e.g., Ge et al., 2011). For the nearby Kharaa basin Hülsmann et al., (2015) concluded that melting of river icings and frozen subsurface is an important factor for a hydrological model. For the Upper Tuul basin, Zang et al., (2008) estimated the sublimation and concluded that almost all snowfall returns to the atmosphere. Chapter 2 found that vapor diffusion in the soil caused by the large vertical temperature differences may have a significant effect on recharge. The importance of freezing and thawing and vapor diffusion makes it clear that a proper assessment of hydrological processes requires assessing not only the water balance but also the energy balance. In addition, in a mountainous area south faces may behave differently from north faces. Soils are dryer and warmer with less permafrost due to the high direct solar radiation at south facing slopes than at north facing slopes. In fact, no permafrost is found at horizontal and south facing areas at low altitudes (Ishikawa et al., 2005 and 2006; Jambaljav et al., 2008; Minderlein and Menzel, 2015).

Numerous methods are available to estimate recharge (Lerner et al., 1990; Scanlon et al., 2002). But most of them require a lot of fieldwork and data, which are always scarce for most sub-arctic and arctic research (e.g., Ye et al., 2009; Karthe et al., 2015), including this study area. One way of estimating recharge with few data is through a physically-based soil water balance to calculate processes such as recharge, evapotranspiration and surface runoff. A number of such models were reviewed by Daniel et al., 2004 and Islam, 2011. They can be used as lumped or distributed according to the spatial description of the basin (Islam, 2011). Examples of these models include TOPMODEL (Beven et al., 1995), SLURP (Kite, 1995), WatBal (Yates, 1996), SWAT (Arnold et al., 1998) or BALAN (Samper et al., 2007). They can be evaluated at a point scale for different land class and then aggregated into sub basin scales. Few such models consider energy balances. The latest version of SWAT (Qi et al., 2016) does, but only considers conduction as a mechanism for heat transport in the soil and not the effect of vapor diffusion. Here, we use

the model of chapter 2, which includes vapor diffusion in both the water and energy balances, but is still sufficiently simple to grant application to basins with limited data.

Thus, the objective of this study are to: 1) evaluate the groundwater recharge in the Upper Tuul basin under freezing and thawing soil condition using water and energy balances, and 2) understand complex hydrological processes in cold regions for different landscapes (vegetation, soil, orientation and slope).

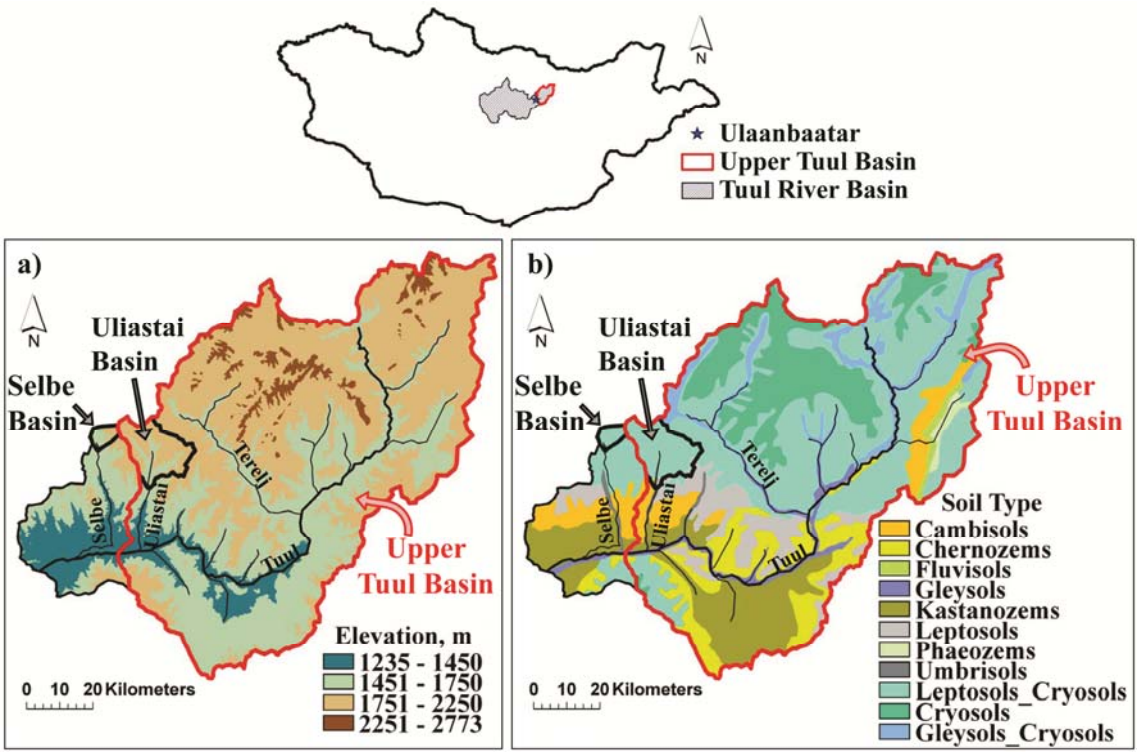

Figure 3.1. Location of the study area. Elevation map (a), Soil map (b).

3.2. Methodology

3.2.1. Study area

The Tuul River (Figure 3.1) flows at its head through mountainous taigas and forest steppesin the Khan Khentii Mountains. Downstream of Ulaanbaatar, it joins the Orkhon

River, which yields to the Baikal Lake. The total area of the basin is 49774 km^2 and total length of the Tuul River is 717 km (Dolgorsuren et al., 2012). The area is characterized by a semi-arid climate, with a hot summer and cold winter (Batima et al., 2007). The area is mountainous with grassland or pasture and forests of Larix and Pinus. Forests dominate the north facing slopes of mountains while grassland dominates the south facing slopes of mountains and the flat areas (Dulamsuren et al., 2008). The region contains discontinuous and sparsely insular permafrost according to the map of permafrost distribution of Mongolia (Gravis et al., 1972; Sharkhuu, 2003). The Tuul River surface is usually frozen from mid-November through end of April, but water still flows under the ice, at least in portions of the river, fed by groundwater discharge (Chapter 4). Small tributaries, such as the Selbe, Uliastai and others, are completely frozen in winter periods (Batima et al., 2004).

The study area comprises the Upper Tuul River basin, which covers some 6400 km^2, with elevations ranging from 1235 to 2773 m above mean sea level (masl) (Figure 3.1.a). The slope increases with elevation with maximum of about 58°. A soil map has been created by Mongolian and Russian researchers using aerophoto and satellite (National Soil Atlas of Mongolia, 1981). The majority of the area (58.8%) is covered by cryosols (including cryosols with leptic and cryosols with gleyic), 12.8% by kastanozems, 9.5% by chernozems,7.3% by leptosols, 6.4% by cambisols, 2.9% by gleysols, 0.7% by chernozems, 0.7% by phaeozems and 0.7% by umbrisols (Figure 3.1.b).

3.2.2. Available data

Daily meteorological data (maximum and minimum temperatures, precipitation, snow depth, wind and relative humidity) are collected by the Institute of Meteorology of Mongolia at two stations within the basin: Ulaanbaatar (elevation 1300 m, 47.90N, 106.92E) and Terelj (elevation 1540 m, 47.98N, 107.45E) stations (Figure 3.2). The Ulaanbaatar station is located in Ulaanbaatar city while Terelj station is situated approximately 40 km to the east.

For the Ulaanbaatar station, the mean air temperature between 1993 and 2013 is 0.6°C. The average annual precipitation for these years is 264 mm. The maximum snow thickness

is 17 cm. The average wind speed is 2 m s^{-1} and average relative humidity 60% for these periods.

For the Terelj station, the mean air temperature between 1993 and 2013 is -3.2°C. The area receives an average of 342 mm of annual precipitation for 21 years with 80% of the annual precipitation falling between June and September. Snow usually falls between mid-October and mid-April, with a maximum thickness of 31 cm. The average wind speed is 1.6 m s^{-1} and average relative humidity 69% for these periods.

It is worth pointing that global database of meteorological data (e.g., WATCH, Weeden et al., 2011) yield values similar to these two stations, which are located at low elevations and may not be representative of the whole basin.

The study area comprises the Selbe-Sanzai, the Uliastai and the Tuul-Ulaanbaatar (Figure 3.2), the three test basins of this study, where gauge stations are available.

The Upper Selbe River basin is located north of Ulaanbaatar between the latitudes 48.12 and 48.18 and the longitudes 106.85 and 106.97. There is no meteorological station within this basin, but the Selbe-Sanzai stationis 47 km away from the Terelj meteorological station and 23 km from the Ulaanbaatar station. It covers an area of 33.4 km^2 and a river length of some 3.6 km, with mean of some 1723 masl. The average river discharge is 0.12 m^3 s^{-1} (113 mm $year^{-1}$) from 1994 to 2013, with a maximum of 7.6 m^3 s^{-1} during one day in 2003.

The Uliastai River basin is located northeast of Ulaanbaatar between the latitudes 48.02 and 48.2 and longitudes 106.97 and 107.22. The Uliastai gauge station covers an area of 202.4 km^2, with a mean elevation of 1841 masl, and a river length of some 14 km. The 1994-2013 average river discharge is 0.49 m^3 s^{-1} (76 mm $year^{-1}$).

The Tuul-Ulaanbaatar station covers most of the Upper Tuul River basin, including a part of the city of Ulaanbaatar, an area of 6395.3 km^2, and a Tuul River length of some 150 km. The elevation ranges from 1290 to 2770 masl. The 1993-2013 average river discharge is 20.3 m^3 s^{-1} (100 mm $year^{-1}$) with a maximum of 721 m^3 s^{-1} during one day in 1993.

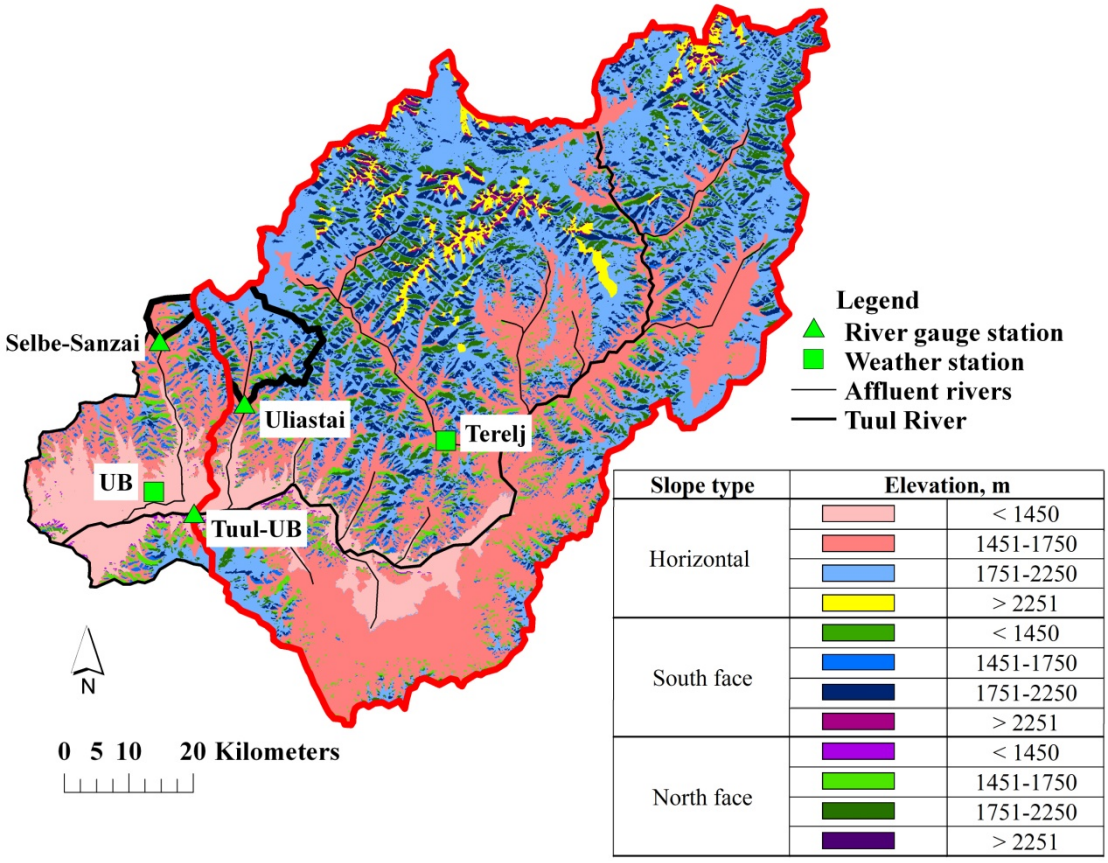

Figure 3.2. Upper Tuul River Basin, showing the location of gauge and whether stations, and the subdivision (color code) according to slope orientation and elevation, which correlate with soil type and vegetation.

3.2.3. Model description

We calculated the water and energy balances using the model of Chapter 2. The water balance accounts for precipitation (P), evapotranspiration (including sublimation), infiltration, surface runoff (SR), and recharge (R). In order to account for the role of freezing, the soil column is divided into a surface (containing vegetation and grass roots) and a subsoil layer. A singularity of this model is that it accounts for vapor diffusion, which is a very relevant water and energy transfer mechanism during late spring, when the soil surface layer is warm, but the subsoil is still melting (Chapter 2). The energy balance includes the advective heat fluxes associated to the above water fluxes, plus net radiation.

Given the relatively high latitude and mountainous nature of the basin, we accounted for slope and orientation in radiation calculations.

We divided the basin in 12 zones with more or less equal slope type (north face, south face, horizontal), altitude range, soil type and vegetation type (Figure 3.2 and Table 3.1). First, we divided the study area according to its slope. North and south face have slopes higher than 10°. Horizontal slopes also include east and west faces of whatever slope. Then, we further subdivided according to altitude range. We did not make further subdivisions according to soil and vegetation type. Instead, we assigned kastanozems (with umbrisols) and chernozems (with leptosols, cambisols and gleysols) to lower elevation zones and cryosols to higher elevation zones, as this more or less reflects the soil map (compare Figure 3.1.b). Forest is virtually restricted to north facing slopes, whereas the rest is covered by grass (Dulamsuren et al., 2008) as can be observed from satellite photos (e.g., Google Earth).

Table 3.1. Description of the 12 model zones

Strike (Slope)	**Altitude, m**	**Soil type**	**Vegetation type**	**Area, km^2**		
				Selbe	**Uliastai**	**Upper Tuul**
Horizontal (EF or WF or (SF or NF and θ<10°))	< 1450	Kastanozems	Grass	-	-	346.1
	1451-1750	Chernozems		17.3	41.3	2012.8
	1751-2250	Cryosols		10.7	105.9	2224.6
	>2250			-	-	180.1
SF and θ>10°	< 1450	Kastanozems		-	-	4.6
	1451-1750	Chernozems		1.1	6.2	178.2
	1751-2250	Cryosols		0.8	21.5	613.6
	>2250			-	-	60.2
NF and θ>10°	< 1450	Kastanozems		-	-	10.1
	1451-1750	Chernozems	Forest	1.8	5.6	189.6
	1751-2250	Cryosols		1.7	21.9	531.6
	>2250			-	-	43.8

θ-slope, SF-south face, NF-north face, WF-west face, EF-east face

We expect rainfall and other climate variables to vary significantly in space due to the complex terrain. Elevation is known to strongly influence atmospheric variables such as precipitation and air temperature. Numerous methods are available to interpolate and estimate atmospheric variables from elevation using graphical (Thiessen, 1911; Taesombat et al., 2009), topographical or linear regression (Houghton, 1979; Shea et al., 2004, Kattel et al., 2013) and geostatistical (Daly et al., 1994; Goovaerts, 2000; Dodson and Marks, 1997) methods. But we have only 2 meteorological stations (Figure 3.2), both located in lowlands, which probably represents a highly biased sample.

Therefore, we used meteorological data from the Ulaanbaatar station for zones with altitudes lower than 1450 m, and from the Terelj station for zones with altitudes between 1451 and 1750 m. When the elevation is higher than 1751 m, precipitation, maximum and minimum air temperature and relative humidity were calculated from the the Terelj station data, corrected for altitude by means of lapse rates (i.e., the change in variable with altitude). Linear regression analysis is the most common method for estimating temperature and precipitation lapse rates (Shea et al., 2004), but again, available data do not suffice to estimate lapse rates, so we relied on regional and literature values.

Precipitation usually increases with elevation (Goodale et al., 1998; Daly et al., 1994). The rate of increase depends on many factors, such as the amount of moisture in the air, distance from large water bodies (e.g., Lake Baikal) and wind direction (Johansson et al., 2003). Precipitation laps rate (Γ_{prec}) in mountain regions have been studied by Hanson et al., 1980, Osborn (1984) and Shea et al., 2004. Recently, Guo et al., (2016) found a precipitation laps rate for the Tibetan Plateau of between 63 and 261 mm km^{-1} year^{-1}, while Oyunbaatar (2001) found a lapse rate for the Selbe basin of about 150 – 250. We extrapolated these rates to daily precipitation using the following expression:

$$P_z = P_0 \left(\frac{P_{0,avg} + \Gamma_{prec}(z - z_0)}{P_{0,avg}} \right) \quad (3.1)$$

where P_z is the precipitation estimated at elevation z (km), P_0 is the observed daily precipitation recorded at the Terelj station (mm day^{-1}), $P_{0,avg}$ is itsyearly average (mm year^{-1}), $z_0$is the elevation of the Terelj station (km). We used a precipitation lapse, Γ_{prec}, of 200 mm km^{-1} year^{-1}.

On a global average, temperature decreases 6.5°C per km increase in altitude (Lutgens and Tarbuck, 1995), but varies with location and season. The relationship between air temperature and elevation has been investigated in many mountain regions (Fontaine et al., 2002; Shea et al., 2004; Blandford et al., 2008; Kattel et al., 2012). Based on these works, we estimated the elevation dependent daily air temperature as:

$$T_z = T_0 + \Gamma_{temp}(z - z_0) \quad (3.2)$$

where T_z is the air temperature at elevation z (km), T_0 is the observed air temperature recorded at Terelj station (°C) and Γ_{temp} is the air temperature lapse rate (°C km^{-1}), which we took as 6°C km^{-1}.

Relative humidity (RH), ratio between actual ($p_{v.air}$) and saturated ($p_{v.sat}$) vapor pressures, was calculated by assuming the actual vapor pressure on a given day does not change with altitude, unless the air becomes saturated. Therefore, the relative humidity can be expressed as:

$$RH_z = \min\left(100\%, \frac{RH_0 p_{v.sat}(T_0)}{p_{v.sat}(T_z)}\right) \quad (3.3)$$

where RH_z is the relative humidity at elevation z and RH_0 is the relative humidity recorded at the Terelj station (%).

The remaining model parameters are shown in Table 3.2. Some parameters depend on slope and soil type. Soil parameters such as wilting point, field capacity, porosity and saturated hydraulic conductivity are obtained from Schroeder et al., (1994) and from Batkhishig and Idirjavkhlan (2009). The soil texture is loam for kastanozem (with umbrisols), silt-clay-loam for Chernozems (with leptosols, cambisols and gleysols) and sandy clay for Cryosols.

Parameters related to evapotranspiration from soil surface and subsoil layers depend on vegetation type. For instance, we adopted a value of 0.8 for the fraction of total transpiration from the surface layer in forest zones, but 1.0 in grass zones, to reflect that forest roots are deeper than grassroots. Thus, transpiration in forests can also take place from the subsoil layer. Forests usually receives lightly larger net shortwave radiation because their albedo (A) is lower (Oke, 1987) than for grass. Asner et al., (2003) presented a database of leaf area indices (LAI), collected from the biomasses of 15 countries, and

gave an average LAI for boreal evergreen needle leaf of 3.1 m^2 m^{-2}. The surface roughness length (z_0) is obtained from Arya (2001).

Table 3.2. Parameters and values

Parameters	Value		Units	Reference
Slope (θ)	0 20 20	for horizontal for North face for South face	degree	
Latitude (φ)	48		degree	
Albedo (A)	0.1 0.23 0.6	for forest for grass for snow	-	Oke, 1987
Soil emissivity (ε_s)	0.94		-	Arya, 2001
Fraction of transpiration from surface layer (α)	0.8 1.0	for forest for grass	-	
Leaf area index (LAI)	3.1 2.1	for forest for grass	m^2 m^{-2}	Asner et al., 2003
Surface roughness length (z_0)	0.8 0.04 0.002	for forest for grass for snow	m	Arya, 2001
Diffusion coefficient (D)	10^{-4}		m^2 s^{-1}	
Field capacity (θ^{fc})	0.307 0.374 0.190	for Kastanozems for Chernozems for Cryosols	m^3 m^{-3}	Schroeder et al., 1994; Batkhisihig and Iderjavkhlan, 2009
Wilting point (θ^{wp})	0.180 0.168 0.050	for Kastanozems for Chernozems for Cryosols	m^3 m^{-3}	Schroeder et al., 1994; Batkhisihig and Iderjavkhlan, 2009
Porosity (ϕ)	0.330 0.397 0.213	for Kastanozems for Chernozems for Cryosols	-	Schroeder et al., 1994
Saturated hydraulic conductivity (K_{sat})	$9.0 \cdot 10^{-6}$ $6.2 \cdot 10^{-6}$ $1.2 \cdot 10^{-7}$	for Kastanozems for Chernozems for Cryosols	m s^{-1}	Schroeder et al., 1994
Surface depth (L_{sf})	0.16		m	

Subsoil depth (L_{ss})	1.5	m	
Soil thermal conductivity	2.9	J s^{-1} m^{-1} K^{-1}	Bristow (2002)
Water thermal conductivity	0.57	J s^{-1} m^{-1} K^{-1}	Bristow (2002)
Ice thermal conductivity	2.2	J s^{-1} m^{-1} K^{-1}	Bristow (2002)

From these models we calculated the total runoff for each basin as the sum of surface runoff (SR) and recharge (R):

$$Q_{calc} = \sum_{i=1}^{12} (R_i + SR_i) * A_i \quad (3.4)$$

where subscript *i* refers to the model zone, Q_{calc} is the computed discharge (m^3 s^{-1}), and A_i is the area of the i^{th} zone (Table 3.1). Since we do not perform routing calculations, we only compare computed and measured river discharge on a cumulative.

3.3. Results

We first asses model validity by comparison with observations and then discuss the hydrological cycle components by assessing non measured variables. The cumulative discharges to rivers calculated using equation 3.4 for the three basins are compared to measured values in Figures 3.3, 3.4 and 3.5. Note that no calibration has been performed. Therefore, model results should be considered a blind prediction. Measured discharge of the Uliastai basin was exceptionally high in 2003. The reason for this anomaly is not clear. Neither Terelj nor Ulaanbaatar stations recorded anomalous high rainfalls that year. Davaa and Oyunbaatar (2010) noted that a flood occurred in 2003 around Ulaanbaatar but yield no further information.

The models yield good overall fits for the Upper Tuul basin (Figure 3.5). Discharge of the Selbe basin is underestimated (red line in Figure 3.3). Comparison to measured discharges for the Uliastai basin is more difficult due to the 2003 anomaly, but ignoring this anomaly the discharge seems to be slightly overestimated (Figure 3.4). These discrepancies may be due to the crude assignment of soil types, which for simplicity was based on elevation (Table 3.1). This gave the Selbe and Uliastai basins two soil types (chernozems and

cryosols, see Figure 3.2), although the soil map only indicates one soil type (cryosols, see Figure 3.1.b). Calculations with only using cryosols increases the discharge, which reflects the relatively low retention capacity (difference between field capacity and wilting point) of cryosols. This change improves the fit for the Selbe basin (blue lines in Figure 3.3) but worsens it for the Uliastai basin (Figure 3.4).

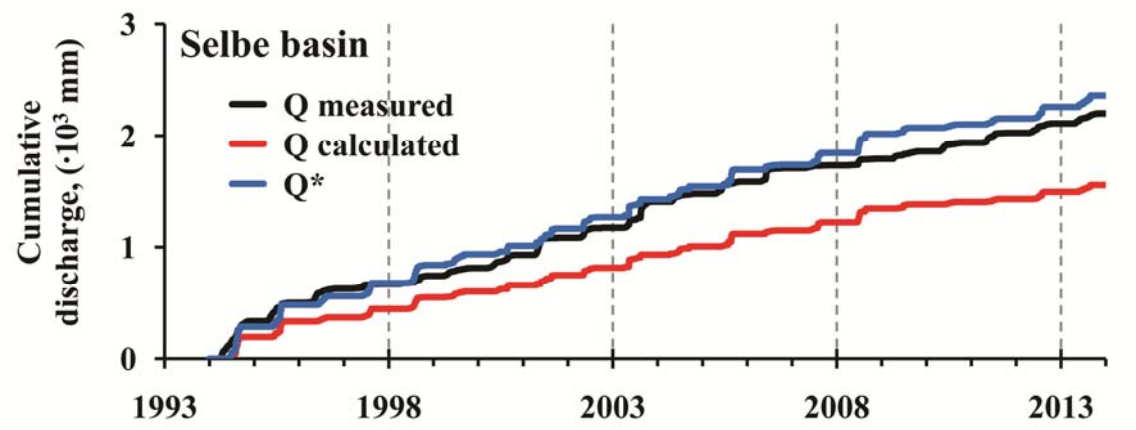

Figure 3.3. Comparison between calculated and observed cumulative discharge (mm) for the Selbe basin from 1994 to 2013. Q* is the cumulative discharge calculated using only one type of soil (cryosols).

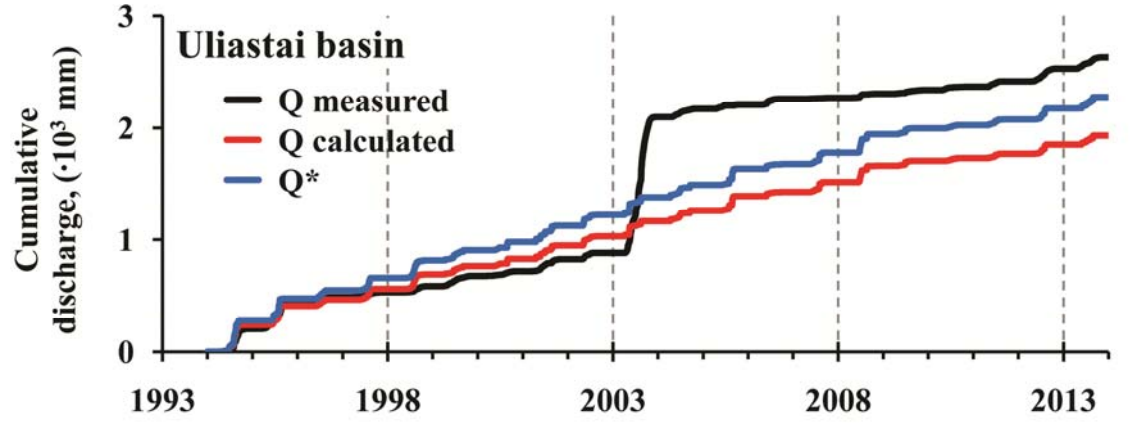

Figure 3.4. Comparison between calculated and observed cumulative discharge (mm) for the Uliastai basin from 1994 to 2013. Q* is the cumulative discharge calculated using only one type of soil (cryosols).

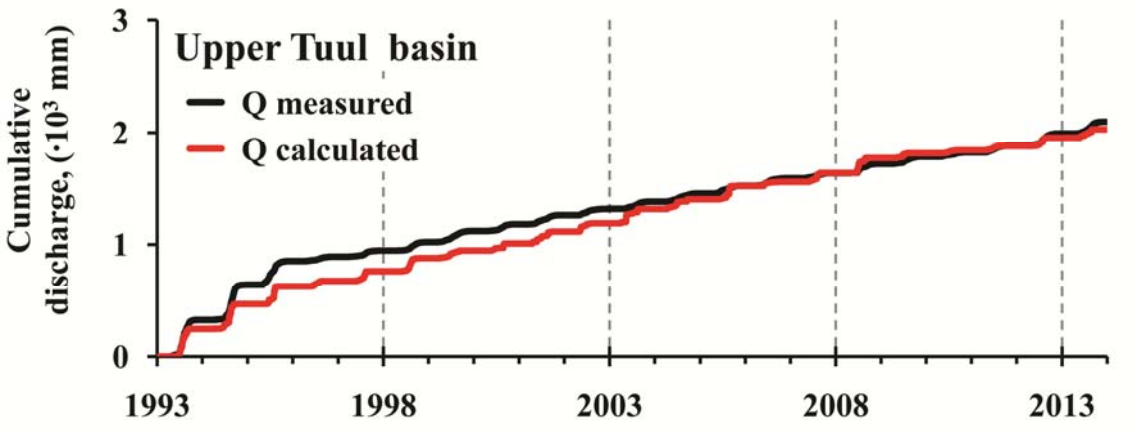

Figure 3.5. Comparison between calculated and observed cumulative discharge (mm) for the whole Upper Tuul basin from 1994 to 2013.

To further verify our model, we compare computed snow depth with snow data from the Ulaanbaatar and Terelj meteorological stations. Our model only computes the total mass of frozen water in the surface layer ($m_{sf,ice}$, in kg m^{-2}), including both snow and pore ice. Therefore, this comparison can only be qualitative. To this end, we estimated snow depth by assuming that part of the ice or snow in the surface layer is within the soil as ice and part is on top of the surface as snow:

$$d_{snow} = \max\left(\left(\frac{m_{sf,ice}}{\rho_{snow}} - \theta_{ice} L_{sf} \frac{\rho_{ice}}{\rho_{snow}}\right), 0\right) \quad (3.5)$$

where d_{snow} is the snow depth (m), ρ_{snow} is the density of snow (kg m^{-3}), θ_{ice} is the volumetric ice content, L_{sf} is the length of surface layer (m) and ρ_{ice} is the density of ice (916.7 kg m^{-3}). We calibrated the snow density and ice content to the measured snow depths. This gave a snow density of 187 kg m^{-3} and ice content of 0.2, which are very reasonable values. The measured data of the Ulaanbaatar and Terelj stations are compared with the horizontal models at elevations lower than 1450 m and 1451-1750 m, respectively, according to the location of the stations (Figure 3.2). Figures 3.6 and 3.7 display the daily computed and measured snow depth for the last 3 years of the Ulaanbaatar and Terelj stations, respectively. Generally, good fits could be obtained, especially for the duration of snow cover, which is much less sensitive to calibration parameters. Nevertheless, the measurements show more short temporary snow packs during autumn and spring than the models.

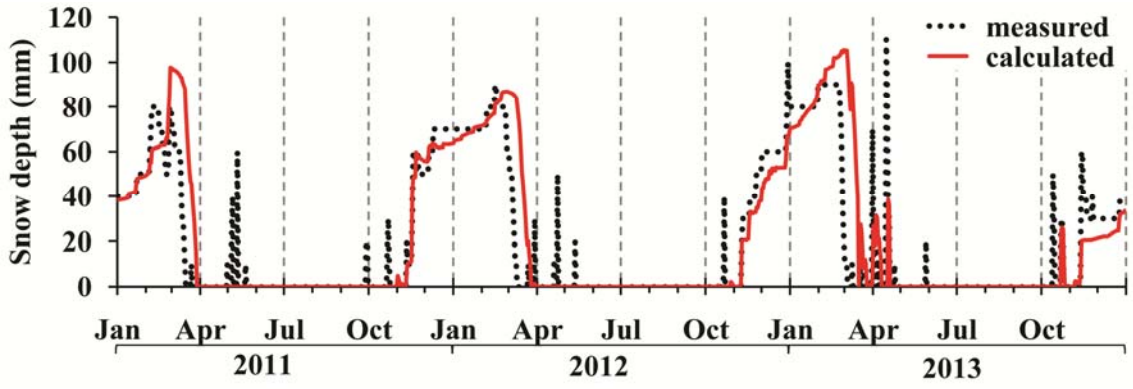

Figure 3.6. Comparison between the daily observed and computed snow depth at elevations below 1450 m with a horizontal slope.

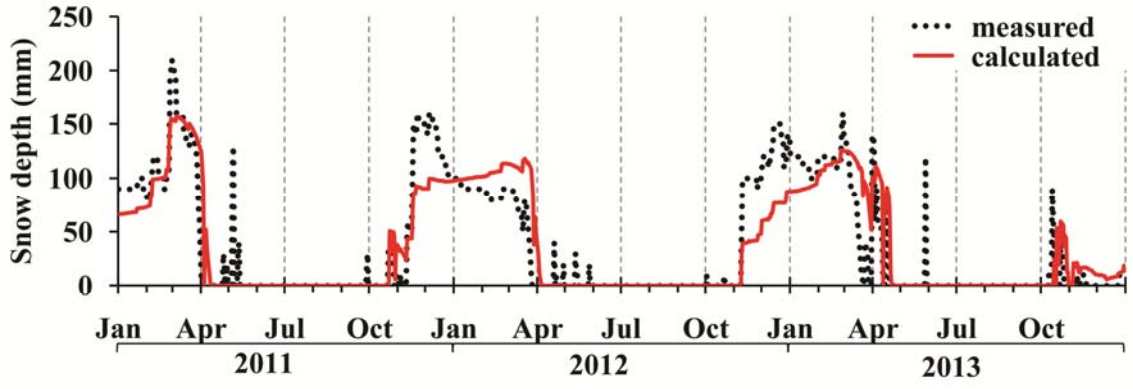

Figure 3.7. Comparison between the daily observed and computed snow depth at elevations ranging from 1451 to 1750 m with a horizontal slope.

Water and energy balance terms, averaged over 21 years (1993-2013), for the 12 model zones and for the 3 basins are summarized in Tables 3.3 and 3.4, respectively. Figure 3.8 displays the evolution of the water balance terms of the largest basin (Upper Tuul basin). A number of unexpected, from a mid-latitudes temperate climate, observations emerge from these calculations.

Precipitation increases with elevation in response to the assumed precipitation lapse rate, with Uliastai being on average the most rainy basin and Selbe the driest (Table 3.3), (but just the opposite to unit discharges reported in Section 2.2 for the three basins). Water

availability causes evapotranspiration (ET_{sf} and ET_{ss}) to also increase with elevation. However, even though evapotranspiration is very low, its ratio over precipitation (ET/P) drops significantly with elevation. For example, the evapotranspiration (ET_{sf}) is about 84% of rainfall for horizontal slopes (85% for south facing slopes) at low areas and 57 % (60 %) at high areas. These ratios are consistent with those obtained in other subarctic regions (Bolton, 2006). Ma et al., (2003) estimated 72% to 85 % for this ratio over the whole Selenge River basin. The large drop of ET/P with elevation reflects not only the reduction in potential evapotranspiration, caused by the lower temperatures and decrease in vapor pressure deficit, but also the reduced water retention capacity of soils in cold regions, probably associated to reduced weathering. This is highlighted by the results in north facing slopes at elevations higher than 1450, mostly occupied by mountain forests, which enhance evapotranspiration not only because of their low albedo and high leaf area index (Table 3.2) but also because forests can evaporate water from both the surface and subsoil layer ($\alpha = 0.8$, Table 3.2). The total ET (sum of ET_{sf} and ET_{ss}) in these zones is about 99%, 95% and 85% of rainfall at elevations of 1451-1750 m, 1751-2250 m and higher than 2251 m, respectively. The evapotranspiration in the Upper Tuul basin does not vary much in time, oscillating around an average of about 302 mm $year^{-1}$ (76 % of rainfall), and follows more or less the same pattern as the rainfall (Figure 3.8).

Like evapotranspiration, recharge and surface runoff increase with elevation because of higher rainfall (Table 3.3). At the north facing slopes, containing forests, the relatively high evapotranspiration leads to relatively low recharge and surface runoff. Recharge is generally larger than surface runoff and both vary a lot from year to year (Figure 3.8). The evolution of recharge follows more or less the same pattern as rainfall. But surface runoff does not, probably because surface runoff occurs mainly during snow melt in spring and does not correlate well with precipitation, which falls mainly in summer.

Vapor diffusion (J_D) between the surface and subsoil layers is positive (downwards) and tends to decrease with elevation, which reflects the decrease of the saturated vapor pressure with temperature. This is further supported by the low variability of yearly vapor diffusion in comparison to recharge and surface runoff (Figure 3.8). While vapor diffusion represents a small fraction of total discharge (12 mm $year^{-1}$ in the Upper Tuul basin, compared to a unit discharge of 96.7 mm $year^{-1}$), it may become an important term of the water balance in dry years with very little rainfall.

Table 3.3. Water fluxes, averaged over 21 years (1993-2013): precipitation (P), evapotranspiration from the surface (ET_{sf}) and the subsoil (ET_{ss}) layer, infiltration (I), surface runoff (SR), vapor diffusion (J_D) and recharge (R). All fluxes are in kg m^{-2} $year^{-1}$. Note that $R=I+ J_D- ET_{ss}$.

Slope type	Elevation, m	P	ET_{sf}	ET_{ss}	I	SR	J_D	R
Horizontal	< 1450	264.0	221.9	0.0	29.1	0.0	13.0	42.1
	1451 - 1750	342.1	277.0	0.0	49.3	0.1	15.6	64.9
	1751 - 2250	442.1	301.1	0.0	88.3	42.5	10.2	98.5
	> 2251	542.1	310.3	0.0	129.7	93.5	8.6	138.3
South face	< 1450	264.0	224.8	0.0	25.4	0.0	13.8	39.2
	1451 - 1750	342.1	283.2	0.0	42.0	0.0	16.8	58.8
	1751 - 2250	442.1	314.7	0.0	83.8	32.7	10.9	94.7
	> 2251	542.1	329.8	0.0	124.7	78.5	9.1	133.7
North face	< 1450	264.0	224.1	0.0	26.3	0.1	13.4	39.8
	1451 - 1750	342.1	315.2	26.6	17.0	0.2	9.7	0.0
	1751 - 2250	442.1	364.2	57.0	59.5	11.2	7.1	9.6
	> 2251	542.1	399.9	40.4	113.8	20.7	7.7	81.1
Basins		**P**	**ET_{sf}**	**ET_{ss}**	**I**	**SR**	**J_D**	**R**
Selbe		381.5	292.4	4.4	61.1	15.0	13.0	69.8
Uliastai		415.8	304.3	6.9	73.4	26.9	11.2	77.7
Upper Tuul		399.2	296.7	5.8	68.1	22.4	11.9	74.3

The energy balances (Table 3.4) produce some further unexpected results. The net radiation absorbed by the south facing slopes is higher than that adsorbed by the horizontal slopes, as expected, because the south facing slopes receive more shortwave solar radiation. But, surprisingly, the net radiation for north facing slope is larger than for horizontal slopes, at all zones with elevations above 1450 masl, which are modeled as covered by forest. This result can be attributed not only to the fact that forests adsorb more solar radiation because of their low albedo, but also to the low temperatures resulting from

high elevation and increased ET. Low temperatures cause lower upward longwave radiation, thus increasing net radiation (Ishikawa et al., 2005).

Table 3.4. Heat fluxes, averaged over 21 years (1993-2013): net radiation (Rn), latent heat (e_g ET), sensible heat (H), heat conduction (G) and vapor convection (e_g J_D). Units of all fluxes are in MJ m^{-2} $year^{-1}$.

Slope type	Elevation, m	Rn	e_g ET	H	G	e_g J_D
Horizontal	< 1450	1787.2	559.9	1230.7	-32.6	32.9
	1451 - 1750	2083.6	697.4	1386.5	-39.9	39.6
	1751 - 2250	2232.8	756.6	1462.6	-25.9	25.8
	> 2251	2325.8	777.8	1513.9	-22.6	21.7
South face	< 1450	2223.9	567.0	1660.4	-34.5	35.0
	1451 - 1750	2663.8	712.8	1951.4	-42.7	42.7
	1751 - 2250	2815.1	790.6	2011.2	-27.6	27.7
	> 2251	2897.1	826.4	2036.7	-23.7	23.0
North face	< 1450	1507.4	565.6	945.5	-33.8	34.1
	1451 - 1750	2501.3	860.8	1644.3	-24.7	24.5
	1751 - 2250	2650.3	1058.6	1585.2	-19.2	18.0
	> 2251	2675.8	1103.9	1544.4	-21.4	19.3
Basins		**Rn**	**e_g ET**	**H**	**G**	**e_g J_D**
Selbe		2219.3	746.4	1468.3	-33.4	33.1
Uliastai		2330.2	782.4	1538.8	-28.7	28.5
Upper Tuul		2283.0	760.8	1514.7	-30.6	30.3

Higher net radiation also leads to higher sensible heat fluxes, which is especially surprising at North facing slopes and elevations above 1450 where it is larger than the corresponding sensible heat fluxes in horizontal slopes and must be attributed the lower atmospheric resistance(higher surface roughness length, z_0) of forests. Generally, the sensible heat flux is higher than the latent heat flux, which reflects the dry climate of regions, with sensible heat consisting of about 66% of the net radiation for all basins and latent heat 34%. The

fraction of sensible heat is a bit higher for the south facing slopes (between 70% and 75%) and lower for the north facing slopes (between 58% and 66%). These fractions are consistent with those of other subarctic regions. Fitzjarrald and Moore (1994) found about 63% for the fraction of sensible heat (H/Rn) and of 29% for the fraction of latent heat (e_gET/Rn) in subarctic climate condition of Canada with forest area. Similar fractions of sensible heat (65%) and of latent heat (29%) were estimated by Tuvshinjargal et al., (2004) in the Terelj area.

There is a downward vapor convection (e_gJ_D), which is compensated by an upward heat conduction (G). Both fluxes are quantitatively small in comparison to the other heat fluxes, but qualitatively relevant as they concentrate on specific periods of the year. Vapor convection is relevant in accelerating ice melt in the subsoil layer during late spring.

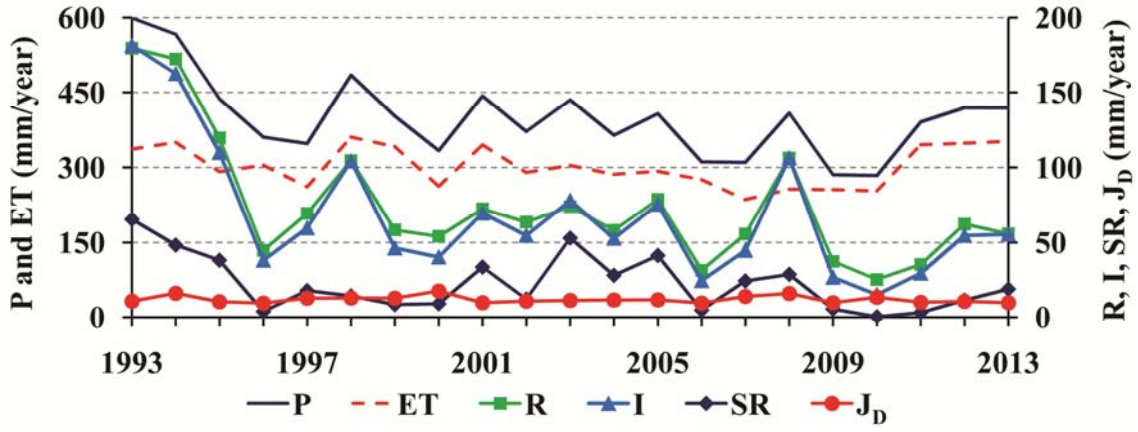

Figure 3.8. The average annual water fluxes evolution in the Upper Tuul basin

The average annual temperatures of the surface and subsoil for different surfaces are shown in Figure 3.9. Average temperatures lower than 0°C, which imply the presence of permafrost, are calculated for elevations higher than 2250 m for north facing slopes, higher than 1750 m for horizontal slopes and higher than 2250 for south facing slopes. The temporal temperature evolution, not shown, is similar to the measurements of Ishikawa et al., (2005) and Jambaljav et al., (2008) for the Terelj area with elevations ranging from 1500 to 1750.

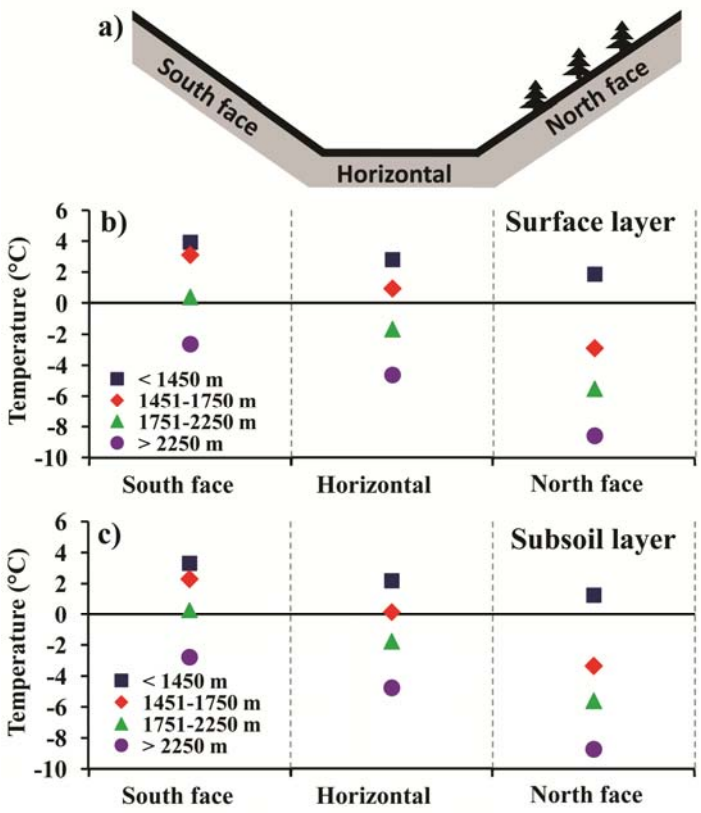

Figure 3.9. Schematic image (a) for landscape, the average annual surface (b) and subsoil layer (c) temperature (1993-2013) in different surfaces. The average annual air temperature was 0.6°C, -3.2°C, -6.2°C and 9.2°C, elevation < 1450 m, 1451-1750 m, 1751-2250 m and > 2251 m respectively.

3.4. Conclusions

A daily water and energy balance accounting for soil water freezing and vapor diffusion was carried out in the Upper Tuul basin, for the period of 1993-2013. Freezing and thawing of the active layer underlain by permafrost or seasonal frozen soil is known to significantly affect hydrological processes in sub-arctic regions (Bolton, 2006), which is our case. To do a realistic, yet simple, model from limited data, the selected area was divided into 12 zones based on elevation ranges, slope, soils and vegetation types obtained from large scale data bases. Daily meteorological data are required. However, data from the two stations (Ulaanbaatar and Terelj) within the basin, which generally agrees with those reported from regional databases for this basin, yielded too low rainfall. We had to

use lapse rates to correct for elevation the direct observations in order to obtain discharges comparable to measurements.

The low rainfall causes direct surface runoff to be also small, where as subsurface runoff contributes more to total discharge because the infiltration increases in summer when the active layer thaws, which is consistent with observations at other subarctic regions (Hülsmann, 2015). Evapotraspiration increases with elevation, due to the increase in precipitation, but the ratio of the evapotranspiration over precipitation (ET/P) decreases, both because the lower temperatures cause a reduced vapor pressure deficit and because cryosols display a low water retention capacity. We found that the vapor diffusion flux is a relevant term of water balance, which may be true for other subarctic regions. This flux transforms into recharge, it is large during late spring, and may become the term controlling overall discharge in dry years.

For the heat fluxes in Upper Tuul basin, the sensible heat is higher than latent heat flux, which reflects the dry climate of region. Due to the low albedo for forest, net radiation at north facing slopes is higher than at horizontal surfaces, but smaller than south facing slopes.

Chapter 4

Surface and groundwater interaction in cold region and leakage

4.1. Introduction

River-aquifer interaction is important both because most riverine hydro-bio-geo-chemical processes depend on this interaction. Water exchanges between groundwater and surface water influence the sustainable groundwater use and also impact on water quality and quantity. Hence, it is not surprising that the topic has received much attention in the hydrological literature (see reviews by Winter, 1995; Sophocleous, 2002; or Kalbus et al., 2006). However, experience is limited in arctic and subarctic zones, where freezing alters both surface and ground water flow and, especially, their interaction. Yet, the issue is

especially important in these regions surface waters freeze in winter months and groundwater becomes the main source for water supply (Dimkic et al, 2008; Jaroslav et al., 2013).

Research in cold regions hydrology has been also intense, and motivated by issues related to climate change, with emphasis on climatic variability, permafrost dynamics and/or ecological issues (e.g., Lyon et al., 2009; Frampton et al., 2011; Bring et. al, 2016). Research on hydrogeological issues is scant (see review by Hinzmanet et al, 2013). River hydrology has largely concentrated on issues related to the ecological impacts of ice and floods caused by ice jams (Fu et al., 2014; Prowse and Beltaos, 2002).

Much less effort has been devoted to the actual mechanisms controlling river flow and its interaction with groundwater during cold periods. Some studies analyze recession curves as driven by permafrost freezing and thawing (Hamilton and Moore, 1996). Kane et al., (1973) observed head differences between the Goldstream Creek River (Alaska) and adjacent aquifer and found that the hydraulic gradient between river and groundwater was high in summer and low in winter. Similar observations were made by (Weber et al., 2013) in Upper East Branch Pecatonica River in Wisconsin.Generally the river water levels increase in summer and drop in winter. However, river levels often increase in early winter, when water starts to freeze-up (Weber et al., 2013; Hamilton, 2004). In fact, the hydrological monitoring and research in northern regions are traditionally focused on the spring and summer high flow period (Moore et al., 2002). These observations explain the reduction in winter streamflow, which is also affected by the increase in viscosity caused by low temperature (Rosenshein, 1988).

In spite of this work, the actual mechanisms controlling groundwater/surface-water interactions in cold regions remain largely unknown. Understanding them is a critical issue (Callegary et al., 2013). Energy balances (Marsh et al, 1990) make it clear river flow under the ice cover is fed by groundwater, which is relatively warm and provides a source of heat to prevent full freezing. In fact river ice thickness may be controlled by groundwater upwelling (Jones et al., 2015). This leads us to conjecture that rive-aquifer interaction in cold regions may be radically different to that from temperate regions. Infiltration may cause streamflow under the ice to disappear, except near the extreme portions of the aquifer (Figure 4.1). At one end, the river may bring water from upstream aquifers

discharge. At the other, the aquifer may discharge into the river. As a result of river flow disappearing, the cone of depression caused by pumping may grow unchecked and become much larger than in temperate regions, where the river continues to flow.

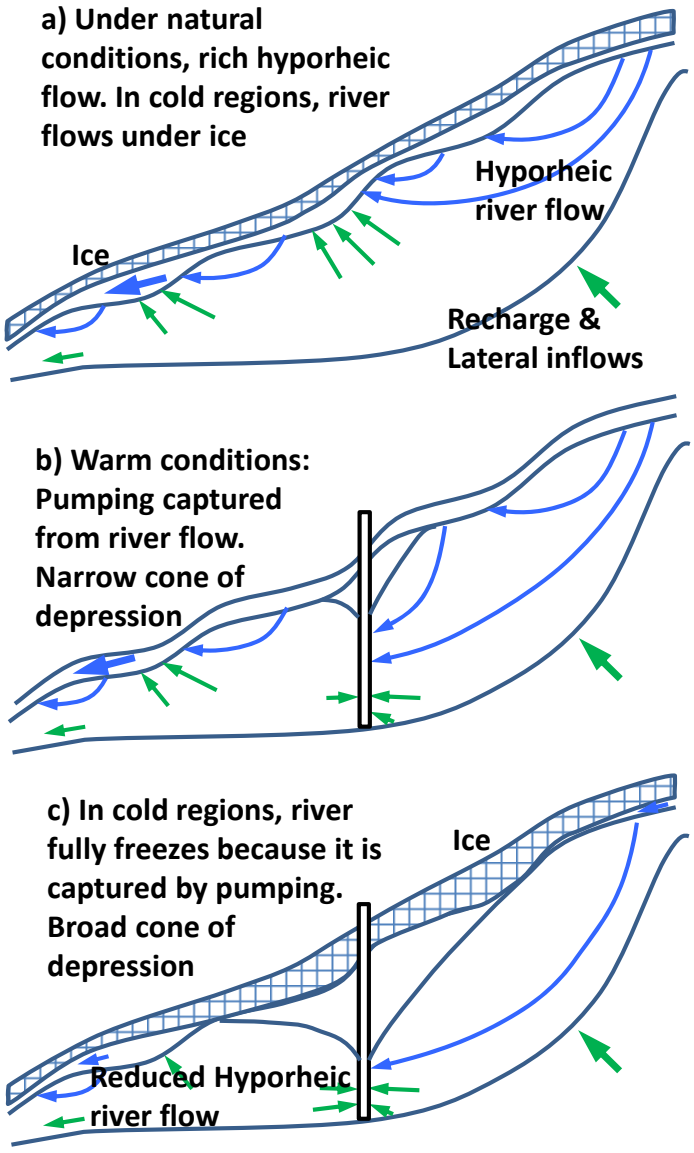

Figure 4.1. River flows under the ice largely because inflows from groundwater, which sustain the flow rate and provide energy to keep water liquid. The resulting flow regime is similar to that without ice (a). Pumping near the river captures river flow, leading to narrow depression cones (b), but it also reduces the inflow of water and energy to the river, which may fully freeze during winter.

The flow regime affects pumping strategies in alluvial aquifers located in cold regions. This work is motivated by the alluvial aquifer of the Tuul River near Ulaanbaatar city, which supplies water to the city (Figure 4.2). Groundwater use in this area has consistently increased since 1960 (Buyankhishig et al., 2007) and is expected to continue increasing (NSO, 2013). For this reason, it is important to assess the interaction between the Tuul River and its alluvial aquifer, but it is challenging due to the scarcity of data, especially during winter. Furthermore, it is clear that some portions of the Tuul River freeze totally during the winter, while the river flows under the ice in others. This raises a number of questions about the feasibility and long term sustainability of pumping.

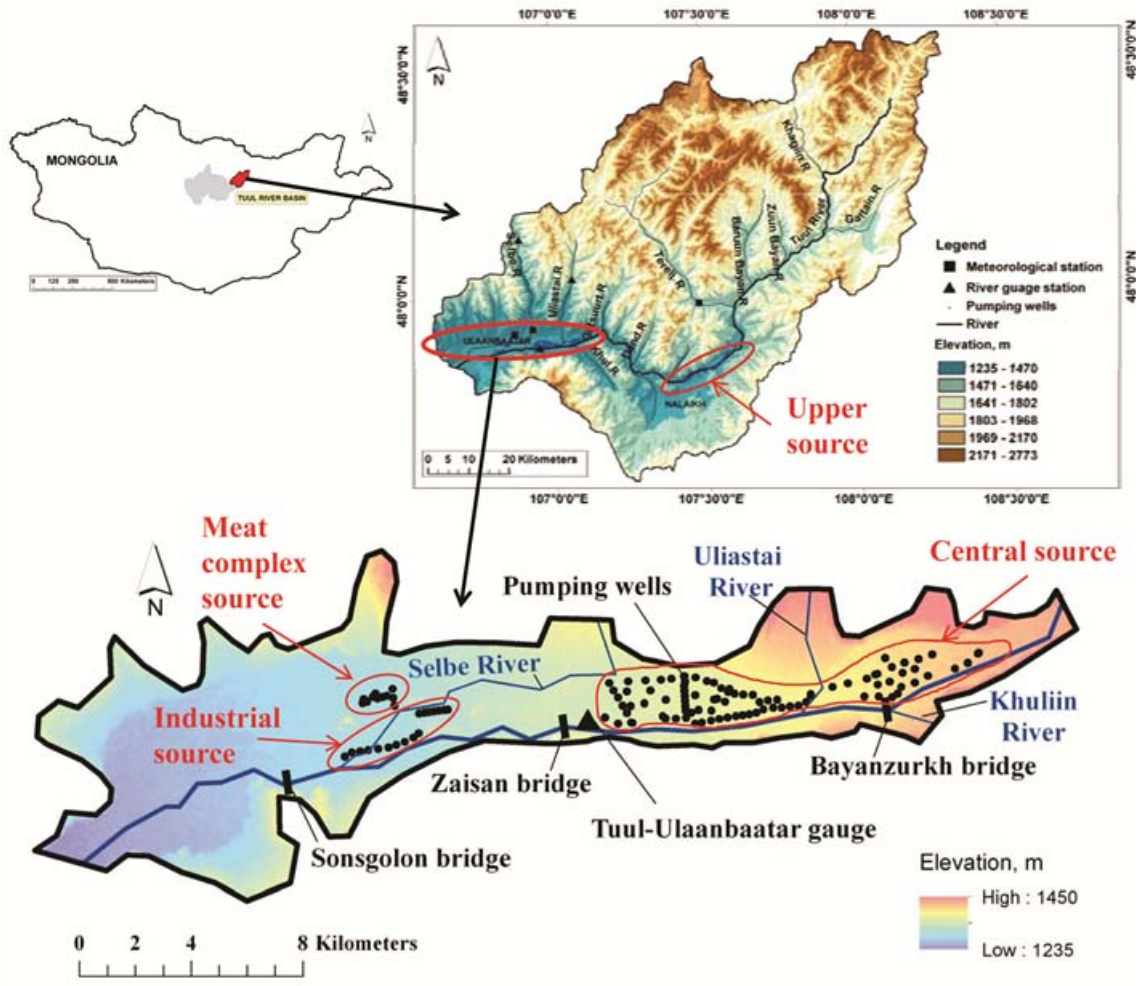

Figure 4.2. Study area, including the whole Upper Tuul River Basin and the Ulaanbataar alluvial aquifer.

The objective of this work is to analyze the Tuul River alluvial aquifer near Ulaanbaatar, the role of river Tuul freezing upon river aquifer interaction and its implications for water supply.

4. 2. Methodology and materials

4.2.1. Study area

This study covers the alluvial aquifer of the Tuul River at Ulaanbaatar (Figure 4.2). This area is characterized by a semi-arid climate, with very cold winters (Batima et al., 2007). The average monthly temperature in Ulaanbaatar varies from a maximum of 22°C in August to a minimum of -25°C in January. As result, the ground is frozen during winter. The average annual precipitation is 264 mm $year^{-1}$ for 1993-2013. Nearly 80% of the annual precipitation falls between June and September. Snow starts to fall in mid-October and the surrounding mountains remain snow covered until early April.

The average (1993-2013) river discharge at Tuul-Ulaanbaatar gauge station (Figure 4.2) is 20.3 m^3 s^{-1}. The Tuul River surface is frozen for some 149 days on average, from Novemberuntil the end of April. The mean depth of the ice cover is 43 cm in November and it increases up to 66 cm in December (Dolgorsuren et al., 2012). The width of the Tuul river valley in the area varies from 0.1 to 0.5 km, but the width of river in the city area is about 35 m. Dalai and Ishiga (2013) found that the riverbed consists of fine-grained sediments near the city area but coarse sediments around the upper source area.

The region around the alluvial aquifer consists mainly of Carboniferous and Devonian sediments (Figure 4.3). These are intruded by Jurassic to Triassic granitoid rocks and locally covered by Cretaceous sedimentary rocks, and by Tertiary and Quaternary deposits (Dorjsuren, 2012). The granitoids are medium and coarse grained porphyritic-granite (Khishigsuren, 2012). The Cretaceous sedimentary rocks occur in the Nalaikh depression, which is one of the coal mining sites in Mongolia. The sediments consist mainly of mudstone, coal, and fine-grained sandstones. Tertiary deposit consists red to yellow clays, sands, and gravels. Quaternary alluvial sediments along the Tuul River valley and its

tributaries are characterized by permeable sands and gravels (e.g., Jadambaa et al., 1981; Unudelger and Banzragch, 1993).

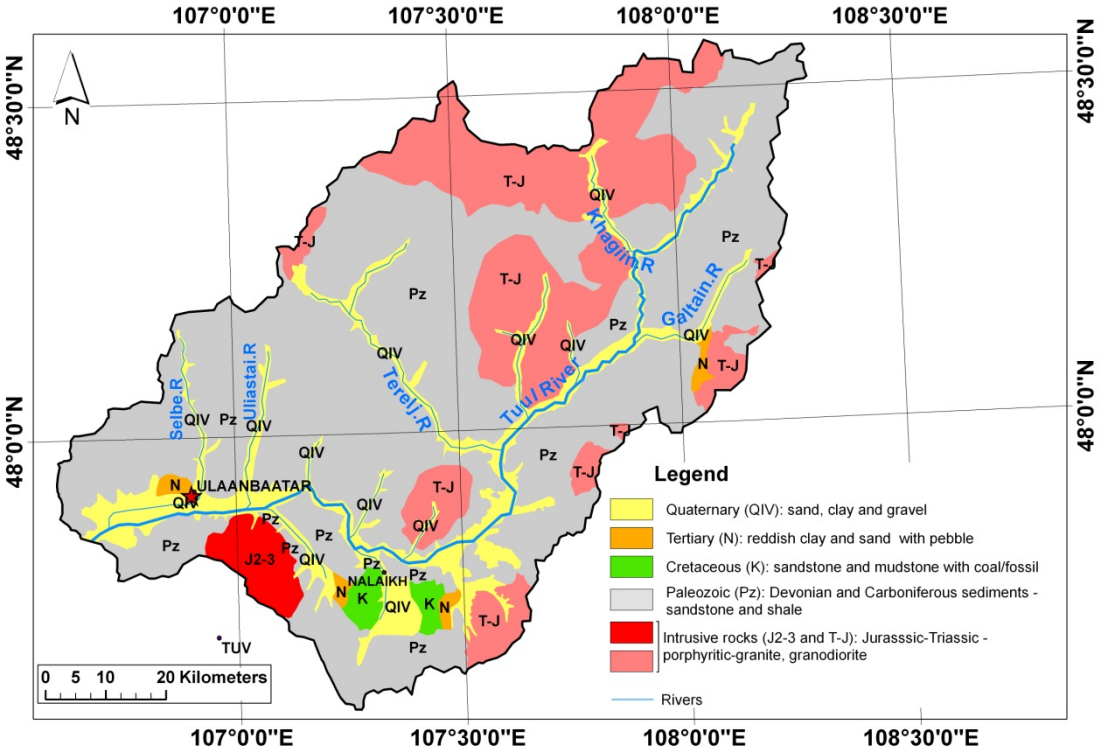

Figure 4.3. Geological map (scale 1: 200 000)

4.2.2. Available data

Exploration boreholes were drilled and sampled in May, 1960 as part of the study of the regional groundwater flow system for alluvial aquifer of Tuul River basin. Aquifer materials were described, heads measured and water samples collected. These data were collected by PNIIIS (1979). Heads ranges from 1254 m to 1316 m above sea level and the aquifer was connected to the river at the time, prior to significant pumping of the aquifer.

Figure 4.4 shows the concentration of total dissolved solids (TDS) measured at exploration boreholes, which ranges between 48 and 250 mg L^{-1}. The highest concentrations (red colors) were found in northeastern part and next of the Selbe River while a low

concentrations were found in a close to Tuul River, which we take as an indication of inflows from the adjacent formations and from the Tuul tributaries, because the average TDS of the Tuul River near Ulaanbaatar is 50-60 mg L^{-1}, whereas that of its tributaries, Selbe and Uliastai rivers 70-190 mg L^{-1} (Altansukh, 2012). Tsujimura et al., (2013) performed End Member Mixing Analysis and found that the Tuul River was the dominant source of water into the alluvial aquifer for the central source area, with some contribution of south and north lateral flow.

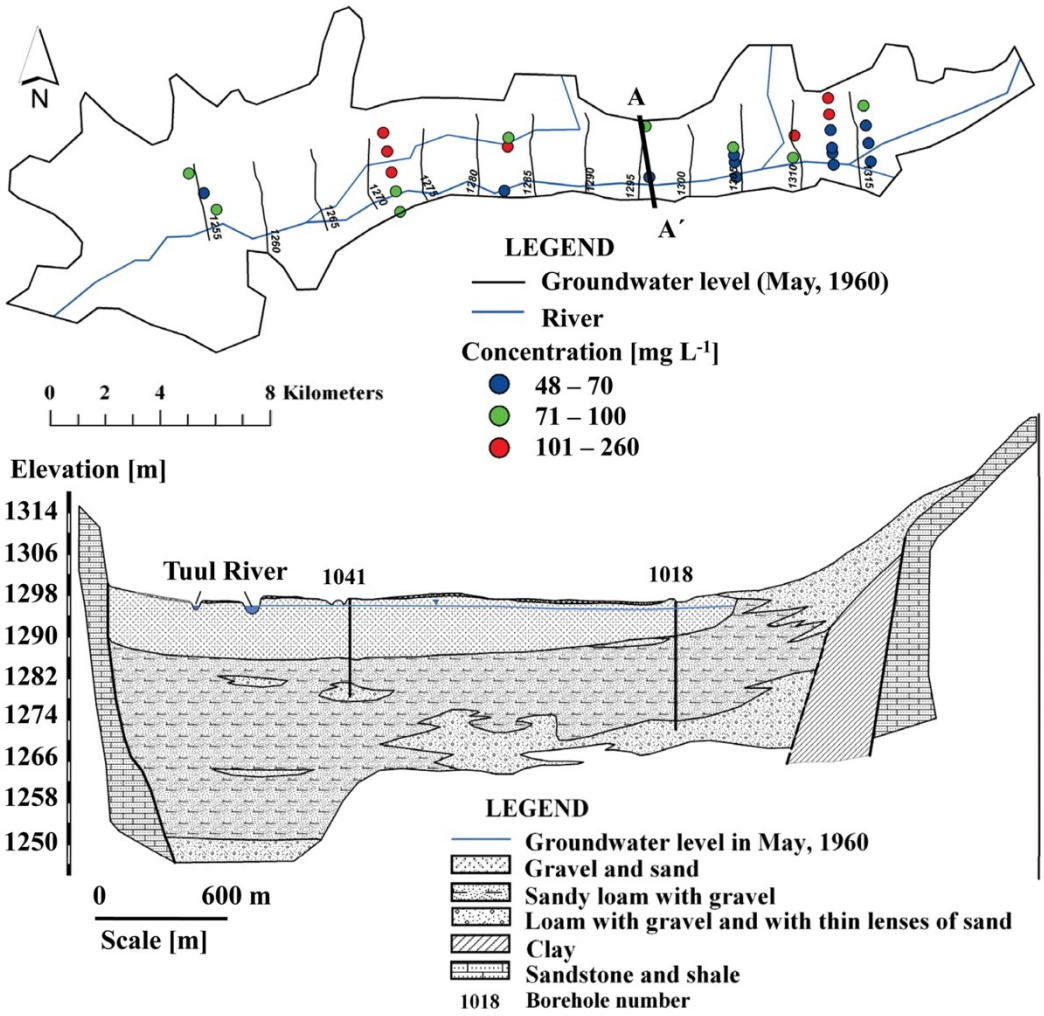

Figure 4.4. Location of exploration boreholes for the May, 1960 campaign, including TDS (color code) and geological cross sections, such as A-A´ shown below (modified from PNIIIS, 1979).

PNIIIS (1979) distinguishes two layers in the alluvial sediment, depending on hydraulic properties: the upper layer contains coarse-grained alluvium with hydraulic conductivities ranging from 50 to 290 m day^{-1}; the lower finer-grained alluvium consists typically of fine sand with silt and clay and displays hydraulic conductivities of about 5 to 35 m day^{-1}. The aquifer thickness derived from the exploration wells ranges from 6 to 28 m in the upper portion, from 10 to 44 m the middle, and about 25 m in the lower part.

Water has been extracted since 1960 from the central source zone, with a 2001-2014 average of 72 000 m^3 day^{-1} from 89 wells. In addition 16 wells have been pumping since 1963 in the Industrial source area (24000 m^3 day^{-1}) and 11 wells in the Meat complex source area from 1965 (13000 m^3 day^{-1}) on average. Pumping rates are rather constant through the year.

Two divers were installed in the alluvial aquifer along the Tuul River in order to measure water head dynamics. One of them was installed in Upper source area (Figure 4.2) and another one in the Industrial source area. We used data for this study from diver belongs to Industrial source area as started to record from February in 2013 to July in 2014. In addition, we obtained data from two divers are located in central source area (Batsaikhan et al., 2011) which were since April in 2012 until July in 2014. These observation wells are away at 1947, 470 and 387 m from Tuul River are referred to as OW1, OW3 and OW8 respectively (see Figure 4.7).

Monthly water temperature and daily water level at Tuul-Ulaanbaatar gauge were collected from 1993 to 2013 during only ice-free periods (Figure 4.2). The maximum water temperature was measured of 17.2°C in July and the minimum water temperature was of 0.2°C in April and in November. The water level was measured of 1.3 m on average between May and November. The maximum water level of 2.1 m was recorded in July, 1993 and the lowest water level occurred in March and April.

Temperature evolution and profiles (Figure 4.5) show that the aquifer does not quite freeze. In fact, heat exchange may be aided by density differences.

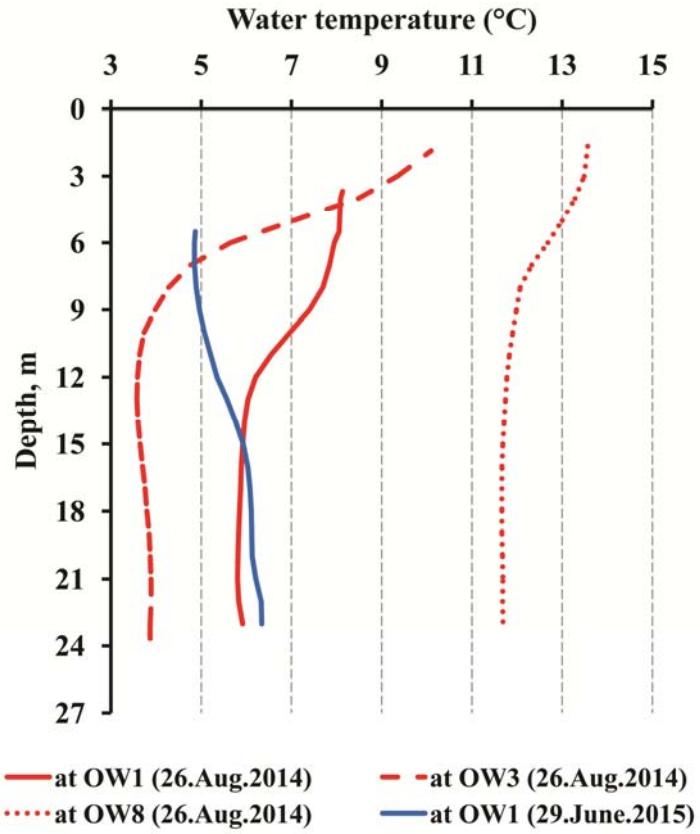

Figure 4.5. Water temperature at observation wells versus depth.

4.2.3. Conceptual model

Several models have been built in the area. The earliest ones performed made by Jadambaa (1977) and PNIIIS (1979) using electric-analog model of the central source area. More recent models have been built by a Japanese group (JICA, 1995) and Buynkhishig (2008). They provide the basis for the conceptual model.

The aquifer system is unconfined, with a no-flow bottom because of the low permeability of the underlying older sedimentary formation. Given its extent to thickness ratio, we adopt Dupuit's approximation and treat it as a two dimensional system. Transmissivity is spatially variable, resulting from multiplying a hydraulic conductivity 60 m d^{-1} (PNIIS, 1979) times a thickness, constant in time because head fluctuations are small. We initially adopted a storage coefficient of 0.13.

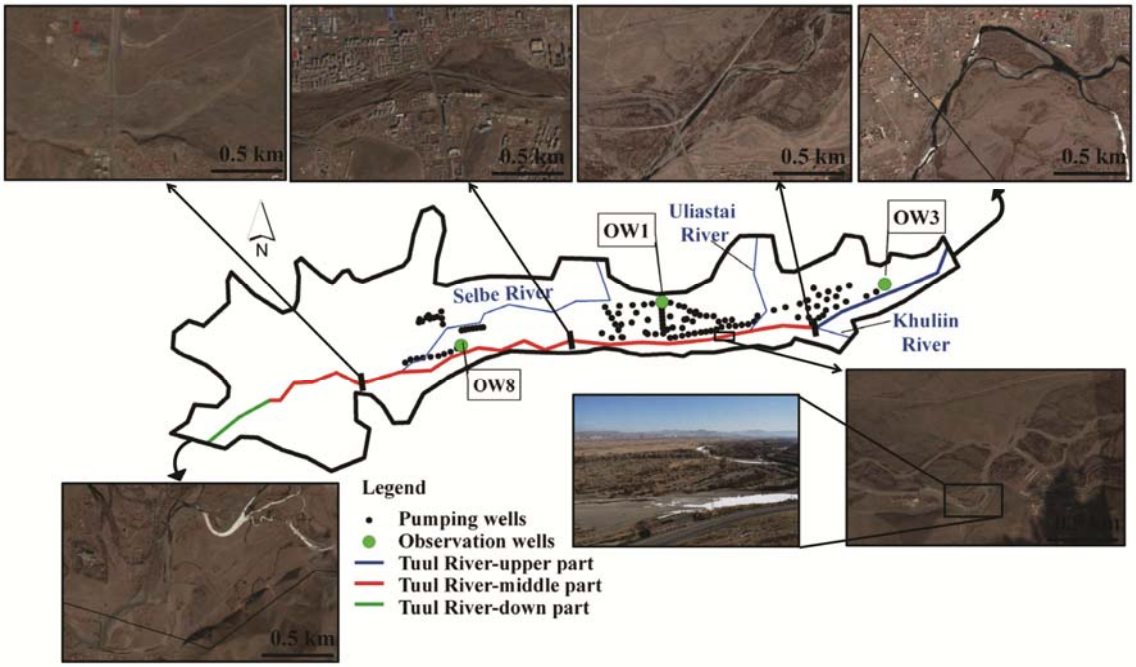

Figure 4.6. Different leakage condition along the Tuul River near Ulaanbaatar. Date of Google Earth images are in April, 2016 and the picture was taken by Tuul River Basin Authority in March, 2016.

We assume that most of the water is extracted by pumping and enters from the rivers, lateral inflows and areal recharge (Figure 4.4). Boundaries adjacent to the older sedimentary formation are treated as a prescribed flow. Rivers and boundaries adjacent to the rivers are treated as leakage inflows:

$$Q = \alpha(H_{river} - h) \quad (4.1)$$

where Q is the stream leakage per unit length of river (m^3 d^{-1}), positive when water enters the aquifer, α is the leakage coefficient (m^2 d^{-1}), h is the computed head or the piezometric head (m) and H_{river} is the river water elevation (m), which was also adopted for the portions of boundaries adjacent to rivers. The leakage coefficient (α) is ideally defined as the product of river width multiplied by hydraulic conductivity times divided by the thickness of the stream bed. Actual leakage is affected by numerous factors, so that equation (4.1) must be considered an approximation (Rötting et al., 2006). In order to approximate some of these factors, we acknowledged the time dependence of temperature,

which affects viscosity and has been found to be relevant (e.g.,Rorabaugh, 1963; Constantz, 1998; Barahona-Palomo, 2014), using (Kestin et al, 1978):

$$\mu(T) = \mu^*(T^*)10^{\left[\frac{20-T}{T+16}\left(1.2348-0.001467(20-T)\right)-\mu^*(T^*)\right]} \quad (4.2)$$

where μ is the viscosity (N s m^{-3}), μ^* is the reference viscosity at reference temperature, T^*, and T is the water temperature (°C). More importantly, we assume that the leakage coefficient may become zero at the regions were the river is fully frozen. Thus, the river length was divided in three zones, depending on where it is fully frozen. To define these zones, we used Google Earth images (Figure 4.6). The upper part extends from the eastern model boundary to Baynzurkh bridge, with length of 7.7 km, where ice is permanent until full snowmelt. The middle part is from Bayanzurkh bridge to after Sonsgolon bridge with a length of 27.2 km. The lower part extends the remaining 3.6 km.

The Tuul river is fully covered by ice in winter, but we selected the middle part as the extension where ice occasionally has disappeared in spring period during the last years. We attribute this disappearance to the nearby pumping, which causes the river to stop flowing under the ice (recall Figure 4.1). As temperatures (and radiation) rise in spring, river ice may disappear either because of sublimation or because melted water infiltrates into the river bed, which becomes dry as shown in Figure 4.1.

The river bed does not disappear in either the upstream or downstream ends of the aquifer. Therefore, we assumed that river flows under ice sheet or aufeis in those two zones. The upstream end of the river is still losing water, which comes from groundwater discharge at the aquifer upstream. Instead, the downstream part remains a gaining stream because the aquifer still discharges.

To represent these changes, the leakage coefficient is treated as:

$$\alpha_i(t) = \alpha_i f_t(t) \quad (4.3)$$

where subscript identifies the leakage zone (Figure 4.6), α_i is a reference value and $f_t(t)$ is used to represent the time variability driven by temperature variability or river freezing, $f_t(t)$ is zero when the river freezes over its whole thickness.

Fluctuations of the Tuul River stage recorded at Tuul-Ulaanbaatar gauge station were extended to the whole river to acknowledge H_{river} variability.

Recharge occurs through the model domain, but concentrates in late spring and summer seasons (lowest in April and in October and highest from June to September), and is zero in winter because the ground is frozen. The average annual recharge was estimated about 15% of rainfall (chapter 3). The model area includes portions of city, where some recharge may come from seepage of the water supply and sewage systems (Vázquez-Suñé et al., 2005).

For transport modeling, we adopted longitudinal and transverse dispersivities of 80 m and 8 m respectively. According to the studies of Altansukh (2012) and Tsujimura et al., 2013, the lowest concentration was applied to Tuul River while the high concentrations for its tributaries. For along aquifer boundaries as following previous information, the high concentration was used at northeast part and low concentration at the south boundary.

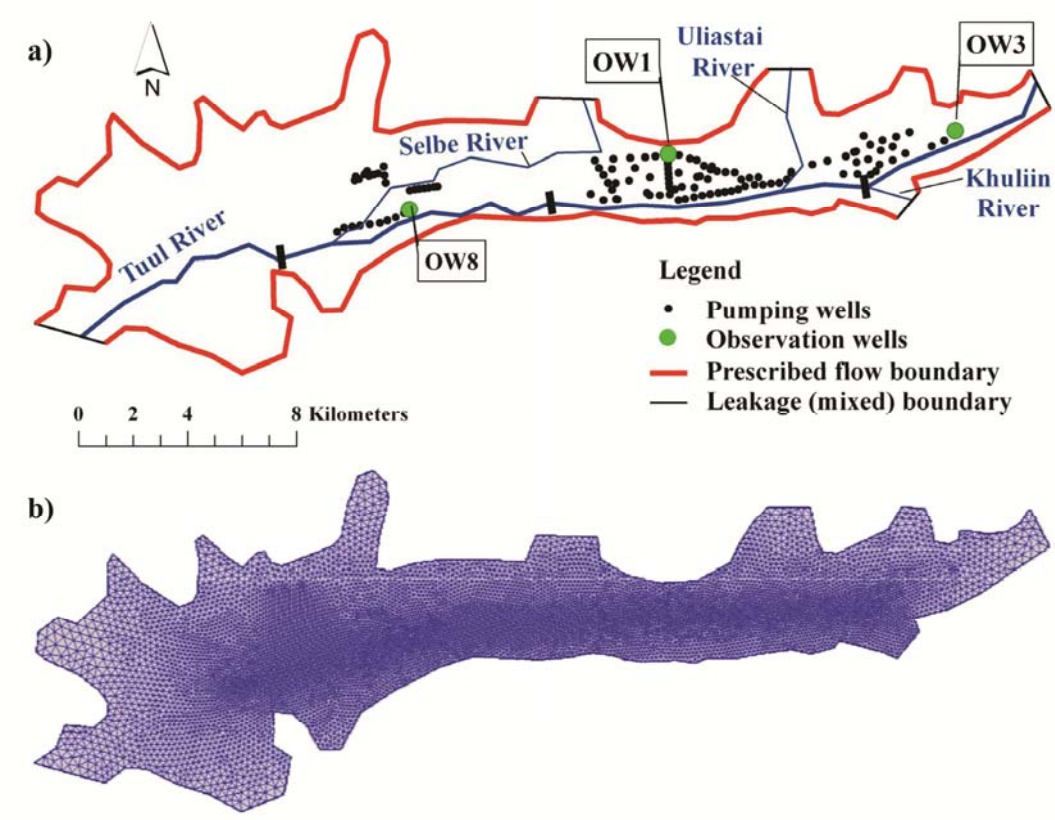

Figure 4.7. a) Conceptual model and boundary conditions and b) model grid.

4.2.4. Numerical model. Calibration strategy

We modelled unconfined alluvial aquifer both for direct simulations and for automatic calibration using the finite element code TRANSIN-IV (Medina and Carrera, 2003), with visual interface of VISUAL TRANSIN IV (UPC, 2003). The model covers an area of 174.16 km^2 (Figure 4.7). The domain was discretized with 9531 nodes, and 18527 elements. The mesh is refined close to the river and where pumping wells are concentrated.

A steady-state groundwater flow and solute transport (TDS) model was calibrated with data from the May, 1960, campaign to obtain preliminary estimates of model parameters and to define an initial groundwater condition. Specifically, this initial calibration yielded the lateral flows from aquifer boundaries and the hydraulic conductivity. All data from exploration wells (Figure 4.4) were used as observation head and concentration.

Using the preliminary parameters from steady-state calibration, we performed several transient runs by sequentially acknowledging the time variability of river stage, lateral inflows, recharge and leakage coefficient. As it turned out, the latter was the most relevant, so that we proceeded by trial-and-error, supported with recent Google Earth images, to identify the river reaches where zero leakage may occur, which we attribute to full freezing of the river. Then we carried out the final calibration for the 1960 to 2014 period using monthly time steps.

4.3. Results

4.3.1. Preliminary calibration

Preliminary parameters were obtained from steady state calibration of flow and solute transport. Computed TDS is shown in Figure 4.8, which reproduces the low salinity throughout most of the aquifer. High salinity is restricted to inputs from lateral inflow and Selbe River, which is generally consistent with observations (Figure 4.4). The computed high salinity zone at the North East boundary is narrower than observed, but would extend

too far and wide downstream if the boundary influx is increased. We attribute the broad high TDS to reduced transmissivity in this region, but preferred to keep the model simple with constant conductivity. As it is, the capture region appears to be well defined, which allows us to set the limits for lateral inflows.

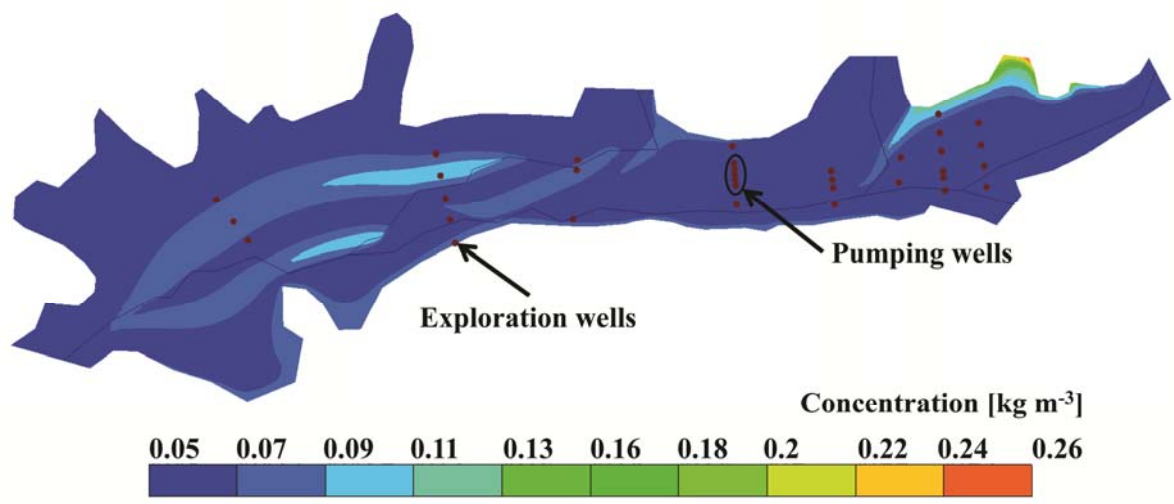

Figure 4.8. TDS concentrations calculated under steady-state flow conditions.

4.3.2. Head fluctuations

The hydraulic conductivity and lateral inflows estimated from the steady-state calibration were used for in the transient flow model. Prior to transient flow calibration we analyzed the impact of time variability of recharge, river water level, lateral flow and leakage coefficient on observed head fluctuation. Figure 4.9 shows a comparison between the observed and calculated heads at observation wells (OW1, OW3 and OW8).

First, the river water level (H_{river}) recorded at Tuul-Ulaanbaatar gauge was considered as variable in time while leakage was and treated as constant and recharge and lateral flows neglected. It is clear that computed head fluctuations in run "only H_{river} (t)" are too small. The same can be said about "Only Recharge (t)" or "Only Lateral Inflows (t)" runs. This lack of sensitivity reflects both the high transmissivity of the aquifer and the low

magnitude of these inputs. Significant fluctuations could only be calculated when leakage was considered as variable in time (Equation 4.3).

Finally, all factors are treated as time dependent which yields the Base Run (black continuous line in Figure 4.9). The groundwater head fluctuations for OW3 and OW8 are very well reproduced, but that of OW1 is not. In this simulation, the fluctuation of leakage coefficient is solely dependent on the river temperature. We assumed that the river water is equal 0°C during winter period. Tuul River water was frozen during winter period because only summer data are available. Moore et al., (2002) noticed that hydrological monitoring and research in northern regions are traditionally focused on the spring and summer high flow period.

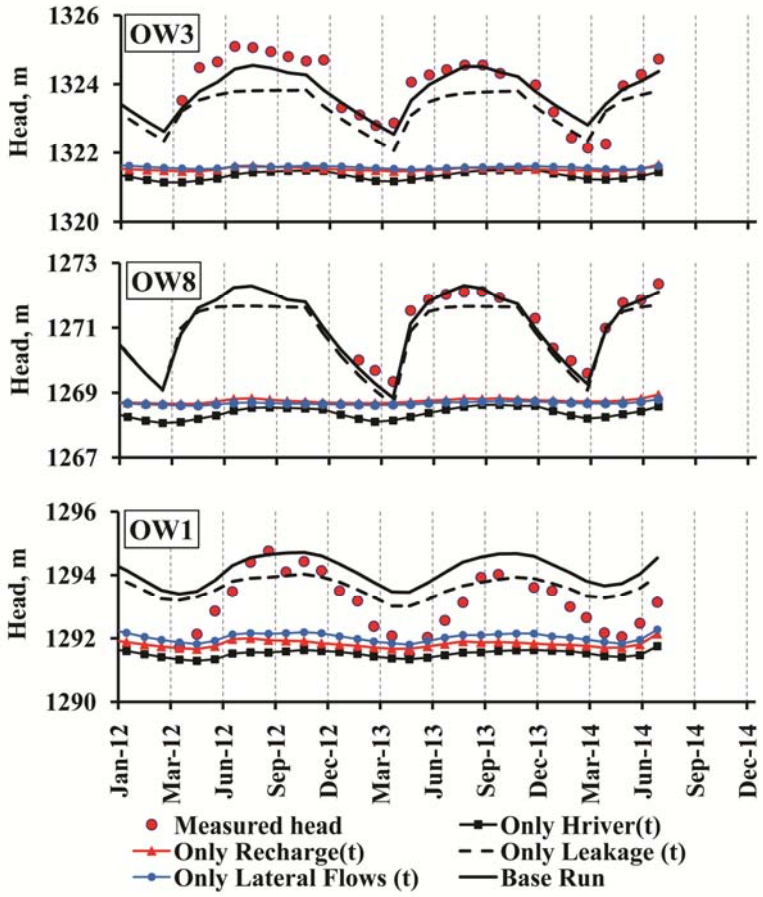

Figure 4.9. Measured (red circles) and computed heads at the three observation wells for the initial base model (using the steady-state calibrated parameters), and acknowledging seasonal fluctuations of only one of the time dependent parameters (recharge, river water stage (H_{river}), lateral flow or leakage coefficient). It is clear that most of the head fluctuation is driven by fluctuations in the leakage factor.

4.3.3. Calibration

The fit between computed and observed heads for the 2012-14 period is shown in Figure 4.10. The fit is overall good and the mass balance (Figure 4.10) consistent with expectations. Therefore, we consider the model appropriate. Still, it is clear that some leakage features are missing. For instance, head at OW8 started to drop from November until April and then water head increases from May. The water head at OW3 declines from December, but during spring the water level is not same as at OW8. The river water may be flows during winter period around of OW3 and river water still infiltrates into alluvial aquifer but it should be small quantity. Therefore we analyzed the sensitivity of heads to leakage along the Tuul River.

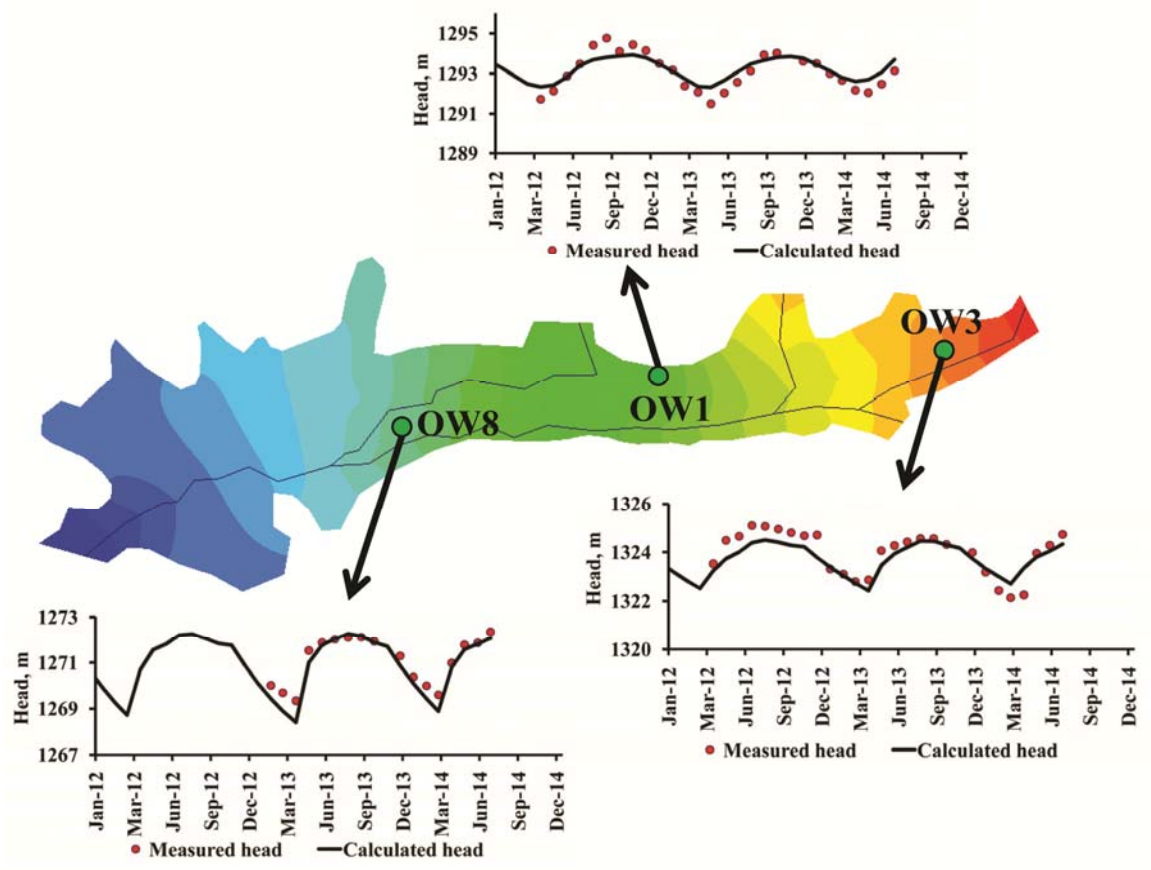

Figure 4.10. Groundwater head fit obtained from calibration at observation wells.

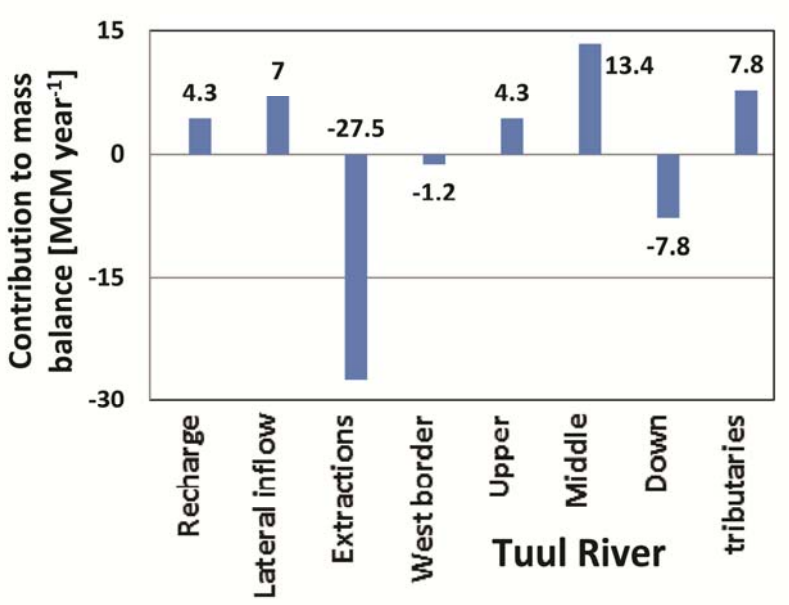

Figure 4.11. Contributions to mass balance (10^6 m^3 $year^{-1}$). Positive values represent inputs.

First, the leakage was 47 which the water temperature is 0.1°C, second and third simulation for leakage were 10 and 1 respectively. The different evolution of water level at observation wells is shown in Figure 4.12.

The water level at OW1 and OW8 are not influenced by these leakage conditions. When higher leakage during winter was used, groundwater head at OW3 is high in spring months. When a small leakage was used, the winter head fall is better reproduced, but heads start to decline from November. Yet, measured water level was still high in December for OW3. This head rise (red ellipses) probably reflects the river water stage growth associate to the formation of the ice sheet, which has been reported in other rivers (e.g., Hamilton 2004).

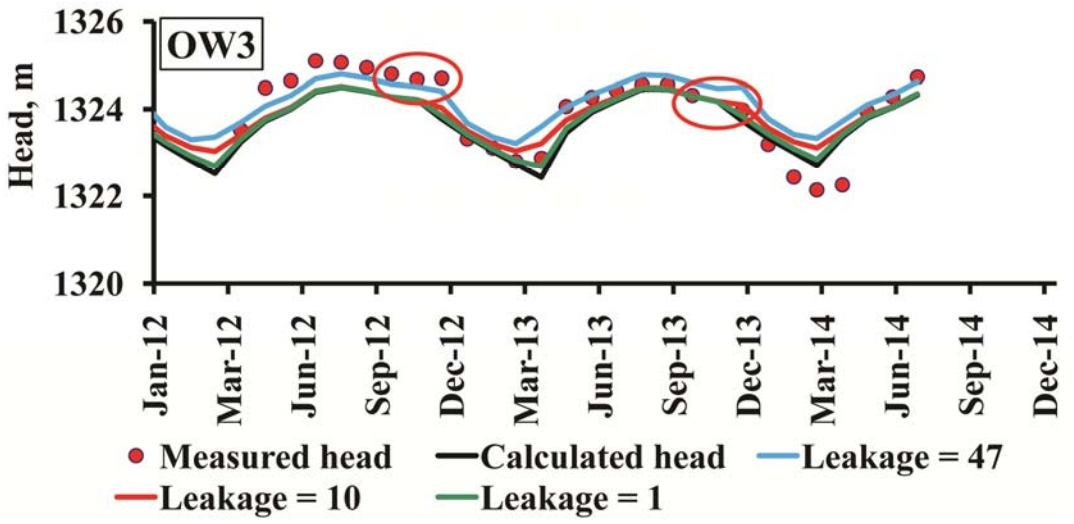

Figure 4.12. Measured and calculated heads OW3, near the river at the upstream edge of the aquifer for several values of the leakage factor. Note that heads rise slightly at the beginning of winter, probably in response to the river head rise during freezing.

4.4. Discussion and Conclusion

The model reproduces quite accurately head fluctuations during recent years and in 1960, prior to intense pumping. Lateral inflows and recharge are consistent with independent estimates. Model parameters are also consistent with hydraulic tests performed in the 1960 campaign. Therefore, we conclude that the model can be considered as a good tool to manage the aquifer and to understand the processes that occur.

The model confirms that river-aquifer interaction is essential for the Ulaanbaatar alluvial aquifer. The vast majority of the water pumped from this aquifer (some 27 MCMd year^{-1}) comes from Tuul River and its tributaries. This is true for alluvial aquifers around the world. What make the Ulaanbaatar alluvial aquifer especial is that the river freezes during winter. The river flow under the ice is sustained by groundwater, which provides the energy to prevent full freezing of the whole river thickness. Groundwater input does not occur where groundwater levels are depleted by pumping. This is the case in the central portion of the model. In this portion, the river becomes fully frozen. In fact, the river bed in

this portion becomes dry in April most years, probably because of sublimation and because water infiltrates into the aquifer immediately after melting.

The river still flows under the ice during winter at both ends of the Ulaanbaatar alluvial aquifer. The downstream end, to the West, receives aquifer discharge (i.e., the river is gainin). At the upstream end, the river is losing water, but maintains its flow for a few kilometers, which we attribute to discharge from the adjacent alluvial aquifers upstream.

If groundwater pumping increases, either at the Ulaanbaatar alluvial aquifer or at the alluvial aquifer near Gachuurt village, it is likely that the currently winter flowing portion of the river will also dry (or, rather, because become fully frozen during winter). This will not be a major problem from a quantitative point of view because aquifer storage is sufficient to support winter pumping, even if abstraction pumping is increased. However, it may have other environmental and cultural implications. Therefore, further study is needed to monitor at both the upper and downstream stream parts of the aquifer.

Chapter 5

General conclusions

The overall objective of this thesis has been to assess water resources in the Upper Tuul River Basin and, by extension, to provide insights into the hydrology of cold regions. To this end, work has been divided into three parts. The main contributions and results of these parts are:

1. A physically based water and energy balance model accounting for phase change (freezing, evaporation and sublimation) and soil vapor diffusion has been developed. To acknowledge the dynamics of the active soil freezing zone, the model is divided into two layers (soil surface and subsoil). It model has been run with daily meteorological data from the Terelj station, northern Mongolia and typical soil properties of the region. The results are qualitatively consistent with observations (amplitude and frequency of soil temperature fluctuations, duration of snow cover, etc.). The most singular result of the model and simulation results is the relative importance of vapor diffusion, which is downwards during

late spring and early summer, when temperature and, therefore, vapor pressure is much larger in the surface than in the still cold subsoil. The associated latent heat flux is essential to melt subsoil ice. Vapor diffusion is upwards during late summer and fall, but the flux is much smaller because subsoil temperature never becomes high and vapor pressure is a non-linear function of temperature. As a result, the net flux is downwards and it is relevant both in terms of water, it controls recharge, and energy balances. Notably, total runoff would be too small, compared to observations, if vapor diffusion is reduced. We conclude that land surface schemes should account for vapor diffusion.

2. This model was applied to the Upper Tuul basin, for period of 1993-2013. Data from two stations (Ulaanbaatar and Terelj) within the basin was used yielded too low rainfall, because they are located at low elevations. In order to obtain realistic meteorological data at high zones, we had to use lapse rates to correct rainfall and temperature for elevation so as to obtain discharges comparable to measurements. Further realism was gained by dividing the basin in 12 zones depending on slope, elevation range and accounting the different type of vegetation and soils. The result is that direct surface runoff is small, and restricted snowmelt period, when the soil is still partly frozen, which hinders infiltration. Infiltration increases in summer when the active layer thaws, so that most of the total discharge results from subsurface runoff. Evapotranspiration increases with elevation due to the increase in precipitation, but the ratio of the evapotranspiration (ET/P) decreases, both because the lower temperatures cause a reduced vapor pressure deficit and because cryosols display a low water retention capacity.

The energy balance is somewhat surprising. North facing slopes receive less direct solar radiation than horizontal or south facing slopes. Yet, net radiation at north facing slope turned out to be larger than at horizontal surfaces, but smaller than south facing slope. We believe that this result is caused by(1) the low albedo of the forests, that cover north facing slopes; and (2) the reduced temperature. The latter is caused by the increased evapotranspiration (forests access much more soil than grass) sensible heat, which is larger than latent heat flux in the 12 zones, but is specially large in forests due to their high roughness length.

3. River-aquifer interaction is essential for the Ulaanbaatar alluvial aquifer. Most of the water pumped from this aquifer comes from Tuul River and its tributaries. This is true for alluvial aquifers around the world. What is especial about the alluvial aquifer near Ulaanbaatar and, we suspect, most alluvial aquifers in arctic and subarctic regions is that the river freezes during winter. River flow under the ice is sustained by groundwater, which provides the energy to prevent full freezing of the whole river thickness, but which may not occur where groundwater levels are depleted by pumping. At present, the river still flows under the ice during winter at both ends of the Ulaanbaatar alluvial aquifer. The downstream end, to the West, receives aquifer discharge, whereas the river is fed by discharge from adjacent alluvial aquifers upstream of the east end. But, in the central portion, the river is fully frozen. In fact, the river bed in this portion becomes dry in April most years, probably because of sublimation and because melted water immediately infiltrates into the aquifer.

If groundwater pumping increases, either at the Ulaanbaatar alluvial aquifer or at the alluvial aquifer near Gachuurt village, it is likely that the currently winter flowing portion of the river will also dry or, rather, become fully frozen during winter. This will not be a major problem from a quantitative point of view because aquifer storage is sufficient to support winter pumping, even if pumping is increased. However, it may have other environmental and cultural implications. Therefore, further study is needed to monitor at both the upper and downstream stream parts of the aquifer.

6. References

Alkhaier, F., Su, Z. and Flerchinger, G.N. (2012)Reconnoitering the effect of shallow groundwater on land surface temperature and surface energy balance using MODIS and SEBS.*Hydrology and Earth System Sciences*, 16(7), 1833-1844.

Allen, R.G., Pereira, L.S., Raes, D. and Smith, M. (1998) Crop evapotranspiration-Guidelines for computing crop water requirements-FAO Irrigation and drainage paper 56. *FAO, Rome*, *300*(9), D05109.

Allen, R. G., Trezza, R. and Tasumi, M. (2006) Analytical integrated functions for daily solar radiation on slopes. Agricultural and Forest Meteorology, 139(1), 55-73.

Altansukh, O., Whitehead, P. and Bromley, J. (2012) Spatial patterns and temporal trends in the water quality of the Tuul River in Mongolia. *Energy and Environment Research*, *2*(1), 62.

Anisimov, O. A. (2007) Potential feedback of thawing permafrost to the global climate system through methane emission.*Environmental Research Letters*, 2(4), 045016.

Arnold J.G., Srinivasan, R., Muttiah, R.S. and Williams, J.R. (1998) Large area hydrological modeling and assessment, part I: Model development. *Journal of the American Water Resources Association.* 34(1), 73-89.

Arya, S.P. (2001) *Introduction to Micrometeorology*. Academic Press, 420 pp.

Asner, G.P., Scurlock, J.M. and Hicke, J.A. (2003) Global synthesis of leaf area index observations: implications for ecological and remote sensing studies. *Global Ecology and Biogeography.* 12(3), 191-205.

Badescu, V. (2002) 3D isotropic approximation for solar diffuse irradiance on tilted surfaces, *Renewable Energy.* 26, 221-233.

Bao, H., Koike, T., Yang, K., Wang, L., Shrestha, M. andLawford, P. (2016) Development of an enthalpy-based frozen soil model and its validation in a cold region in China. *Journal of Geophysical Research: Atmospheres*.

Barahona-Palomo, M. (2014) Estimation of aquifers hydraulic parameters by three different tecniques: geostatistics, correlation and modeling.Doctorate thesis in UniversitatPolitecnica de Catalunya, UPCBarcelonaTech, Spain.

Batima, P., Nyamsuren, B. and Buyndalai, B. (2004) Trends in river and lake ice in Mongolia. *Assessments of impacts and adaptations to climate change (AIACC). Working Paper*, (4).

Batima, P., Natsagdorj, L. and Batnasan, N. (2007) Vulnerability of Mongolia's Pastoralists to Climate Extremes and Changes. *Climate change and Vulnerability.* Edited by Neil Leary, Cecilia Cande, Jaoti Kulkarni, Anthany Nyong and Juan Pulhin. London. pp 67-87.

Batkhishig, O. and Iderjavklan, S. (2009) Digital soil map of the Kharaa river basin. *Internal Report*. Soil Sciences Laboratory, Institute of Geography, Mongolian Academy of Sciences.

Batsaikhan, N., Woo, N.C. and Nemer, B. (2011) Groundwater quality and sustainability in Ulaanbaatar, the fast growing Capital of Mongolia. In *AGU Fall Meeting Abstracts* (Vol. 1, p. 1334).

Beven, K. J., Lamb, R., Quinn, P., Romanowicz, R. and Freer, J. (1995) "TOPMODEL" In: Singh, V.P., (Ed.), *Computer Models of Watershed Hydrology, 18. Water Resources Publications*, Highlands Ranch, CO, (Chapter 18); pp.

Blad, B.L. and Rosenberg, N.J. (1976) Evaluation of Resistance and Mass Transport Evapotranspiration Models Requiring Canopy Temperature Data, *Agron. J.* 68, 764–769.

Blandford, T. R., Humes, K. S., Harshburger, B. J., Moore, B. C., Walden, V. P. and Ye, H. (2008) Seasonal and synoptic variations in near-surface air temperature lapse rates in a mountainous basin. *Journal of Applied Meteorology and Climatology*, *47*(1), 249-261.

Boland, J., Ridleya, B. and Brown, B. (2008) Models of diffuse solar radiation. *Renewable Energy.* 33, 575-584.

Bolton, W.R. (2006) Dynamic modeling of the hydrological processes in areas of discontinuous permafrost. Dissertation, University of Alaska, Fairbanks

Bring, A., Fedorova, I., Dibike, Y., Hinzman, L., Mård, J., Mernild, S. H., Woo, M. K. (2016). Arctic terrestrial hydrology: A synthesis of processes, regional effects and research challenges. Journal of Geophysical Research: Biogeosciences.

Bristow, K.L. (2002) Thermal Conductivity. *Methods of Soil Analysis: Part 4 Physical Methods*. 1209-1226.

Brutsaert, W.H. (1975) On a derivable formula for long-wave radiation from clear skies. *Water Resources Research*. 11(5), 742-744.

Brutsaert, W.H. (1982) *Evaporation into the Atmosphere*. R. Deidel Publishing Company, Dordrecht, Holland.

Buyankhishig, N., Masumoto, M. and Aley, M. (2007) Parameter estimation of an unconfined aquifer of the Tuul River basin Mongolia.

Buyankhishig, N. (2008) Doctorate thesis in Mongolian University of Science and Technology. Ulaanbaatar. (in Mongolian).

Buyankhishig, N., Aley, M. and Enkhbayar, D. (2009) Abstraction influence on alluvial aquifer of the Tuul River, Mongolia. *IAHS-AISH publication*, 80-88.

Callegary, J. B., Kikuchi, C. P., Koch, J. C., Lilly, M. R., and Leake, S. A. (2013) Review: groundwater in Alaska (USA). Hydrogeology Journal, 21(1), 25-39.

Cass, A., Campbell, G. S. and Jones, T. L. (1984)Enhancement of thermal water vapor diffusion in soil. *Soil Science Society of America Journal*. 48(1), 25-32.

Callegary, J. B., Kikuchi, C. P., Koch, J. C., Lilly, M. R., and Leake, S. A. (2013) Review: groundwater in Alaska (USA). Hydrogeology Journal, 21(1), 25-39.

Constantz, J. (1998) Interaction between stream temperature, stream flow, and groundwater exchanges in alpine streams. *Water resources research*, *34*(7), 1609-1615.

Côté, J. and Konrad, J.M. (2005) A generalized thermal conductivity model for soils and construction materials. *Canadian Geotechnical Journal*. *42*(2), 443-458.

Cussler, E. L. (1997) *Diffusion: Mass Transfer in Fluid Systems (2nd ed.). New York: Cambridge University Press.* ISBN 0-521-45078-0

Dalai, B. and Ishiga, H. (2013) Geochemical evaluation of present-day Tuul River sediments, Ulaanbaatar basin, Mongolia. *Environmental monitoring and assessment*, *185*(3), 2869-2881.

Daly, C., Neilson, R. P. and Phillips, D. L. (1994) A statistical-topographic model for mapping climatological precipitation over mountainous terrain.*Journal of applied meteorology*, *33*(2), 140-158.

Dandar, E., Carrera, J. and Nemer, B. (2016) Evaluation of groundwater resources in the upper Tuul River basin, Mongolia.*Water and Environment in the Selenga-Baikal Basin: International Research Cooperation for an Eco region of Global Relevance,*Columbia University Press.

Daniel, E. B., Camp, J. V., LeBoeuf, E. J., Penrod, J. R., Dobbins, J. P. and Abkowitz, M. D. (2011) Watershed modeling and its applications: A state-of-the-art review. *The Open Hydrology Journal*, *5*(1).

Davaa, G. and Oyunbaatar, D. (2010) Floods in around Ulaanbaatar. *Information and Research Institute of Meteorology, Hydrology and Environment*, Mongolia. (in Mongolia)

Debele, B., Srinivasan, R. and Gosain, A.K. (2010) Comparison of Process-Based and Temperature-Index Snowmelt Modeling in SWAT.*Water Resources Management.* 24, 1065-1088, doi:10.1007/s11269-009-9486-2.

Dimkic, M., Brauch, H. J. and Kavanaugh, M. C. (Eds.). (2008) *Groundwater management in large river basins*. IWA Publishing.

Dodson, R. and Marks, D. (1997) Daily air temperature interpolated at high spatial resolution over a large mountainous region. *Climate Research*, *8*(1), 1-20.

Dolgorsuren, G., Chagnaa, N., Bron, J. and van der Linden, W. (2012) Tuul River basin integrated water resources management assessment report. *Strengthening Integrated Water Resources Management in Mongolia.* Ulaanbaatar.

Dulamsuren, C., Hauck, M., Bader, M., Osokhjargal, D., Oyungerel, S., Nyambayar, S. and Leuschner, C. (2008) Water relations and photosynthetic performance in Larixsibirica growing in the forest-steppe ecotone of northern Mongolia. *Tree physiology*. 29(1), 99-110.

Ek, M. B., Mitchell, K. E., Lin, Y., Rogers, E., Grunmann, P., Koren, V., Gayno, G. and Tarpley, J. D. (2003). Implementation of Noah land surface model advances in the National Centers for Environmental Prediction operational mesoscale Eta model. *Journal of Geophysical Research: Atmospheres,* 108(D22).

Emerton, L., Erdenesaikhan, N., De Veen, B., Tsogoo, D., Janchivdorj, L., Suvd, P., Enkhtsetseg, B., Gandolgor, G., Dorisuren, Ch., Sainbayar, D. and Enkhbaatar, A. (2009) The Economic Value of the Upper Tuul Ecosystem. *Mongolia Discussion Papers, East Asia and Pacific Sustainable Development Department*. Washington, D.C.: World Bank.

Evett, S.R., Prueger, J.H. and Tolk, J.A. (2011) Water and energy balances in the soil-plant-atmosphere continuum. *Handbook of Soil Sciences: Properties and Processes.*6-1.

Fontaine, T. A., Cruickshank, T. S., Arnold, J. G. and Hotchkiss, R. H. (2002) Development of a snowfall–snowmelt routine for mountainous terrain for the soil water assessment tool (SWAT). *Journal of hydrology*, *262*(1), 209-223.

Frampton, A., Painter, S., Lyon, S. W. and Destouni, G. (2011) Non-isothermal, three-phase simulations of near-surface flows in a model permafrost system under seasonal variability and climate change. Journal of Hydrology, 403(3), 352-359.

Fu, C., Popescu, I., Wang, C., Mynett, A. E. and Zhang, F. (2014) Challenges in modelling river flow and ice regime on the Ningxia-Inner Mongolia reach of the Yellow River, China. Hydrology and Earth System Sciences, 18(3), 1225.

Fuka, D.R., Easton, Z.M., Brooks, E.S., Boll, J., Steenhuis, T.S. and Walter, M.T. (2012) A simple process-based snowmelt routine to model spatially distributed snow depth and snowmelt in the SWAT model. *Journal of the American Water Resources Association.* 48(6), 1151-1161.

Ge, S., McKenzie, J., Voss, C. and Wu, Q. (2011) Exchange of groundwater and surface-water mediated by permafrost response to seasonal and long term air temperature variation. *Geophysical Research Letters*, *38*(14).

Goodale, C. L., Aber, J. D., and Ollinger, S. V. (1998) Mapping monthly precipitation, temperature, and solar radiation for Ireland with polynomial regression and a digital elevation model. *Climate Research*, *10*(1), 35-49.

Goovaerts, P. (2000) Geostatistical approaches for incorporating elevation into the spatial interpolation of rainfall. *Journal of hydrology*, *228*(1), 113-129.

Gran, M., Carrera, J., Olivella, S. and Saaltink, M. W. (2011) Modeling evaporation processes in a saline soil from saturation to oven dry conditions. *Hydrology and Earth System Sciences*, *15*(7), 2077-2089.

Gravis, G.F., Gavrilova, M.K., Zabolotnik, S.I., Lisun, A.M., Suhodrovsky, V.L. and Tumurbaatar, L. (1972) Geocryological conditions in Mongolia. Yakutsk. Russia. (in Russian).

Guo, X., Wang, L. and Tian, L. (2015) Spatio-temporal variability of vertical gradients of major meteorological observations around the Tibetan Plateau. *International Journal of Climatology*.

Gusev, Y. M. and Nasonova, O. N. (2002) The simulation of heat and water exchange at the land–atmosphere interface for the boreal grassland by the land surface model SWAP. Hydrological processes, 16(10), 1893-1919.

Hamilton, A. S. and Moore, R. D. (1996) Winter streamflow variability in two groundwater-fed sub-Arctic rivers, Yukon Territory, Canada. *Canadian Journal of Civil Engineering*, *23*(6), 1249-1259.

Hamilton, S. (2004) Winter streamflow as a source of uncertainty in water balance calculations. *IAHS Publications-Series of Proceedings and Reports*, *290*, 249-256.

Hanasaki, N., Kanae, S., Oki, T., Masuda, K., Motoya, K., Shen, Y. and Tanaka, K. (2007) An integrated model for the assessment of global water resources? Part 1: Input meteorological forcing and natural hydrological cycle modules. *Hydrology and Earth System Sciences.* 4(5), 3535-3582.

Hanson, C. L., Morris, R. P., Engleman, R. L., Coon, D. C, and Johnson, C. W. (1980) Spatial and Seasonal Precipitation Distribution in Southwest Idaho. USDA, SEA, ARM-W-13, 15 pp.

Hargreaves, G.H. and Samani, Z.A. (1985) Reference crop evapotranspiration from air temperature.*Applied engineering in agriculture*. 1(2), 96-99.

Hargreaves, G.H. and Allen, R.G. (2003) History and Evaluation of Hargreaves Evapotranspiration Equation.*Journal of Irrigation and Drainage Engineering.* 129(1), 53-63. doi: 10.1061(ASCE)0733-9437(2003)129:1(53).

Hiller, B. T. and Jadamba, N. (2006) Groundwater use in the Selenge river basin, Mongolia. In *The full papers of the 34th congress of International Association of Hydrogeologists, Bejing,* China.

Hinzman, L. D., Destouni, G. and Woo, M. K. (2013) Preface: Hydrogeology of cold regions. Hydrogeology Journal, 21(1), 1-4.

Ho, C. K, and Webb, S. W. (Eds.). (2006) *Gas transport in porous media* (Vol. 20). Dordrecht: Springer.

Hülsmann, L., Geyer, T., Schweitzer, C., Priess, J. andKarthe, D. (2015) The effect of subarctic conditions on water resources: initial results and limitations of the swat model applied to the Kharaa river basin in Northern Mongolia.*Environmental Earth Sciences*, *73*(2), 581-592.

Houghton, J. G. (1979) A model for orographic precipitation in the north-central Great Basin. *Monthly Weather Review*, *107*(11), 1462-1475.

Ishikawa, M., Sharkhuu, N., Zhang, Y., Kadota, T. and Ohata, T. (2005) Ground thermal and moisture conditions at the southern boundary of discontinuous permafrost, Mongolia. *Permafrost and Periglacial Processes.*16(2), 209-216.

Ishikawa, M., Zhang, Y., Kadota, T. and Ohata, T. (2006) Hydrothermal regimes of the dry active layer. *Water resources research*, *42*(4).

Islam, Z (2011) A Review on Physically based hydrologic modeling, *Technical report*, University of Alberta.

Jadambaa, N. (1977) Groundwater recharge and flow in artesian aquifers in Ulaanbaatar area and estimation of water resources in these aquifers or use of waer supply of city. Doctorate thesis in Geology and Mining. Moscow. (in Russian).

Jadambaa, N., Tserendorj, Z. and Enkhshishig, P. (1981) Hydrogeological investigations on groundwater in aquifers in Tuul River Basin in Ulaanbaatar area.Report. Ulaanbaatar. (In Russian).

Jadambaa, N. (2010) "Hydrogeology" In: *Geology and Mineral of Mongolia*, (VIII), Ulaanbaatar, (in Mongolian).

Jambaljav, Ya.,Dashtseren, A., Solongo, D., Saruulzaya, D. and Battogtokh, D. (2008) The temperature regime in boreholes at Nalaikh and Terelj sites in Mongolia. *Proceedings of the Ninth International Conference on Permafrost.* University of Alaska, Fairbanks, Volume 1, pp. 821-825.

JICA-Japan International Cooperation Agencey. (1995) The study on water supply system in Ulaanbaatar and its surroundings. *Report 01-1056*. Ulaanbaatar.

Johansson, B. and Chen, D. (2003) The influence of wind and topography on precipitation distribution in Sweden: Statistical analysis and modelling.*International Journal of Climatology*, *23*(12), 1523-1535.

Jones, C., Kielland, K. and Hinzman, L. (2015) Modeling groundwater upwelling as a control on river ice thickness. Hydrology Research, 46(4), 566-577.

Kalbus, E., Reinstorf, F. and Schirmer, M. (2006) Measuring methods for groundwater surface water interactions: a review. *Hydrology and Earth System Sciences Discussions*, *10*(6), 873-887.

Kane, D. L., Carlson, R. F., and Bowers, C. E. (1973) Groundwater pore pressures adjacent to subarctic streams.In *Proceedings of the 2nd international conference on permafrost, North American contributions, Yakutsk. National Academy of Sciences, Washington, DC* (pp. 453-458).

Karthe, D., Hofmann, J., Ibisch, R., Heldt, S., Westphal, K., Menzel, L., Avlyush, S. and Malsy, M. (2015) Science-based IWRM implementation in a data-scarce central asian region: experiences from a research and development project in the Kharaa River Basin, Mongolia. *Water*, *7*(7), pp.3486-3514.

Kato, H., Mariko, S., Urano, T. and Sugita, M. (2006) Influence of grazing on vegetation, surface energy balance and water balance over the Mongolian steppe. *Rn*, *8*(12), 158.

Kattel, D. B., Yao, T., Yang, K., Tian, L., Yang, G. and Joswiak, D. (2013). Temperature lapse rate in complex mountain terrain on the southern slope of the central Himalayas. *Theoretical and applied climatology*, *113*(3-4), 671-682.

Katul, G.G. and Parlange, M.B. (1992) A Penman-Brutsaert Model for wet surface evaporation. *Water Resources Research.* 28(1), 121-126.

Kestin, J., Sokolov, M. and Wakeham, W. A. (1978) Viscosity of liquid water in the range −8°C to 150°C. *Journal of Physical and Chemical Reference Data*,*7*(3), 941-948.

Kite, G.W. (1995) "The SLURP Model" In: Singh, V.P., (Ed.), *Computer Models of Watershed Hydrology, 15. Water Resources Publications*, Highlands Ranch, CO, (Chapter 15); pp.

Kunkel, K. E. (1989) Simple procedures for extrapolation of humidity variables in the mountainous western United States. J. Climate, 2, 656–669.

Lerner, D. N., Issar, A. S. and Simmers, I. (1990) Groundwater recharge, a guide to understanding and estimating natural recharge.*International Association of Hydrogeologists*, Kenilworth, Rep 8, 345 pp

Lutgens, F. K. and Tarbuck, E. J. (1995) *The atmosphere.* Prentice-Hall

Ma, X., Yasunari, T., Ohata, T., Natsagdorj, L., Davaa, G. and Oyunbaatar, D. (2003) Hydrological regime analysis of the Selenge River basin, Mongolia. *Hydrological Processes.* 17(14), 2929-2945.

McMahon, T.A., Peel, M.C., Lowe, L., Srikanthan, R. and McVicar, T.R. (2013) Estimating actual, potential, reference crop and pan evaporation using standard meteorological data: a pragmatic synthesis. *Hydrology and Earth System Sciences.* 17(4), 1331-1363.

Medina, A. and Carrera, J. (2003) Geostatistical inversion of coupled problems: dealing with computational burden and different types of data. *J. Hydrol*. 281 (4), 251–264.

Minderlein, S. and Menzel, L. (2015) Evapotranspiration and energy balance dynamics of a semi-arid mountainous steppe and shrubland site in northern Mongolia. *Environmental Earth Sciences*, *73*(2), 593-609.

Monteith, J.L. and Unsworth, M.H. (1990) *Principles of Environmental Physics.*Academic Press, 291 pp.

Murray, F.W. (1967) On the computation of saturation vapor pressure. *J. Appl. Meteor.* **6,** 203–204.

National soil atlas of Mongolia. (1981) (Scale 1:1000 000)

Nicolsky, D. J., Romanovsky, V. E., Alexeev, V. A. and Lawrence, D. M. (2007)Improved modeling of permafrost dynamics in a GCM land-surface scheme.*Geophysical Research Letters*, 34(8).

Noorian, A. M., Moradi, I. and Kamali, G. A. (2008) Evaluation of 12 models to estimate hourly diffuse irradiation on inclined surfaces. *Renewable energy.* 33(6), 1406-1412.

NSO. (2013) *Statistic of Ulaanbaatar*, Mongolia

Oke, T.R. (1987) *Boundary Layer Climates.*2nd edition, Halsted, New York.

Osborn, H. B. (1984) Estimating precipitation in mountainous regions. *Journal of Hydraulic Engineering*, *110*(12), 1859-1863.

Oyunbaatar, D. (2001) Runoff and rainfall distribution in the Selbe river basin. In *Proceedings of the International Workshop on GAME-ANN/Radiation, 7–9 March 2001, Phunket* (pp. 102-106).

Penman, H.L. (1948) Natural evaporation from open water, bare soil and grass.*InPorceedings of the Royal Society of London A: Mathematical, Physical and Engineering Sciences.* Vol.193, 120-145.

PNIIIS - Engineering Geological Scientific-Research and Industrial Institute.(1979) Exploration for evaluation exploitable groundwater resources of an alluvial aquifer in the Tuul River basin (Central water part).*Report 01-983*. (in Russian).

Priestley, C.H.B. and Taylor, R.J. (1972) On the assessment of surface heat flux and evaporation using large scale parameters. *Mon. Weather Rev*. 100, 81-92.

Prowse, T. D. and Beltaos, S. (2002) Climatic control of river-ice hydrology: a review. Hydrological processes, 16(4), 805-822.

Qi, J., Li, S., Li, Q., Xing, Z., Bourque, C.P.A. and Meng, F.R. (2016) A new soil-temperature module for SWAT application in regions with seasonal snow cover. *Journal of Hydrology.* 538, 863–877, doi: 10.1016/j.jhydrol.2016.05.003.

Ransley, T., Tottenham, R., Sundaram, B. and Brodie, R. (2007) Development of Method to Map Potential Stream-Aquifer Connectivity: a case study in the Border Rivers Catchment. *Bureau of Rural Sciences, Canberra*.

Reilly, T. E., and Harbaugh, A. W. (2004) *Guidelines for evaluating ground-water flow models* (p. 30). US Department of the Interior, US Geological Survey.

Ripple, C.D., Rubin, J. and Van Hylckama, T.E.A. (1970) *Estimating Steady-state Evaporation Rates from bare Soils under Conditions of High Water Table*, U.S. Geol. Sur., Open-file Report Water Res. Div., Menlo Park, California, 62 pp.

Rötting, T. S., Carrera, J., Bolzicco, J., Salvany, J. M. (2006) Stream-stage response tests and their joint interpretation with pumping tests. Groundwater, 44(3), 371-385.

Rorabaugh, M. I. (1963) Streambed Percolation in Development of Water Supplies. In R. Bentall (Ed.), Methods of Collecting and Interpreting Groundwater Data (Vols. 1544-H, pp. 47-62).U.S. Geological Survey Water Supply Paper.

Rosenberg, N.J., Blad, B.L. and Verma, S.B. (1983) Evaporation and Evapotranspiration.*Chapter7 of the Book Microclimate – The Biological Environment.* Wiley-Interscience, John Wiley and Sons, 209–287.

Rosenshein, J. S. (1988) Region 18, alluvial valleys. *Hydrogeology: The Geology of North America*, *2*.

Saito, H. and Šimůnek, J. (2009) Effects of meteorological models on the solution of the surface energy balance and soil temperature variations in bare soils. *Journal of Hydrology.* 373(3), 545-561.

Samper, J., Vera, M. G., Pisani, B., Alvares, D., Marques, J. E., Varela, A., Losada, J.A., Ferreira, J.P.L. and Vieira, J.M.P. (2007) Using hydrological models and Geographic Information Systems for water resources evaluation: GIS-VISUAL-BALAN and its application to Atlantic basins in Spain (Valiñas) and Portugal (Serra da Estrela). *IAHS publication*, *310*, 259.

Sapriza-Azuri, G., J. Jódar, J. Carrera, andH.V. Gupta(2015)Toward a comprehensive assessment of the combined impacts of climate change and groundwater pumping on catchment dynamics. *Journal of Hydrology*, 529, 1701-1712.

Scanlon, B. R., Healy, R. W. and Cook, P. G. (2002) Choosing appropriate techniques for quantifying groundwater recharge. *Hydrogeology Journal*,*10*(1), 18-39.

Schroeder, P.R., Dozier, T.S., Zappi, P.A., McEnroe, B.M., Sjostrom, J.W. and Peyton, R.L. (1994) The hydrologic evaluation of landfill performance (HELP) model: engineering documentation for version 3. *Environmental Protection Agency, United States*.

Sharkhuu, N. (2003) Recent changes in the permafrost of Mongolia. *In Porceedings of the 8th International Conference on Permafrost.*Zurich, Switzerland, pp.1029/1034.

Shea, J. M., Marshall, S. J. and Livingston, J. M. (2004) Glacier distributions and climate in the Canadian Rockies. *Arctic, Antarctic, and Alpine Research*,*36*(2), 272-279.

Shuttleworth, W. J. (1979) *Evaporation*, Institute of Hydrology, Wallingford.

Shvetzov, P.F. (1978) Conditions and geothermal consequences of the moisture exchange between the lithosphere and the atmosphere in permafrost regions. *Third international conference on permafrost.*Ottawa, Ontorio.

Sicart, J.E., Pomeroy, J.W., Essery R.L.H. and Bewley, D. (2006) Incoming longwave radiation to melting snow: observations, sensitivity and estimation in northern environments. *Hydrol.Processes.* 20, 3697-3708, doi: 10.1002/hyp.6383.

Sophocleous, M. (2002) Interactions between groundwater and surface water: the state of the science. *Hydrogeology journal*, *10*(1), 52-67.

Sproul, A.B. (2007) Derivation of the solar geometric relationships using vector analysis. *Renewable Energy.* 32(7), 1187-1205, doi: 10.1016/j.renene.2006.05.001.

Taesombat, W. and Sriwongsitanon, N. (2009) Areal rainfall estimation using spatial interpolation techniques. *Science Asia.* 35, 268-275.

Tian, Y.Q., Davies-Colley, R.J., Gong, P. and Thorrold, B.W. (2001) Estimating solar radiation on slopes of arbitrary aspect.*Agricultural and Forest Meteorology.* 109, 67-74.

Thiessen, A.H. (1911) Precipitation averages for large areas. Monthly Weather Rev. 39 (7), 1082–1084.

Tsujimura, M., Ikeda, K., Tanaka, T., Janchivdorj, L., Erdenchimeg, B., Unurjargal, D. and Jayakumar, R. (2013) Groundwater and surface water interactions in an alluvial plain, Tuul River Basin, Ulaanbaatar, Mongolia. *Sciences in Cold and Arid Regions*, *5*(1), 0126-0132.

Tuvshinjargal, D. and Saranbaatar, L. (2004) Thermal balance features in the Terelj valley (Mongolia). *In proceedings of the 3rd International Workshop on Terrestrial Change in Mongolia.* Tsukuba, Japan

Unudelger, G. and Banzragch, B. (1993) Hydrogeological investigations in Ulaanbaatar area (1990-1992).*Report*. Ulaanbaatar. (in Mongolian)

UPC, (2003) Codigo Visual Transin 1.1 R65.Developed in the Department of Geotechnical Engineering and Geosciences (ETCG).UPC.

Vázquez-Suñé, E., Sánchez-Vila, X. and Carrera, J. (2005) Introductory review of specific factors influencing urban groundwater, an emerging branch of hydrogeology, with reference to Barcelona, Spain. *Hydrogeology Journal*,*13*(3), 522-533.

Verdhen, A., Chahar, B.R. and Sharma, O.P. (2014) Snowmelt Modelling Approaches in Watershed Models: Computation and Comparison of Efficiencies under Varying Climatic Conditions. *Water Resources Management.* 28, 3439–3453, doi: 10.1007/s11269-014-0662-7.

Weber, M. D., Booth, E. G. and Loheide, S. P. (2013) Dynamic ice formation in channels as a driver for stream-aquifer interactions. *Geophysical Research Letters*, *40*(13), 3408-3412.

Weedon, G. P., Gomes, S., Viterbo, P., Shuttleworth, W. J., Blyth, E., Österle, H., Adam, J.C., Bellouin, N., Boucher, O. and Best, M. (2011) Creation of the WATCH forcing data and its use to assess global and regional reference crop evaporation over land during the twentieth century. *Journal of Hydrometeorology*, *12*(5), 823-848.

Winter, T.C. (1995) Recent advances in understanding the interaction of groundwater and surface water. *Reviews of Geophysics*, *33*(S2), 985-994.

Woo, M. K. (2012) *Permafrost hydrology*. Springer Science and Business Media.

Wu, T., Wang, Q., Zhao, L., Du, E., Wang, W., Batkhishig, O. and Watanabe, M. (2012). Investigating internal structure of permafrost using conventional methods and ground-penetrating radar at Honhor basin, Mongolia. *Environmental earth sciences*, *67*(7), 1869-1876.

Xu, C.Y. and Singh, V.P. (2002) Cross comparison of empirical equations for calculating potential evapotranspiration with data from Switzerland. *Water Resources Management.* 16(3), 197-219.

Yates, D.N. (1996) WatBal: An Integrated Water Balance Model for Climate Impact Assessment of River Basin Runoff. *International Journal of Water Resources Development.* 12(2), 121-140, doi: 10.1080/07900629650041902.

Ye, B., Yang, D., Zhang, Z. and Kane, D. L. (2009) Variation of hydrological regime with permafrost coverage over Lena Basin in Siberia. *J. Geophys. Res.*, 114, D07102, doi:10.1029/2008JD010537.

Zabel, F., Mauser, W., Marke, T., Pfeiffer, A., Zängl, G. and Wastl, C. (2012) Inter-comparison of two land-surface models applied at different scales and their feedbacks while coupled with a regional climate model. *Hydrology and Earth System Sciences.* 16(3), 1017-1031.

Zandaryaa, S., Borhculuun, U. and Munkhtuya, S. (2003) Reserves, consumption and contamination of groundwater in Ulaanbaatar, Mongolia.*Atlas of Urban Geology*, *14*, 445-488.

Zhang, Y., Suzuki, K., Kadota, T. and Ohata, T. (2004) Sublimation from snow surface in southern mountain taiga of eastern Siberia. *Journal of Geophysical Research: Atmospheres.* 109(D21).

Zhang, Y., Ishikawa, M., Ohata, T. and Oyunbaatar, D. (2008) Sublimation from thin snow cover at the edge of the Eurasian cryosphere in Mongolia. *Hydrological processes*, *22*(18), 3564-3575.

Zhou, J., Pomeroy, J. W., Zhang, W., Cheng, G., Wang, G., and Chen, C. (2014) Simulating cold regions hydrological processes using a modular model in the west of China.*Journal of Hydrology*, 509, 13-24.

Annexes

Position of the sun

For the calculation of the position of the sun and the zenith, it is convenient to define two unit vectors: **p**, which is orthogonal to the land surface and **s**, which points to the sun (Figure A1). Their first component points eastwards, the second northwards and the third upwards. Vector **p** can be calculated from the strike (σ) and dip (θ) (see also figure A2):

$$\mathbf{p} = \begin{pmatrix} p_{east} \\ p_{north} \\ p_{up} \end{pmatrix} = \begin{pmatrix} \cos\sigma \sin\theta \\ -\sin\sigma \sin\theta \\ \cos\theta \end{pmatrix} \quad \text{(A1)}$$

Vector **s** depends on the time of the day, the sun declination (δ), solar angle (ω) and the latitude (φ). It can be calculated according to Sproul (2007) as:

$$\mathbf{s} = \begin{pmatrix} s_{east} \\ s_{north} \\ s_{up} \end{pmatrix} = \begin{pmatrix} -\cos\delta \sin\omega \\ \sin\delta \sin\varphi - \cos\delta \sin\varphi \cos\omega \\ \cos\delta \cos\varphi \cos\omega + \sin\delta \sin\varphi \end{pmatrix} \quad \text{(A2)}$$

The product of both vectors ($\mathbf{p}^T\mathbf{s}$) equals the cosine of the angle between them. Note, that on a horizontal surface (θ = 0), $\mathbf{p}^T$ is (0,0,1) and $\mathbf{p}^T\mathbf{s} = s_{up}$. At night $s_{up} < 0$, at daylight $s_{up} > 0$ and at sunrise and sunset $s_{up} = 0$. Furthermore, an inclined surface is in the shade when $\mathbf{p}^T\mathbf{s} < 0$.

The sun declination (δ) is the angle between the direction of the sun and the equator. It can be calculated by a yearly sinusoidal function:

$$\delta = -\delta_{\max} \sin\left(2\pi \frac{t - t_s}{d_a}\right) \quad \text{(A3)}$$

where $\delta_{\max}$ is the maximum sun declination (0.4091 rad = 23.26°), t is time (s) , t_s is time at September equinox, approximately September 21st, (s) and d_a is the duration of year (=365.241 days =3.15568×10^7 s).

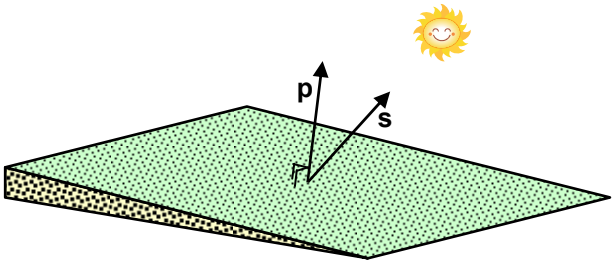

Figure A1. Illustration of vectors **p** and **s**

The extraterrestrial solar radiation on a horizontal surface can be simplified by:

$$\begin{aligned} R_{S,et,hor} &= S_0 f_e s_{up} = S_0 f_e(\cos\delta\cos\varphi\cos\omega + \sin\delta\sin\varphi) && \text{If } s_{up} > 0 \\ R_{S,et,hor} &= 0 && \text{otherwise} \end{aligned} \tag{A4}$$

where S_0 is the sun constant (1367 J m^{-2} s^{-1}) and f_e is the factor that corrects for the eccentricity of the earth´s orbit. It can be calculated from (Allen et al., 1998):

$$f_e = 1 + 0.033\cos(2\pi\frac{t - t_{ph}}{d_a}) \tag{A5}$$

where t_{ph} is the time at perihelion, approximately January3rd, (s).

For the daily averaged extraterrestrial solar radiation on a horizontal surface, integrating equation (A4) between sunset and sunrise and dividing by the duration of a day (d_d) gives:

$$R_{S,et,hor} = \frac{S_0 f_e}{d_d}\int_{-\omega_{ss}}^{\omega_{ss}} s_{up}\,dt = \frac{S_0 f_e}{d_d}(\cos\delta\cos\varphi\sin\omega_{ss} + \omega_{ss}\sin\delta\sin\varphi) \tag{A6}$$

where the sunset angle, ω_{ss}, is the solar angle when s_{up} equals 0:

$$\omega_{ss} = \cos^{-1}(\max(\min(-\tan\varphi\tan\delta, 1), -1) \tag{A7}$$

The min and max functions guarantee that $\omega_{ss} \in [0, \pi]$. Thus, equation (A6) also works for days when the sun doesn't set or rise (i.e., in polar regions).

Correction for an inclined surface

The strike (σ) of an inclined plane is the orientation of a horizontal line on this plane, expressed as an angle relative to the north in clockwise direction. The dip (θ) is the maximum angle between a horizontal plane and the incline plane (figure A2).

The extraterrestrial solar radiation on an inclined surface is the solar radiation without taking into account the reduction of it by the atmosphere. It can be expressed as:

$$\begin{aligned} \mathrm{R}_{\mathrm{S},et,inc} &= \mathrm{S}_0 f_e \max(\mathbf{p}^T\mathbf{s}, 0) && \text{If } s_{up} > 0 \\ \mathrm{R}_{\mathrm{S},et,inc} &= 0 && \text{otherwise} \end{aligned} \tag{A8}$$

Note that for a horizontal surface ($\theta = 0 \Rightarrow \mathbf{p}^T\mathbf{s} = s_{up}$) equation (A8) reduces to (A4).For the daily averaged extraterrestrial solar radiation on an inclined surface, we have to integrate equation (A8):

$$\mathrm{R}_{\mathrm{S},et,inc} = \frac{\mathrm{S}_0 f_e}{\mathrm{d_d}} \int_{-\omega_{\mathrm{ss}}}^{\omega_{\mathrm{ss}}} \max(\mathbf{p}^T\mathbf{s}, 0)\mathrm{dt} \tag{A9}$$

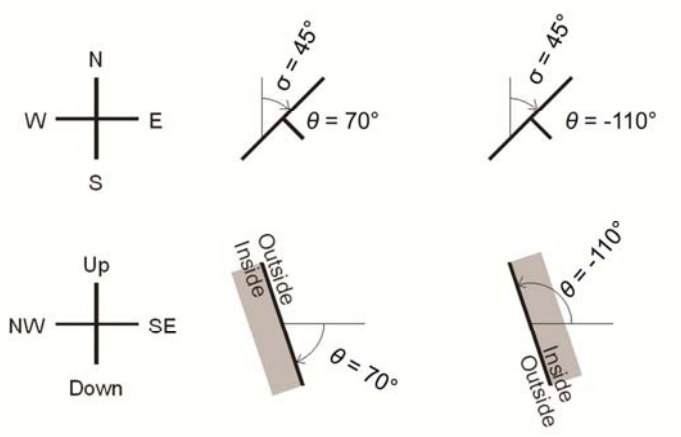

Figure A2. *Illustration of strike (σ) and dip (θ). Note that a dip between -0.5π and 0.5π (-90^0 and 90^0) refers to a plane with its outside facing upwards. A dip between 1.5π and 0.5π*

(90^0 and 270^0) or between -1.5π and -0.5π refers to a plane with its outside facing downwards.

However, we have to take into account that the surface can be in the shade during part of the day, which complicates the calculations. The integral of $\max(\mathbf{p}^T\mathbf{s}, 0)$ can be calculated by dividing it into different periods, when it is in the shade or not:

$$\int_{-\omega_{ss}}^{\omega_{ss}} \max(\mathbf{p}^T\mathbf{s}, 0)\, dt = \max\left(\int_{-\omega_{ss}}^{\omega_1} \mathbf{p}^T\mathbf{s}dt, 0\right) + \max\left(\int_{\omega_1}^{\omega_2} \mathbf{p}^T\mathbf{s}dt, 0\right) + \max\left(\int_{\omega_2}^{\omega_{ss}} \mathbf{p}^T\mathbf{s}dt, 0\right) \tag{A10}$$

$$\omega_1 = \min\left(\max(-\omega_{ss}, \omega_{io1}), \omega_{ss}\right)$$

$$\omega_2 = \min\left(\max(-\omega_1, \omega_{io2}), \omega_{ss}\right)$$

where ω_{io1} and ω_{io2} are the two solar angles in a day when the inclined surface comes out of or into the shade, that is, when $\mathbf{p}^T\mathbf{s} = 0$. They are calculated from:

$$\text{if } -1 \geq \frac{b}{a\sqrt{1 + b^2/a^2}} \geq 1 \text{ and } -1 \geq \frac{c}{a\sqrt{1 + b^2/a^2}} \geq 1 \text{ then}$$

$$\omega_{io1} = \min(\mathrm{mod}(\pi - \omega_b + \omega_c, 2\pi) - \pi, \mathrm{mod}(-\omega_b - \omega_c, 2\pi) - \pi)$$

$$\omega_{io2} = \max(\mathrm{mod}(\pi - \omega_b + \omega_c, 2\pi) - \pi, \mathrm{mod}(-\omega_b - \omega_c, 2\pi) - \pi)$$

$$\omega_b = \frac{b}{a\sqrt{1 + b^2/a^2}} \tag{A11}$$

$$\omega_c = \frac{c}{a\sqrt{1 + b^2/a^2}}$$

else (there is no solution for $\mathbf{p}^T\mathbf{s} = 0$)

$$\omega_{io1} = -\pi$$

$$\omega_{io2} = \pi$$

where mod is a function that returns the remainder of the first argument after it is divided by the second argument. This guarantees that ω_1 and $\omega_2 \in [-\pi, \pi]$. Moreover, the min and

max functions guarantee that $\omega_{io1} \leq \omega_{io2}$. When there is no solution for $\mathbf{p}^T\mathbf{s} = 0$, it means that during the whole day the inclined surface is facing the sun or not.The integral of $\mathbf{p}^T\mathbf{s}$ can be calculated by using equations (A1) and (A2):

$$\int_{\omega_{ini}}^{\omega_{fin}} \mathbf{p}^T\mathbf{s}\, dt = \int_{\omega_{ini}}^{\omega_{fin}} (\mathrm{a}\sin\omega + \mathrm{b}\cos\omega - \mathrm{c})dt = \tag{A12}$$

$$= \frac{d_d}{2\pi}[-a(\cos\omega_{fin} - \cos\omega_{ini}) + b(\sin\omega_{fin} - \sin\omega_{ini}) - c(\omega_{fin} - \omega_{ini})]$$

with

$$a = -\cos\sigma\sin\theta\cos\delta$$

$$b = \sin\sigma\sin\theta\cos\delta\sin\varphi + \cos\theta\cos\delta\cos\varphi \tag{A13}$$

$$c = \sin\sigma\sin\theta\sin\delta\cos\varphi - \cos\theta\sin\delta\sin\varphi$$

Sky view factor

The sky view factor (f_{sv}), is the proportion of the sky above the inclined surface that is not blocked from view by the surrounding horizontal plane (figure A3). It ranges from 0.5 for a vertical to 1 for a horizontal surface. In general one can use the formula of Badescu (2002):

$$f_{sv} = \frac{\cos(2\theta) + 2}{4} \tag{A14}$$

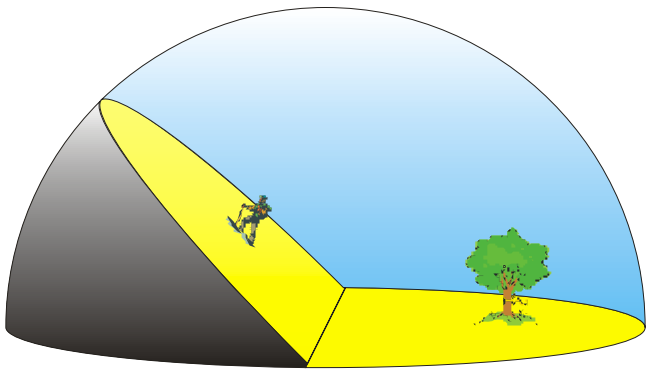

Figure A3. *Illustration of the sky view factor, f_{sv}.*